

Josef Lechner, BSc.

# **Design and Experimental Evaluation of 3D printed Microreactors for Reactions in Continuous Flow**

## **MASTER'S THESIS**

to achieve the university degree of

Diplom-Ingenieur

Master's degree programme: Chemical and Pharmaceutical Engineering

submitted to

**Graz University of Technology**

Supervisor

Assoc.Prof. Dipl.-Ing. Dr.techn. Heidrun Gruber-Wölfler

Institute of Process and Particle Engineering

Graz, January 2019

---

# AFFIDAVIT

I declare that I have authored this thesis independently, that I have not used other than the declared sources/resources, and that I have explicitly indicated all material which has been quoted either literally or by content from the sources used. The text document uploaded to TUGRAZonline is identical to the present master's thesis.

29. January, 2019

Date

Signature

---

# Abstract

Continuous flow processes in pharmaceutical industry have gained a lot of interest by research, authorities and industry in recent years. Especially microfluidic technology is a promising alternative to the present discontinuous processes. 50% of reactions in the pharmaceutical industry could benefit from continuous processes, mainly by using microreaction systems (MRS) [1]. Detailed reactor design requires information about the intrinsic reaction kinetics, without limitations due to heat or mass transfer. In organic synthesis, undesired side reactions may be promoted by bad mixing, decreasing yield and selectivity. Therefore, fast mixing devices are inescapable for successful chemical reactions and a reliable determination of reaction kinetics.

This thesis focuses on the characterisation of the mixing performance of 3D printed microreactors made of stainless steel and ceramics. Additive manufacturing was chosen as fabrication process, to create highly complex micro structures. Stainless steel and ceramic devices were produced by using selective laser melting (SLM) and lithography-based ceramic manufacturing (LCM) as fabrication techniques, respectively. Passive mixing was realised with designs consisting of split-and-recombine (SAR) elements or spherical mixing chambers. Active mixing with external forces was achieved with a cascade consisting of ten connected continuous stirred-tank reactors (CSTR-cascade) with internal magnetic stirrers.

The mixing performance was characterised by determining residence time distribution (RTD) and a set of mixing sensitive reactions. A consecutive-competitive diazo coupling of 1-naphthol and diazotised sulfanilic acid, published by Bourne et al. [2], was chosen as mixing sensitive reaction. The reaction was analysed by measuring UV/VIS absorption and least square fitting. The influence of different geometries, materials, fabrication techniques and rotational speed of the stirrers on the mixing performance was investigated. The gained data was used to compare different reactor elements concerning their mixing efficiency and to develop optimisation approaches.

The investigated designs are due to their good mixing performance suitable to be used for fast reactions. In order to perform kinetic measurements in flow, using the 3D printed reactors, a set-up for the determination of the reaction kinetics was designed. An aerobic oxidation of Grignard reagents was chosen as model reaction, since it requires fast mixing. Testing the complex reaction set-up resulted in new challenges for further development, based on this thesis.

---

# Kurzfassung

Bei kontinuierlichen Prozessen in der pharmazeutischen Industrie besteht ein wachsendes Interesse von Forschung, Industrie und Behörden. Besonders die Mikroreaktionstechnik ist eine vielversprechende Alternative zu den derzeit etablierten diskontinuierlichen Prozessen. 50 % der Reaktionen in der pharmazeutischen Industrie könnten von kontinuierlichen Prozessen, großteils von Mikroreaktionssystemen (MRS), profitieren [1]. Die detaillierte Berechnung von Reaktoren benötigt Informationen über die intrinsische Reaktionskinetik, ohne Limitierungen durch Wärme- oder Stoffübertragung. In der organischen Synthese kann schlechtes Mischen unerwünschte Nebenreaktionen begünstigen. Deswegen sind schnell mischende Elemente für eine selektive chemische Reaktion und eine zuverlässige Bestimmung der Reaktionskinetik unumgänglich.

Diese Arbeit beschäftigt sich mit der Charakterisierung des Mischungsverhaltens von 3D gedruckten Mikroreaktoren aus Edelstahl und Keramik. Additive Fertigung wurde als Herstellungsprozess von komplexen Mikrostrukturen gewählt. Edelstahl und Keramik Elemente wurden mittels selektivem Laserschmelzen (SLM) und Lithographie-basierter Keramik Fertigung (LCM) hergestellt. Als passive Mischer wurden Designs mit split-and-recombine (SAR) Elementen oder mit kugelförmigen Mischkammern verwendet. Aktives Mischen wurde durch eine Rührkesselkaskade mit zehn miteinander verbundenen Rührkesseln und internen Magnetrührstäbchen realisiert.

Das Mischungsverhalten wurde durch die Bestimmung der Verweilzeitverteilung (RTD) und mit mischungssensitiven Reaktionen charakterisiert. Eine seriell-kompetitive Reaktion von 1-Naphthol mit diazotierter Sulfanilsäure, publiziert von Bourne et al. [2], wurde zur Charakterisierung gewählt. Die Analyse wurde durch Messung der UV/VIS Absorption und einer Regression der kleinsten Fehlerquadrate durchgeführt. Der Einfluss von Geometrie, Material, Herstellungsverfahren und Drehzahl der Rührer auf die Mischleistung wurde untersucht. Anhand der erhaltenen Informationen wurden die Elemente hinsichtlich ihrer Mischleistung verglichen und Optimierungen entwickelt.

Die zuvor untersuchten Reaktoren eignen sich, aufgrund ihrer guten Mischleistung, zur Verwendung für schnelle Reaktionen. Ein Versuchsaufbau zur Bestimmung der Reaktionskinetik mit den 3D gedruckten Reaktoren wurde erstellt. Als Modellreaktion wurde eine aerobe Oxidation von Grignard Reagenzien zu den entsprechenden Phenolen gewählt, da für diese Reaktion ein schnelles Mischen der Komponenten unumgänglich ist. Erste Tests des komplexen Aufbaus führten zu neuen Herausforderungen für auf diese Arbeit aufbauende Weiterentwicklungen.

---

# Acknowledgement

In meinem Leben hatte ich Berufswünsche wie Sand am Meer. Von Betonmischwagenfahrer über Musicalstar bis Pilot war alles dabei. Als Favoriten herauskristallisiert haben sich letztendlich Naturwissenschaft und Technik. Dies liegt nicht nur an den fehlenden Gesangskünsten sondern auch ganz viel an jenen Menschen, die mich durch Studium und Leben begleitet haben.

Ganz besonders möchte ich mich bei meiner Professorin Heidrun Gruber-Wölfler und bei Manuel C. Maier für die Betreuung dieser Masterarbeit bedanken. Eure fachlichen und persönlichen Anregungen haben mir beim Verfassen und kontinuierlichen Verbessern dieser Arbeit sehr geholfen. Vielen Dank für die Möglichkeit diese Arbeit durchzuführen, die Geduld während des Schaffens sowie die herzliche Aufnahme in der Arbeitsgruppe. Das angenehme und lustige Verhältnis zu allen CoSy Bros macht jeden Tag zum Vergnügen.

Ein besonderer Dank gilt auch meinen Freunden aus dem Bachelorstudium und der CPE-Task Force. Wir haben es mit viel Kaffee, Teamwork, Nachtschichten und ein, zwei Bier geschafft unser Studium zu bewältigen. Ich bin froh diese schöne Zeit mit euch verbracht zu haben und hoffe auf weitere lustige Jahre mit euch. Besonders hervorheben möchte ich Nika, Eli, Ingrid, Larissa und Sascha. Durch Streicheleinheiten, fachliche Hilfe, tränenreiche Lernnächte und lustige Stunden habt ihr diese Zeit unvergesslich gemacht. Auch die ACFC-Crew hat mein Studium geprägt wofür ich euch, besonders Berni und Tobi, danken möchte.

Eine wichtige Rolle in meinem Grazer Leben spielen meine nicht-Chemie-Freunde. Anti, Chrissi, Christof, Fil, Georg, Janine, Makei, Hannes und noch ganz viele andere. Mit Diskussionen auf unterschiedlichsten Niveaus, unvergesslichen Nächten und Ausflügen habt ihr mir den Studienalltag versüßt. An dieser Stelle möchte ich mich auch bei den Daheimgebliebenen bedanken. Jakob, Luki, Resa, Julia und alle für die hier leider kein Platz mehr ist, dank euch genieße ich jeden Tag in der Heimat. Die Erinnerungen an die Zeit am See, am Berg, in der WunderBAR oder im Urlaub sind unbezahlbar.

Zu guter Letzt möchte ich meinen Eltern und Geschwistern danken. Vielen Dank für die Unterstützung und die Geduld während meines Studiums. Eure Hilfe, ob finanziell, persönlich, durch Verköstigungen oder Taxidienste hat mir dieses Studium ermöglicht. Ihr seid die besten Geschwister der Welt, denn ihr habt mir alle Rechte bei den Eltern erkämpft und wart trotzdem immer für mich da. Herzlichsten Dank, dass ihr euch so gut um euer Nesthäkchen gekümmert habt.

---

# Contents

<b>1</b>	<b>Introduction</b>	<b>1</b>
<b>2</b>	<b>Theoretical Background</b>	<b>3</b>
2.1	Continuous Processes . . . . .	3
2.2	Microreaction Systems . . . . .	5
2.2.1	Design of Microreaction Systems . . . . .	7
2.2.2	Increasing the Production Capacity . . . . .	10
2.3	Fabrication of Microfluidic Devices . . . . .	11
2.3.1	Polydimethylsiloxane - Soft Lithography . . . . .	11
2.3.2	Additive Manufacturing - 3D printing . . . . .	12
2.3.3	Stainless Steel - Selective Laser Melting (SLM) . . . . .	12
2.3.4	Ceramics - Lithography-Based Ceramic Manufacturing (LCM) . . . . .	13
2.4	Mixing in Microfluidic Devices . . . . .	13
2.4.1	Passive Mixing Principles . . . . .	16
2.4.2	Active Mixing Principles . . . . .	19
2.5	Characterisation of Mixing . . . . .	21
2.5.1	Residence Time Distribution (RTD) . . . . .	21
2.5.2	Mixing Sensitive Reactions . . . . .	24
2.6	Model Reaction - Aerobic Oxidation of Grignard Reagents . . . . .	29
2.7	UV/VIS Spectroscopy . . . . .	30
<b>3</b>	<b>Results and Discussion</b>	<b>32</b>
3.1	Description of the 3D printed Microfluidic Devices . . . . .	33
3.2	Macromixing - Residence Time Distribution . . . . .	36
3.2.1	Split-and-Recombine-Reactor . . . . .	37
3.2.2	CSTR-Cascade v1 . . . . .	38
3.3	Micromixing - Mixing Sensitive Reactions . . . . .	40
3.3.1	Calibration of the Dyes . . . . .	41
3.3.2	Passive Mixers . . . . .	44
3.3.3	Active Mixers - CSTR-Cascade . . . . .	47
3.4	Material Influence on the Mixing Performance . . . . .	50
3.5	Optimisation Approaches of the CSTR-Cascade v1 . . . . .	52

---

3.6 Kinetic Measurements in Flow . . . . .	54
<b>4 Conclusion and Outlook</b>	<b>59</b>
<b>5 Experimental</b>	<b>61</b>
5.1 Equipment . . . . .	61
5.2 Preparation of Reagents . . . . .	62
5.3 UV/VIS Calibration of the Dyes . . . . .	64
5.4 Mixing Sensitive Reactions . . . . .	64
5.5 Residence Time Distribution . . . . .	65
<b>6 References</b>	<b>66</b>
<b>7 List of Figures</b>	<b>74</b>
<b>8 List of Tables</b>	<b>79</b>
<b>9 Appendix</b>	<b>80</b>
9.1 Abbreviations and Symbols . . . . .	80
9.2 Substance Data . . . . .	82
9.3 Results Residence Time Distribution . . . . .	83
9.4 Results Mixing Sensitive Reactions . . . . .	85
9.5 List of Chemicals . . . . .	89
9.6 SOP-Residence Time Distribution . . . . .	90
9.7 SOP-Mixing Sensitive Reaction . . . . .	91

---

# 1 Introduction

Pharmaceutical and fine chemical industry usually produce in discontinuous (batch) processes, at multiple production sites as illustrated in Figure 1.1. Batch processes in general are less efficient than continuous ones, but their flexibility and versatility promote the wide use in pharmaceutical industry [1, 3]. The active pharmaceutical ingredient (API) for example, is synthesised usually in Asia and then transported to Europe or USA for the final drug formulation. This procedure causes long production times, inconstant product quality and supply chain disruptions [4, 5]. Production times of more than 200 days from raw material to the final product lead to a loss of \$50 billion a year for the pharmaceutical industry, due to inefficient processes [6]. The U.S. Food and Drug Administration (FDA) has reported more than 200 drug shortages related to batchwise manufacturing over the period 2011-2014 [4, 7]. A promising alternative are continuous processes which received a lot of attention by academic research and industry within the last few years [5, 8]. They are already state of the art in petrochemical industry and food processing. More than ten years ago, the FDA started an initiative encouraging and assisting the pharmaceutical industry to implement continuous manufacturing. In June 2018, the International Council of Harmonisation began to develop work plans and guidelines for continuous manufacturing [9–11]. This confirms the urge of authorities to promote continuous manufacturing in pharmaceutical industry.

Pharmaceutical engineering is highly complex due to a multi-step API synthesis and purification in the primary manufacturing, followed by several unit operations within the secondary manufacturing [8]. Although this leads to a challenging development of fully continuous processes, a compact system which continuously produces drugs from the starting material to the final tablet has been

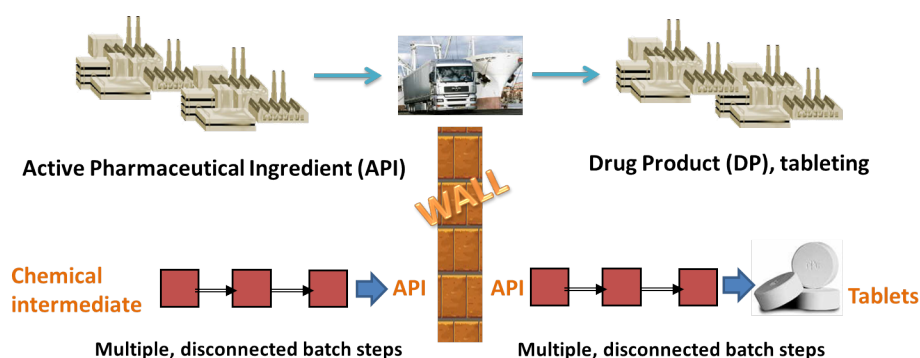


**Figure 1.1:** Illustration of a pharmaceutical production chain with multiple, disconnected batch processes for primary (left) and secondary (right) manufacturing [6].

reported by Adamo et al. in 2015 [4].

Continuous processes run with constant product quality all the time, as long as the parameters of the input material are constant. A steady quality control is done with process analytical technology (PAT), performing time resolved measurements. If the input parameters are changing, the process parameters can be adjusted, allowing a better understanding and control of the process. Advantages of continuous processes are a higher process safety, the ability to work with hazardous or unstable substances and highly exothermic reactions. This opens a field of reactions which was unreliable in traditional batch chemistry. Detailed analyses by Roberge et al. [1] showed that 50% of the reactions in pharmaceutical industry would benefit if they were carried out in flow. In contrast, batch processes suffer from varying product quality, shut down times and heating and cooling phases [3, 8, 12]. A highly promising field in continuous manufacturing are microreactor systems (MRS). Due to their high surface-to-volume ratio, MRS enhance heat and mass transfer which results in a higher process safety. The used small amounts enable the handling of hazardous, explosive or unstable substances and extreme process conditions, which can result in higher selectivity, faster reactions and cost reduction [8, 12–15].

Contrary low flow rates of MRS cause the absence of turbulences, resulting in a diffusion dependent mixing process. Yield and selectivity of chemical reactions are influenced by the flow conditions, if the reaction kinetics are in the time scale of the mixing process. The mixing performance is improved by two approaches, active and passive mixing. While passive mixing is only influenced by the geometry of the mixing structure, active mixing applies external forces to enhance the mixing efficiency [15–20]. To characterise the mixing performance, numerical methods like computational fluid dynamics (CFD) and experimental methods like particle tracking and mixing sensitive reactions are used [14, 21–25]. The low reactor volumes only allow the production of small amounts. This can be compensated by parallelisation of optimised elements, called numbering-up.

The design of MRS was limited to chips made of glass or polymers, with a two dimensional pattern of flow channels. Recent development in additive manufacturing i.e. 3D printing opened completely new possibilities concerning materials and geometry of the devices. By building the structure layer-by-layer, nearly every arbitrary geometry is possible. The use of stainless steel or ceramics increases the resistances against chemicals, temperature and pressure [26–29].

Aim of this thesis is to experimentally characterise 3D printed microfluidic devices made of stainless steel and ceramics, for the usage as more efficient reactor elements in MRS. This characterisation includes evaluation of element mixing capacities by mixing sensitive reactions published by Bourne et al. [2], and residence time distributions (RTD). The influence on the mixing performance and RTD is examined by utilising different reactor materials and their manufacturing method. Based on the obtained information, reactor elements were compared to each other and possible geometry optimisations were made. The characterised reactors can then be used to determine reaction kinetics in flow to later provide necessary data for a detailed reactor design.

---

## 2 Theoretical Background

### 2.1 Continuous Processes

Unit operations can be divided into discontinuous and continuous processes which are illustrated in Figure 2.1. In batch manufacturing all materials are charged before and discharged after processing. In semi-batch some material is added during the process but everything is discharged at the end of processing. In continuous manufacturing charging and discharging is done simultaneously throughout duration of the process [30, 31].

These definitions can be applied to all unit operations either thermal, mechanical or chemical. In petrochemical industry or food processing, continuous manufacturing is already well established. Pharmaceutical companies still produce mostly in batch because of complex multi-step processes and the easy traceability of the final product. Within the last years a promising trend from batch to continuous manufacturing of drugs evolved [3, 8, 9]. Advantages of the batch reactor are the flexibility in operation and low instrumentation costs. Different reactions can be performed by using the same equipment. Disadvantages are the high labor and handling costs, shutdown times and a varying product quality over several batches. Hence batch is well suited to produce small amounts of many different products by using only one piece of equipment [32]. Product analysis is usually done offline between different unit operations, which takes additional time until the result is available. If the intermediate does not meet quality requirements it may be discarded.

In continuous manufacturing the product of one unit operation is directly sent to the next unit operation for further processing. Critical parameters of each process need to fulfill defined quality characteristics. Extending the processing time of single unit operations, to achieve a higher quality, is not possible as it would cause disruptions for the downstream unit operations. As compensation buffers between single processes are used. Continuous manufacturing compared to batch manufacturing needs a higher level of process design to achieve a desired quality [3]. Critical quality attributes are defined, measured and monitored to ensure a product quality within defined limits. Advantages are a better process and quality control by using real time inline measurements leading to a consistent product quality. Scale up is done with dimensionless numbers referred to geometrical, mechanical, thermal and chemical similarity. Many parameters (e.g. heat and mass transfer) are influenced by the reactor size resulting in a challenging scale up. Continuous processes need less manual handling during production which increases the process safety. This reduces costs compared to batch processes [3, 30, 32].

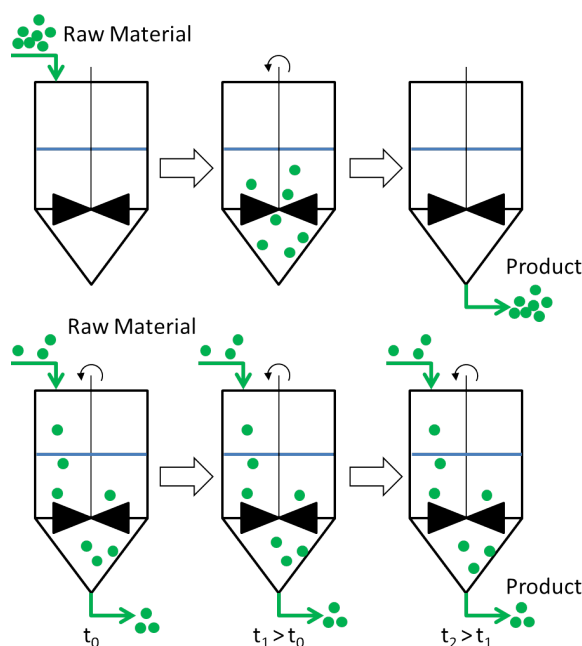


**Figure 2.1:** A simple depiction of batch (top) and continuous (bottom) manufacturing. Adapted from [3].

For reasons mentioned above, authorities and organisations are encouraging companies to switch to continuous manufacturing. It is not yet the state of the art but there is a trend to implement more continuous unit operations in the pharmaceutical industry. Literature studies show that miniaturisation of reactions offers many advantages for organic synthesis, especially for pharmaceutical applications microreactors appear suitable [1, 8–11, 13–16, 30].

### Continuous Organic Synthesis - Challenges

An efficient organic synthesis is a key factor of pharmaceutical or fine chemical production. Goals are fast, selective and cost efficient production of substances with high purity. API synthesis is a highly complex multi-step process consisting of chemical reactions, quenching and purification. This complexity in combination with low production volumes and instability of products favours flexible batch reactors [8, 33]. However, the mentioned advantages of continuous processes lead to a growing number of scientists who investigate continuous organic synthesis.

Roberge et al. [1] proposed that 50% of reactions in the pharmaceutical industry would benefit from continuous processes, especially when carried out in micro scale. Focusing on small scale continuous technology using MRS, special challenges concerning process- and equipment design occur. Firstly to mention is the material and fabrication technique of MRS. So far, most microreactors are chips made of polydimethylsiloxane (PDMS) manufactured by soft lithography. This technique is limited to 2D geometries. The low compatibility with organic solvents is the main limitation of PDMS. The application of high temperatures and pressures is hindered due to the low mechanical

strength [26, 34].

Another challenge is referred to mass transfer MRS. Reactions at micro scale suffer from diffusion dependent mixing, because the low flow rates imply low Reynolds numbers, which indicate the absence of turbulences. The resulting laminar flow profile makes mixing mostly dependent on molecular diffusion which is a rather slow process [14, 17].

Heterogeneous reactions, like gas-liquid reactions, benefit from the enhanced mass transfer in micro scale due to the higher surface-to-volume ratio [35, 36].

To run a continuous process with predefined quality requirements, a time resolved analysis of the critical quality parameters is necessary. PAT is defined as a tool to design, analyse and control manufacturing through time resolved measurements. This includes physical, chemical and biological methods as well as data acquisition and analysis. Although the analysis of a whole process is challenging, it opens the opportunity for better understanding and control of manufacturing processes [37].

## 2.2 Microreaction Systems

Ever since chemists work in their laboratories, they perform reactions in round-bottom flasks using several milligrammes to grammes of their starting material. Optimisation of the reaction parameters consumes a lot of energy, time and material, until scale up leads to new challenges. To overcome these problems, continuous flow with MRS came up as an alternative. MRS include all necessary equipment to run a process like micro heat exchanger, micro absorber, pumps and others. Over the past years, MRS have evolved from simple chips to highly complex multi-step synthesis devices. MRS are mostly present in academic research and engineering applications but also biological research has shown an increasing adoption [13, 16, 33, 38].

Roberge et al. [1] analysed 86 reactions in pharmaceutical and fine chemical industry and proposed to divide reactions into three classes, depending on their kinetics and if continuous manufacturing would be beneficial:

- **Type A** reactions are very fast (half life <1 s) which are usually mixing controlled because the reaction is much faster than mixing. To ensure a good temperature control, a highly efficient heat transfer is necessary. Reactive species like halogens and amides as well as organometallic reactions are included in this group.
- **Type B** reactions are kinetics controlled and usually occur between 1 s and 10 s. Here mixing is not critical and scale up issues can be prevented by using the same surface area to volume ratio. Microstructures would improve the heat transfer for these reactions.
- **Type C** reactions suit well for batch processes according to their kinetics. Continuous processing would increase the product quality and reduce safety risks.

In general, hazardous chemicals or autocatalytic reactions would benefit from continuous processes because the reduced volume also reduces the danger. Significant cost savings can be expected either due to a higher yield or cost reduction due to lower labor costs. Additionally MRS could provide new pathways such as hazardous reactions and solvent free reactions [39]. Based on Roberge's studies, 50 % of the reactions would benefit if they were carried out continuously, especially in MRS. Unfortunately 60 % of these cannot be done in flow due to problems with solids [1].

Microfluidic devices are defined as devices with fluidic channels with a characteristic length scale of 10  $\mu\text{m}$  to 1 mm. A clear distinction between microreactor and micromixer is not possible because mixing and reaction act simultaneously due to high reaction rates. MRS offer a variety of advantages compared to standard batch equipment. Obviously less space, material and energy is needed for the equipment. The small channel diameters lead to a high surface-to-volume ratio which directly increases the effective exchange surface for heat and mass transfer. These transfer processes take place at the phase boundaries. With a high specific surface area, transport rates are increased and the equilibrium is reached faster. The surface-to-volume ratio is inverse proportional to the characteristic length of the object. The smaller the channel gets, the larger grows the effective area for transport processes [37]. Table 2.1 gives approximate values of the surface-to-volume ratio for different reactor types [5]. The low volume in combination with the high effective exchange surface

**Table 2.1:** Surface-to-volume ratios for various reactors. Calculated for half filled round-bottom flasks with static liquid. Adapted from [5].

Type of reactor	Surface-to-volume ratio [ $\text{m}^2\text{m}^{-3}$ ]
250 mL round-bottom flask	38
50 mL round-bottom flask	66
5 mL round-bottom flask	141
tube reactors	50 - 2000
gas-liquid microchannel	3400 - 18000

results in shorter response time and simpler process control. For example in huge batch reactors it is nearly impossible to keep a highly exothermic reaction at isothermal condition. The temperature is not homogeneously distributed, resulting in hot spots which promote different reaction rates. This is no problem with MRS due to the enhanced heat and mass transfer. The reduction of the active volume reduces the risk of hazardous reactants. An MRS can thus practically increase the safe operation of runaway reactions or explosive gas regimes [8, 12–15, 40].

Small channel diameters also allow the application of extreme process conditions for process intensification, known as novel process windows (NPW). Thereby mentioned are high temperature and pressure, reactions with high concentrations or solvent free reactions. Small channels resist high

pressure because of the low surface area [8, 41].

Thinking about sustainability, MRS are a promising route to green chemistry which is proven by a wide range of studied applications and concepts. NPW and small amounts of chemicals used for experiments are preventing waste production. Compared to batch processes, no heating up and cooling phases are necessary, reducing the energy demand. Microwave technology reduces the reaction time. The photon-flux for photochemical reactions is increased resulting in higher energy efficiency compared to classical batch reactors [8, 12, 13, 42].

Not only the energy demand is reduced, also the yield and selectivity of many reactions is improved using microfluidic devices, resulting in a win-win situation. This is usually correlated with the increased heat and mass transfer and the intensified process conditions. An impressive example is the condensation of *o*-phenylenediamine with acetic acid, where the time until full conversion was reduced from nine weeks to just 30 s using high temperature, pressure and microwave technology [41, 43]. Also multi-step reactions including purification and quenching steps have been reported [8, 12, 16, 33].

Unfortunately there are also challenges in microreactor technology. There is a lack of equipment suppliers for micro applications especially concerning inline analysis tools or pumps, but the situation is getting better. Handling of solids is one of the biggest challenges. If precipitation inside the microreactor channel takes place, it will be blocked. Slow reactions are not suitable for microreactors as they would need high volumes which are hard to realise. The choice, if batch or MRS is the better process management, depends on different parameters, demonstrated in reaction type A-D by Roberge et al. [1, 9, 12, 15, 17].

## 2.2.1 Design of Microreaction Systems

### General Set-up

In Figure 2.2 a standard set-up of an MRS is depicted. A fluid and reagent delivery system is needed to feed the exact reagent amounts into the system. This can be liquids or gases whereby pumps or mass flow controllers (MFC) are used respectively. Depending on the solvent, pressure and flow rate, either piston pumps, syringe pumps or peristaltic pumps are used [5]. In the next zone the reagents are mixed and the chemical reaction starts before entering the reactor unit. Optionally the reagents can be pre-tempered prior mixing or reaction zone. In the reaction zone the chemical reaction takes place and the module is connected to the quenching unit. This ensures accurate control of the residence time [5]. To ensure a constant system pressure, a back pressure regulator (BPR) is connected prior to sampling. Elevated pressures allow the performance of reactions above the boiling point of the reaction media. When working with gaseous or volatile substances a BPR is necessary for reproducibility since pressure deviations lead to generation or absorption or formation of gaseous bubbles. Fixed and adjustable BPRs are used and in general they do not measure the actual pressure [5]. Purification and analysis units can be implemented additionally. It is noticeable

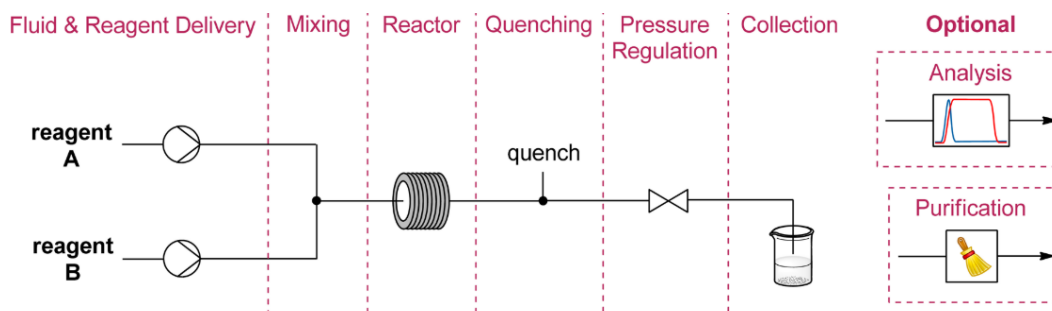


**Figure 2.2:** Zones of a standard two feed microfluidic system. The modules can be used repetitively and interchangeably to enlarge the system [5].

that all these modules are interchangeable and can be used repetitively. This enables an infinite number of configurations to perform highly complex syntheses [5, 12]. Connection of the zones is realised with standard HPLC connectors and tubings. The wetted parts are made of perfluorinated polymers (PFA, PEEK, PTFE and FEP) or stainless steel, depending on pressure, solvent and other parameters [5].

### Design of Microfluidic Devices

Accurate reactor design is strongly dependent on the knowledge about reaction kinetics. This information is only valuable if it captures the intrinsic kinetics without any limitations due to heat and mass transfer, which is challenging for very fast reactions [44].

A commonly used dimensionless number in microfluidic technology is the Reynolds number. It represents the ratio of inertia forces over viscous forces and is defined as:

$$Re = \frac{u \cdot L_{char}}{\nu} = \frac{u \cdot L_{char} \cdot \rho}{\eta} \quad (2.1)$$

Here  $u$  is the fluid velocity,  $L_{char}$  is the characteristic length, i.e. the hydraulic diameter  $d_h$ ,  $\nu$  and  $\eta$  are the kinematic and dynamic viscosity and  $\rho$  is the density of the fluid. For flow in pipes, above a critical value of approximately  $Re \approx 2300$  turbulent flow occurs at the macro scale. Small channel diameters and low volumetric flow rates in MRS lead to Reynolds numbers between 0.1 and 1000 resulting in a laminar flow profile [14, 17]. Low Reynolds numbers imply that viscous forces are dominating over inertia forces, minimizing turbulences which would be beneficial for mixing effects [17, 45].

Hessel [46] published a five step methodology for dimensioning and layout of MRS: In **step 1** the channel diameter  $d$  is designed which plays a crucial role for heat and mass transfer. The required channel diameter, depending on the reaction kinetics and heat generation of the reaction is depicted in Figure 2.3. A small channel diameter reduces the mixing length and mixing time. The time scales of heat and mass transfer should be smaller than the time scale for mixing. Additionally the adiabatic temperature rise of the reaction has to be taken into account, in order to avoid hot spot

formations by too wide channels [46]. Contrary, very narrow channels induce a prohibitive pressure drop  $\Delta p$  (equation 2.2), increasing the energy demand and costs of pumps.

$$\Delta p = \lambda_f \cdot \frac{l \cdot \rho}{d \cdot 2} \cdot u^2 \quad (2.2)$$

For laminar flow in circular channels, the channel friction factor is defined as  $\lambda_f = C_f/Re = 64/Re$  with the Reynolds number  $Re$  being defined in equation 2.1. The pressure drop determines mixing and transport phenomena which are described by the energy dissipation rate  $\varepsilon_{diss}$ . This is a measure for the interface generation between components based on vortex generation [14]:

$$\varepsilon_{diss} = \frac{\Delta p \cdot u}{\rho \cdot \Delta l} \quad (2.3)$$

The pressure drop is also influenced by the channel length which is dimensioned in **step 2**. To ensure a full reaction within the reactor, the mean residence time  $t_{res}$  needs to be higher than the reaction time. From the channel diameter  $d$  and the volumetric flow rate  $Q$  the flow velocity  $u$  is defined:

$$u = \frac{Q}{A} = \frac{4 \cdot Q}{d^2 \cdot \pi} \quad (2.4)$$

By knowledge of the reaction time, the residence time in the micro channel is given and via  $t_{res} = l/u$  connected with the length of the channel  $l$ . The derived channel dimension can again lead to an elevated pressure drop. It should be focused on a compromise between a narrow RTD and a low pressure drop [14, 46]. In **step 3** the thickness of channel walls is determined. In order to ensure isothermal conditions, the channel walls need to provide sufficient heat transfer, especially for exothermic reactions. To avoid unwanted temperature gradients the time scale for heat conduction in the channel walls should be lower than the residence time of the fluid. In general the ratio of generated heat by reaction and removed heat should be lower than one [44, 46].

After the channel dimensions are fixed, **step 4** determines the number of flow channels to ensure the required production capacity. In production applications the number of channels is given by the total production amount. In research applications a small number of channels might be preferable, because analysis can be more difficult for a high number of channels [46].

In the last **step 5** the layout of a flow distribution system, for feeding the starting material to the different channels, is designed. Major requirements are an equal distribution to all channels and a narrow RTD [46].

Another useful tool to design hydraulic diameter  $d_h$ , length  $l$  and cross sectional area  $A$  are transport phenomena described by Damkohler numbers. Damkohler numbers can be used in step one to three of the design methodology. These dimensionless numbers represent ratios of different time

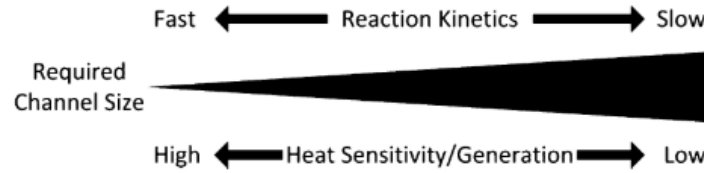


**Figure 2.3:** Illustration of the required channel diameter depending on the reaction kinetics and the heat sensitivity/generation of the reaction [47].

scales for a satisfactory performance and are given in equations 2.5, 2.6 and 2.7 [47, 48].

$$Da_I = \frac{\text{residence time}}{\text{time for consumption}} = k_r \cdot c^{n-1} \cdot \frac{V_R}{Q} > 1 \quad (2.5)$$

$$Da_{II} = \frac{\text{mixing time}}{\text{time for consumption}} = t_m \cdot k_r \cdot c^{n-1} < 1 \quad (2.6)$$

$$Da_{IV} = \frac{\text{rate of heat generation}}{\text{rate of heat removal}} = k_r \cdot c^n \cdot \Delta H_r \cdot \frac{4 \cdot \rho \cdot d_h}{U_t \cdot \Delta T_w} < 1 \quad (2.7)$$

Here  $k_r$  is the reaction rate constant,  $n$  the order of the reaction,  $V_R$  the reactor volume,  $t_m$  the mixing time,  $\Delta H_r$  is the heat of reaction,  $U_t$  is the overall heat transfer coefficient and  $\Delta T_w$  is the fluid-to-wall temperature difference. The Damkohler numbers can be explained the following way [48]:

- $Da_I > 1$  for complete reaction within the channel.
- $Da_{II} < 1$  for sufficient fast mixing and radial mass transfer.
- $Da_{IV} < 1$  for sufficient heat transfer in the channel. In practical applications often  $Da_{IV} < 0.2$  is chosen.

## 2.2.2 Increasing the Production Capacity

The small size of microfluidics imply a low volume and low production capacities. There are three ways to increase the production capacity of continuous processes [49]:

- **Scale-up** is defined as increasing the reactor size.
- **Numbering-up** is the parallelisation of multiple identical reactors or channels.
- **Scale-out** is running a reaction for a longer period of time.

In MRS numbering-up and scale-out are the favoured methods. Numbering-up means that a microfluidic device is used multiple times in parallel. The devices are combined with a flow splitting unit, ensuring equal flow rates to the reactors. This concept is known as external numbering-up. The other concept named 'internal numbering-up' is the connection of functional elements (e.g. channels) instead of complete devices. These elements are put together in a stack and fed via a special designed

distribution unit. Internal numbering-up benefits of its compact structure and is advantageous for a high degree of parallelisation. External numbering-up preserves all transport processes and is useful for multiphase reactions. However it is chosen for simple, practical reasons if the degree of parallelism is low [46].

## 2.3 Fabrication of Microfluidic Devices

The choice of a suitable fabrication technique is depending on many different parameters [37]. Several tasks concerning the demands on the device (accuracy, dimensions, special design), demands on the material (chemical, thermal or mechanical resistance) and demands on the fabrication technique are factors of the manufacturing process [37]. Driven by these parameters the optimum for the desired application should be found. Originally, microfluidics were made of silicon and glass but then the focus shifted to polymers like PDMS, because of the low price and easy fabrication. Nowadays a huge variety of materials can be used including different polymers, metals, ceramics, silicon and glass [28, 37, 50]. The most important factors for the choice of material are resistance against temperature, pressure and corrosion as well as the thermal properties [37]. This includes heat transfer properties which are very important for highly exothermic or endothermic reactions.

So far, microfluidics used in academic research and laboratories are mostly fabricated from PDMS by using soft lithography [8, 34, 50]. The focus of this thesis is on microreactors made of stainless steel and ceramics. Metal reactors were fabricated using selective laser melting (SLM) while the ceramic ones used lithography-based ceramic manufacturing (LCM). These are additive manufacturing techniques, i.e. 3D printing which open the possibility to produce nearly every imaginable structure.

### 2.3.1 Polydimethylsiloxane - Soft Lithography

PDMS is a polymer belonging to a group of organosilicon compounds. Soft lithography is a technology based on molding of an elastomer, giving inexpensive polymeric devices. This means that a structure is replicated using stamps, molds or masks [34]. However, soft lithography is limited to 2D objects. The production of 3D objects is possible by stacking multiple layers together but this increases fabrication steps and time [8, 50]. Advantages of PDMS are the low price and easy fabrication of 2D chips and the well suited physicochemical properties for biomedical and physical science applications. The optical clarity of the material makes PDMS suitable for optical analysis [28, 50]. Reactors made of PDMS found limited application in organic synthesis. This is due to their low chemical compatibility with organic solvents demonstrated by swelling with nonpolar solvents. Furthermore, the low temperature stability and mechanical strength prohibit the use of high temperatures and pressures [26, 34, 51].

### 2.3.2 Additive Manufacturing - 3D printing

Additive manufacturing is an upcoming technology in chemical reaction engineering. The main advantage of 3D printing is that objects are manufactured layer-by-layer under precise digital control. This makes nearly every arbitrary structure possible as the layer thickness can go down to a few micrometers. 3D printing benefits from the digital approach of CAD design. The files can be easily shared or edited with collaborators. Computational methods allow fast prediction and analysis of mechanical or flow properties. The variety of possible structures is especially for reactor design beneficial. Highly complex mixing structures are possible to create, which were not accessible with classical methods. Also complete reactors including all modules mentioned in section 2.2.1 (multiple inlets, cooling, heating, quenching or analysis) are possible to fabricate in one step. Additive manufacturing allows the realisation of parts, within a short time period and rapid optimisation of the designed geometry. Parts produced by rapid prototyping method are found in aerospace, biomedical implants and prostheses as well as chemical microreactors. Concerning economics 3D printing is favored for low- and mid-scale productions [26–29, 50, 52, 53].

### 2.3.3 Stainless Steel - Selective Laser Melting (SLM)

SLM is a powerful additive manufacturing technique where an increasing number of materials can be used, including aluminium, copper, stainless steel, hastelloy, tantalum and tungsten [26, 52]. In contrast to PDMS, these materials provide heat conductivity, thermal resistance, mechanical strength and are chemical compatible with most organic solvents, providing a well suited material for organic synthesis [26, 27, 52].

SLM is a powder-based 3D printing process of a pure metal alloy, where the particles are fully melted. In selective laser sintering (SLS) the precursor is not fully melted, but heated to a point where the powder is fused together, called sintering [28]. A scheme of the process is depicted in Figure 2.4. The geometry is designed in a CAD-file and then sliced with another software to generate cross-sectional layers. A high energy laser beam scans over the surface of a powder bed and thereby selectively melts the powder of a layer defined by the sliced CAD-file. In a next step the powder bed is lowered by a defined height and a new powder bed is deposited above the previous layer and again selectively melted, thereby building up a 3D structure layer-by-layer. Except of some post-processing steps SLM/SLM is mostly automatable [28, 37, 52, 53]. Unused powder is blown off with compressed air and can be recycled after sieving it. Parameters like the laser beam power, laser spot size, particle size, scanning speed and layer thickness affect the SLM process [53]. The achievable wall thickness is defined by the laser spot size which is between 0.3 and 0.7 mm. Parts manufactured by SLM suffer from a certain surface roughness which has considerable effects in the design of microfluidics. [27, 52, 53].

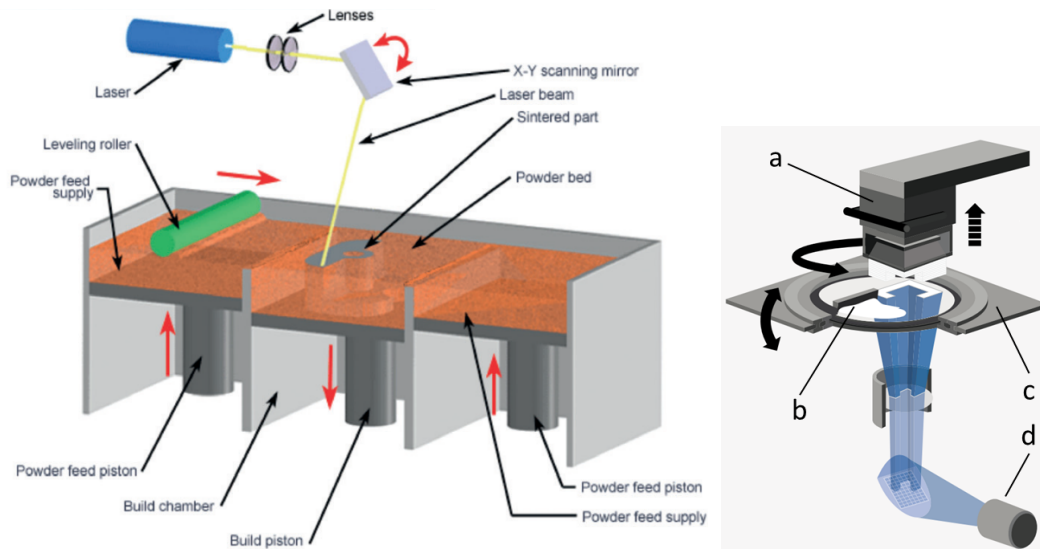


**Figure 2.4:** Left: Scheme of the selective laser melting/sintering (SLM/SLS) manufacturing process. SLS sinters the material together while SLM uses the laser to achieve a full melt of the material [28]. Right: Scheme of the lithography-based ceramic manufacturing (LCM) technique. a) building platform, b) wiper blade, c) vat, d) light source. Adapted from [54].

### 2.3.4 Ceramics - Lithography-Based Ceramic Manufacturing (LCM)

Ceramics are a promising material for chemical reactions with aggressive reactants at elevated temperatures because of their high thermal and chemical stability. This qualifies ceramics for applications which are not covered by metals or polymers. The mechanical strength is high but ceramics are very brittle. The properties of the final product do not only depend on the material, they are also influenced by the fabrication process [37, 55]. The lithography-based ceramic manufacturing technique is used for reactor production in this thesis and depicted in Figure 2.4. Aluminium oxide is dispersed in a photo-sensitive matrix consisting of photo initiator, monomers and additives giving a slurry as precursor. The slurry is exposed to light from the bottom and thereby the monomers start a polymerisation reaction giving a solid structure on the building platform. Then the building platform is lifted up and a rotating vat applies fresh slurry. The building platform dips again into the slurry and light is applied, generating the next layer. This is done layer-by-layer until the structure is finished. The polymer defines the structure with ceramic particles being encapsulated, giving the green body. This object is heat treated to remove the polymer and then sintered to give the final ceramic object [56, 57].

## 2.4 Mixing in Microfluidic Devices

In general, mixing is a process of homogenisation of two or more substances and occurs at three different scales [58–60]:

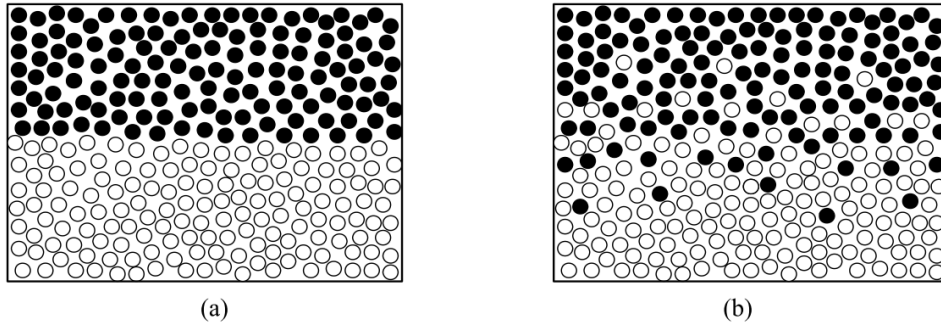


**Figure 2.5:** Illustration of the exchange of molecules through an interfacial area by molecular diffusion: a) initial conditions with complete separation of two fluids; b) random state during diffusion process [62].

- **Macromixing** is driven by the largest scales of motion in the fluid. It refers to mean concentration and concentration distribution over the reactor.
- **Micromixing** is mixing on the smallest scales of motion and at the scales of molecular diffusion. As described by Roberge et al. [1] this is the limiting step of the very fast type A reactions.
- **Mesomixing** is described as the mixing behaviour at a smaller scale than macromixing but on a larger scale than micromixing where molecular diffusion becomes important.

Suppose two miscible liquids are present in one container and the aim is to homogeneously mix both substances. In the region near the interface both substances have different properties leading to random molecular motion and permeation of each fluid into one another. This motion is called diffusion and is illustrated in Figure 2.5. It only takes place through the interfacial area and continuous diffusion over sufficient long time leads to complete homogenisation of both fluids. This homogenisation forces the diffusion to occur slower because the concentration gradients are decreased. This effect is described by Fick's law giving the proportional constant, the molecular diffusion [21, 61, 62].

Two dimensionless numbers, the Reynolds number ( $Re$ , equation 2.1) and the Peclet number ( $Pe$ , equation 2.8) are commonly used to characterise mixing in microfluidics [16, 17, 45]. Introducing the Peclet number gives the ratio of mass transport due to convection and mass transport referred to diffusion and is given as:

$$Pe = \frac{u \cdot L_{char}}{D_{mol}} \quad (2.8)$$

Where  $u$  is the fluid velocity,  $L_{char}$  is the characteristic length, i.e. the length of the mixing path and  $D_{mol}$  is the molecular diffusion coefficient. Low Peclet numbers, which are usual in MRS, indicate that mixing is highly dependent on diffusion effects. Diffusive mixing occurs at much slower rates than time scales associated with fluid motion. This implies that complete mixing by diffusion takes an unacceptable long residence time when talking about continuous reactors [18, 22, 63, 64]. As mentioned, diffusive mixing only takes place at the interface between two fluids. Considering fast reactions, where the reaction rate is higher than the mixing rate, reactions already started before full



**Figure 2.6:** Illustration of the effect of multilamination of streams. The interfacial area is increased and at the same time the diffusion path length is decreased leading to an enhanced mixing efficiency. Adapted from [62].

homogenisation took place, which is disadvantageous for organic syntheses. This does not only affect the overall reaction time, it also promotes unfavoured side reactions resulting in a lower yield of the desired product. This wastes raw materials and complicates downstream work-up processes. So it is crucial to develop highly efficient and fast mixers in order to optimise MRS [18, 21, 23]. As diffusion only takes place at the interface between fluids, manipulation of the mixing rate can be done by increasing the interfacial area and in parallel minimising the diffusion path length, as illustrated in Figure 2.6. This is induced by multilamination of the streams or chaotic mixing [21, 45, 62, 64]. Another possibility is the use of elevated temperatures to enhance diffusion. However, this is limited by the chemical stability and other parameters of the process.

Mixing in microfluidic devices can be divided into two major categories, active and passive mixing. Passive mixing is achieved by changing the geometries, orientation or arrangement of fluid channels using obstacles or split-and-recombine (SAR) approaches. Passive mixing elements are integrated during fabrication of the microfluidic device. The main advantage is that there are no moving parts and no additional energy input is necessary, simplifying operation and production. However, the mixing performance is defined by the geometry and can only be adjusted by changing the flow rate. Active mixing is achieved by an additional energy input using stirring, pressure gradients or other techniques. A clear benefit is the high variability of operation conditions and the possibility to increase the mixing performance even at low flow rates. Contrary an additional energy input is necessary and moving parts can lead to troubles [16–18, 20, 25, 62, 63, 65–67]. Hessel [20] and Nguyen [67] classified different mixing approaches which are illustrated in Figure 2.7.

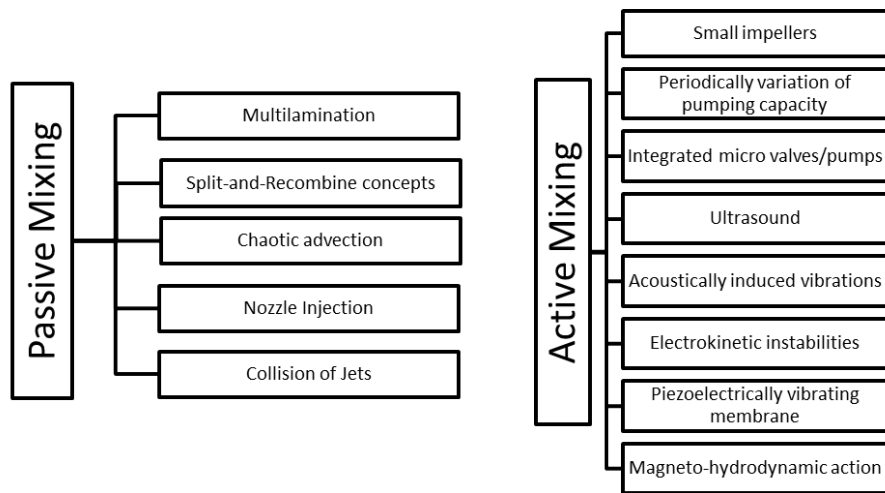


**Figure 2.7:** Examples of active and passive mixing approaches. Active mixing is induced by external forces and passive mixing solely uses the mixer geometry [20, 67].

### 2.4.1 Passive Mixing Principles

Passive mixing is induced by forcing the fluid through small channels or by clever alternations of channels walls. Thereby the interfacial area is increased and the diffusion path length is decreased, resulting in an enhanced mixing performance.

#### Homogeneous Systems

In the basic case, two streams are combined and go on in one channel which is usually done with a basic T-mixer or Y-mixer as depicted in Figure 2.8a,b. At laminar flow, the two streams flow side by side of each other and mixing only takes place by diffusion, thus is very slow. At high flow rates turbulences are induced leading to a better mixing performance. Wang et al. [68] illustrated this scenario with the use of  $\mu$ -LIF-experiments (micro laser induced fluorescence) as shown in Figure 2.8. The mixing efficiency can be improved by roughening of the channel wall or throttling of the channel entrance [20, 67]. A simple way to reduce the diffusion path length is to force the fluid stream through multiple tiny channels which is called lamination as seen in Figure 2.8c. The increased contact surface leads to a better performance but the pressure drop is increased. This miniaturisation of channels is limited by the fabrication technology of the device [20, 45, 65, 67]. Another concept is hydrodynamic focusing which reduces the stream width and as a result the Reynolds number is increased and the diffusion path length is reduced. As seen in Figure 2.8d the middle stream is a sample stream and solvent streams from the other two inlets work as sheath flow [20, 67].

Another approach for passive mixing is the SAR method. Lamination and chaotic advection contribute the most to this type of mixing process. Basically three steps are necessary, flow splitting, flow recombination and flow rearrangement [20]. The exact structure of SAR-mixers differs in the

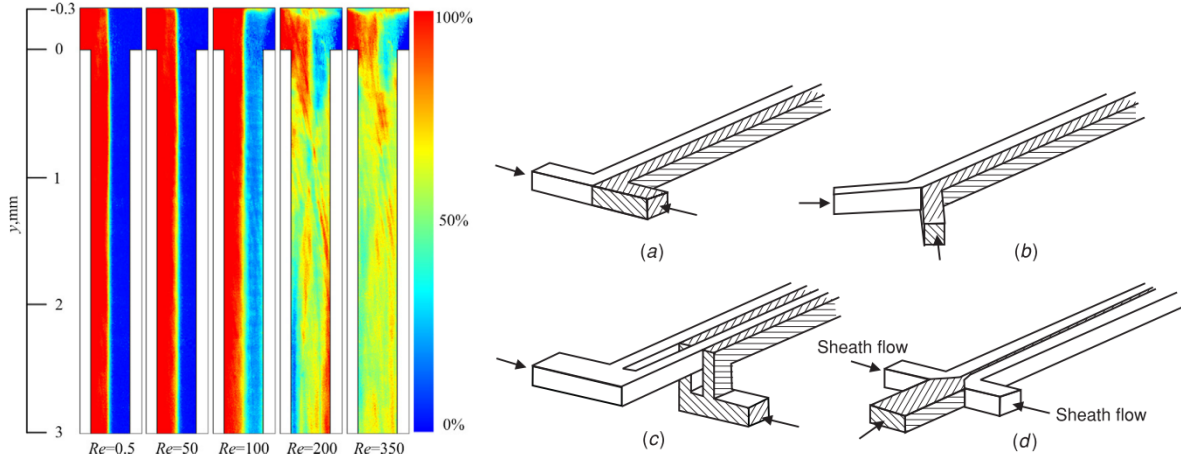


**Figure 2.8:** Left: Colored experimental  $\mu$ -LIF results for increasing  $Re$  numbers (from left to right) for a T-mixer. Pure red denotes 100 % liquid A and pure blue denotes 0 % [68]. Right: Schematic illustration of basic passive mixer designs: a) T-mixer, b) Y-mixer, c) concept of parallel lamination and d) concept of hydrodynamic focusing [67].

arrangement of the streams. Basically the principle of SAR-mixers is similar to the multi-lamination method. Kim et al. [69] designed, simulated and fabricated an F-shaped micromixer which achieved fast mixing (Figure 2.9 left). Hardt et al. [70] reported experimental and simulation results of the mixing performance of a SAR-mixer with a chain-like structure (Figure 2.9 right). Splitting and recombining streams is more effective than diffusion of two streams, but it still appears slowly especially at low Reynolds numbers [17].

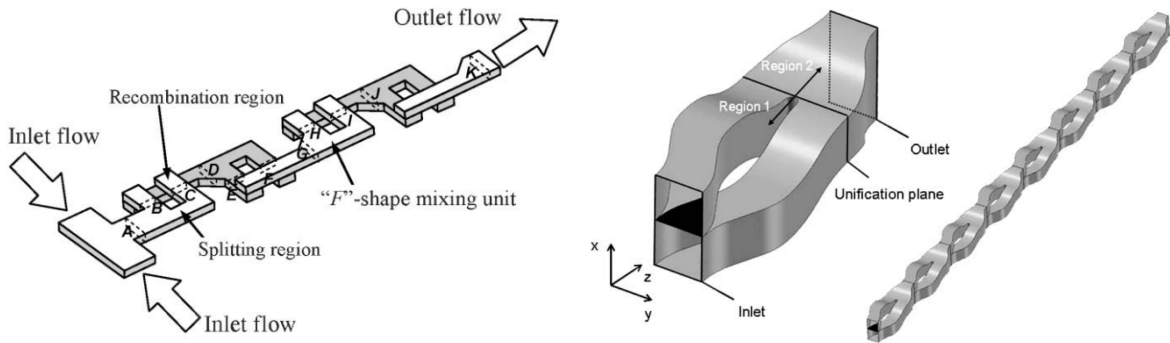


**Figure 2.9:** Examples of SAR-mixers: Left: F-shaped SAR concept published by Kim et al. [69]; Right: Chain-like SAR concept published by Hardt et al. [70].

Besides diffusion, chaotic advection is also a promising principle to improve the mixing efficiency. It is defined as the splitting, stretching, folding and breaking of the flow by internal elements but can also be induced by external forces [37, 67]. This increases the interfacial area by forming recirculation or eddies in the flow regime [20, 65]. The fabrication of highly complex structures is possible

due to achievements in additive manufacturing and other fabrication techniques. Many structures were investigated and promising flow configurations for different Reynolds numbers were found [67]. At  $Re > 200$  the asymmetric arrangement of obstacles in the channel or at the wall improves the mixing efficiency significantly. Also zig-zag-arrangements are well suited because they produce recirculation around the turns [67]. A scheme of the arrangement is illustrated in Figure 2.10 (left). A famous mixer for intermediate Reynolds numbers  $10 < Re < 100$  is the staggered herringbone micromixer published by Stroock et al. [20, 71]. The asymmetric arrangement of obstacles on one side of the channel influences the whole flow pattern and produces large and small vortices, as depicted in Figure 2.10 (right). This micromixer achieves very good mixing [17, 20, 37, 67].

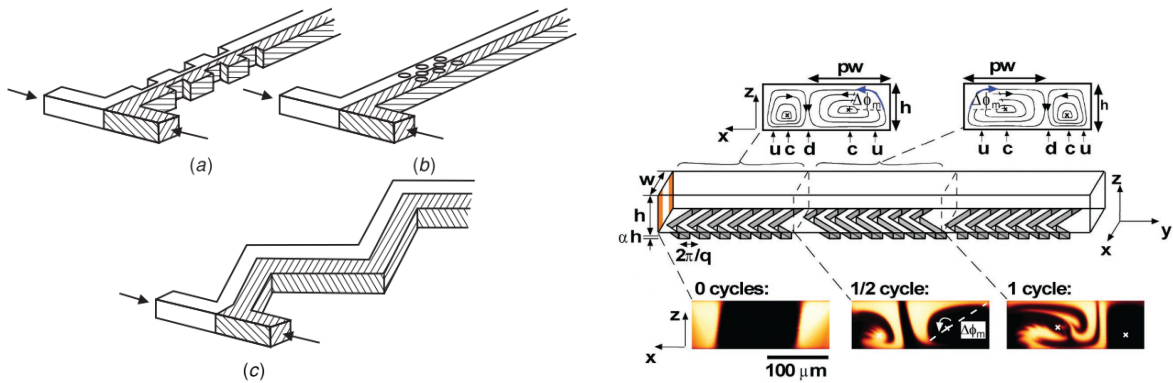


**Figure 2.10:** Examples for chaotic advection: Left: At high Reynolds numbers obstacles at the wall (a), in the channel (b) or zig-zag arrangements (c) showed good mixing performance [67]; Right: Scheme of the staggered herringbone micromixer and the produced vortices [71].

## Heterogeneous Systems

Mixing is also crucial for multiphase systems consisting of immiscible liquids or gases and liquids because a high interfacial area is desired. Song et al. [72] studied a multiphase system with droplets transported by a carrier fluid. They formed droplets consisting of three fluids within an immiscible carrier fluid as depicted in Figure 2.11. While flowing through winding channels, shearing of the droplet with the channel wall caused chaotic advection inside the droplets [17, 72]. With this approach no dispersion of the reactive liquids was achieved and each droplet is comparable with a tiny batch reactor. Afterwards, separation of the immiscible liquids is simple done by a capillary separator and so the product is a single phase [17, 73].

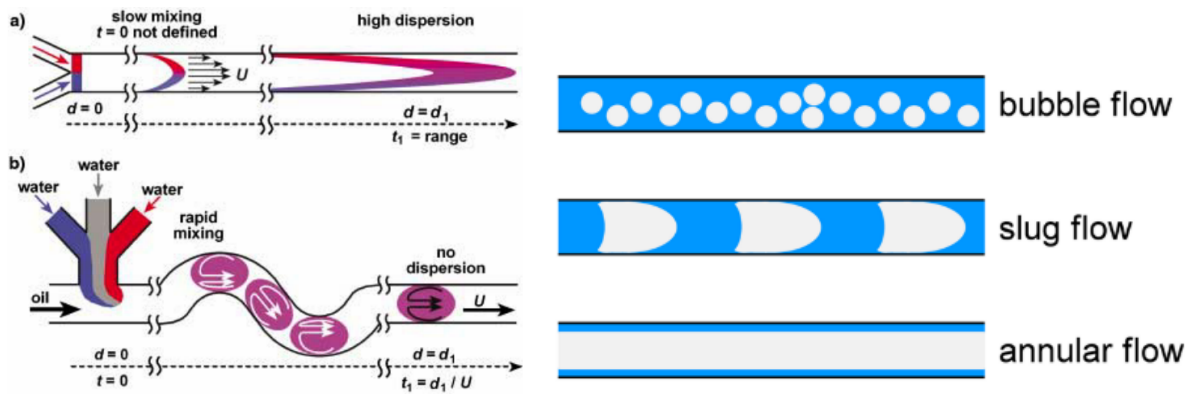


**Figure 2.11:** Left: a) Scheme of two inlets in a standard micro channel with slow mixing and high dispersion. b) Proposed multiphase micromixer with efficient mixing inside the droplets [72]. Right: Illustration of different gas-liquid flow regimes in microstructures. The gas flow rate increases from top to bottom [5].

Heterogeneous systems include gas-liquid and liquid-liquid regimes. Three different flow regimes called bubble flow, slug flow or annular flow (Figure 2.11 right) are obtained, depending on the superficial velocity of both phases [5, 73–75]. In bubble flow and slug flow gas bubbles are located between liquid segments. Bubble flow has bubbles smaller than the channel diameter. Slug flow is most common in microchannels and has bubbles which are longer than the channel diameter [36]. In annular flow, a steady gas channel is in the core of the channel with a thin liquid film at the channel walls [36, 75]. If the gas phase is a reactive component mass transfer between both phases is of major importance. A chemical reaction can take place in the major liquid body and in the film between the two phases. This effects between two phases on the reaction rate can be described by the Hatta Modulus, described in [32]. Many parameters like Henry's law constant, the rate constants in each phase as well as the concentration ratio between the phases affect the Hatta modulus. A possibility to describe the conditions in this complex system is the two film model. Continuous flow in microfluidics is advantageous and increases the surface-to-volume ratio significantly as seen in Table 2.1 - this enhances the mass transfer which can be rate limiting [5, 36]. Detailed information is given by Levenspiel et. al. [32].

## 2.4.2 Active Mixing Principles

Active mixing, compared to passive mixing, offers a variety of additional possibilities to control the degree of mixing. This is achieved by the use of external forces like pressure, ultrasonic, electromagnetic fields or other technologies. This goes hand in hand with a complex fabrication technique and additional costs, due to moving parts and energy demand [16, 20, 44, 65].

Mixing with stirring bars or impellers is the most common way in laboratory or industrial scale. Micro stirrers were fabricated and investigated by Lu et al. [76]. Mixing is enhanced by a micro impeller which acts in a rotating magnetic field causing turbulences in the fluid. The use of multiple micro impeller showed fast mixing within a channel or a mixing chamber. The mixing efficiency

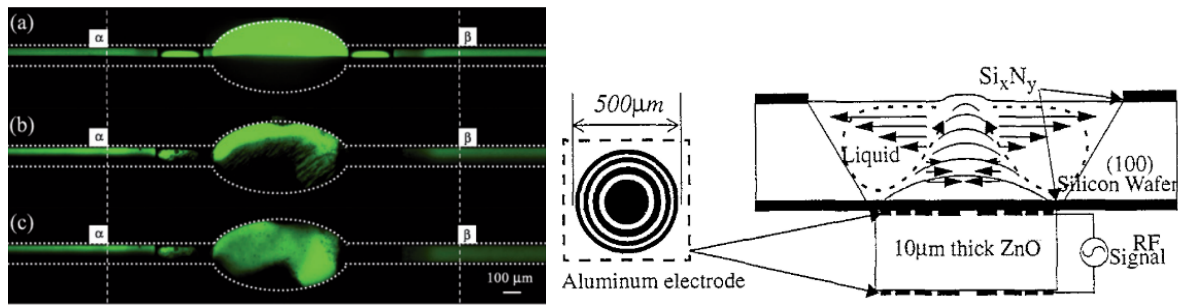


**Figure 2.12:** Left: Fluorescence micrographs of a fluorescent and a non-fluorescent stream in a mixing chamber: a) Chamber without particles shows no mixing enhancement, i.e. diffusive mixing. b) Non-rotating magnetic particles in the chamber lead to enhanced but incomplete mixing. c) Mixing chamber with rotating particles generates efficient mixing. Adapted from [77]. Right: Scheme of an acoustically driven micromixer published by Zhu et al. [78].

increased with the rotational speed [20, 76]. Far away from the stirrer, mixing enhancement is bad. To overcome this problem, stirrer and microfluidic device are designed in a way that the diameters of stirrer and chamber are nearly of the same size and by the use of multiple stirrers [17]. Lee et al. [77] published a magnetic mixing enhancement method, using magnetic particles which act as stirring bars inside a mixing chamber. This configuration showed efficient mixing enhancement as depicted in Figure 2.12.

Acoustic waves have also been used for enhancement of micromixing [17, 20]. A mixing chamber with a zinc-oxide membrane at the bottom has been reported [67, 78]. Vibrations of this membrane are controlled by varying frequency and voltage of the input signal. An illustration is given in Figure 2.12. Another approach is to penetrate an air bubble inside a liquid by an acoustic field, thus the bubble surface acts like a vibrating membrane. This induces friction forces around the bubble resulting in a flow disturbance and a higher mixing efficiency [17, 20]. Active mixing can also be achieved by ultrasonic generated from piezoelectric membranes [20, 65]. Problems occur for biological and chemical analysis due to the temperature rise induced by acoustic waves. Furthermore, ultrasonic waves around 50 kHz are harmful to biological samples [67].

An obvious way to enhance mixing is to disturb the pressure field inside the channel, which is mostly done by pulsing of the inlet streams. This pulse is achieved by varying the flow rate of one or more pumps. Simple implementation is possible because no additional equipment is needed. Glasgow et al. [79] simulated a T-mixer with a periodically pulsed side flow at low Reynolds numbers. Pulsing of both streams with a 90 degree phase difference lead to a five times better degree of mixing than without pulsing, as shown in Figure 2.13 [17, 79]. Although 90 degree phase difference mixes slightly better, 180 degree phase difference provides a constant outlet flow rate so this is the preferable configuration [79].

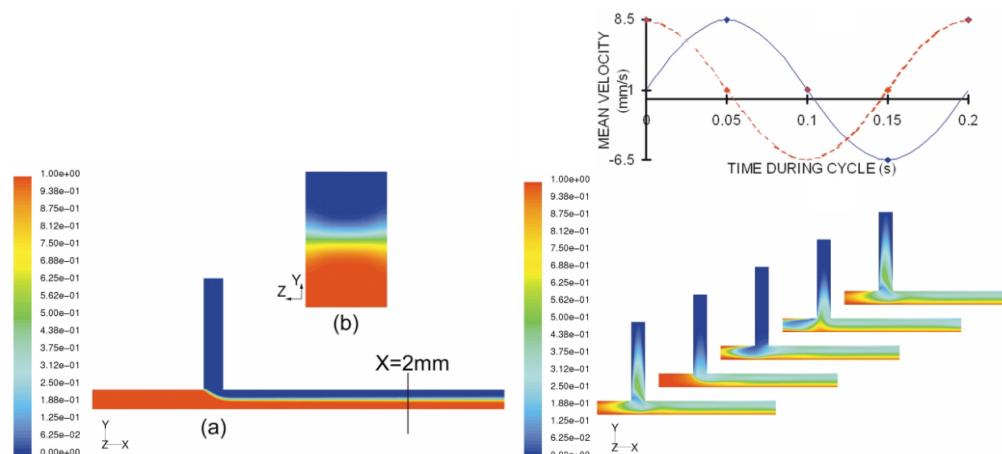


**Figure 2.13:** Numerical simulation of pulsed flow in a simple T-mixer with a mean velocity of  $1 \text{ mm s}^{-1}$  for both inlet streams. Left: Control case without any pulsing indicates bad mixing. Right: Pulsed flow with a 90 degree phase difference. The graph shows the mean velocities as a function of time. The numerical simulation shows enhanced mixing for various times. Adapted from [79].

## 2.5 Characterisation of Mixing

Fast mixing is necessary to ensure a selective reaction progress. In order to find the optimum, the characteristics of a microfluidic device are required to match the reaction kinetics of the desired reaction. Thereby heat and mass transfer are the most important parameters [80]. To compare mass transfer, i.e. the mixing efficiency of microfluidic devices, methods to get qualitative and quantitative results are needed. In general the characterisation of mixing can be divided into physical and chemical methods. Physical methods do not use a chemical reaction. The analysis solely depends on physical effects in the macroscale. This provides mixing information for reactor analysis and design [58]. An easy way is to dilute a coloured solution with a second stream and use optical methods like microscopes or high speed cameras to follow this process. Therefore coloured or fluorescent dyes can be used [22, 81]. Complete mixing is indicated by a uniform concentration of the dye. This method is simple to implement but gives inappropriate information about complex multi-layered mixing patterns because the information is averaged over the depth of the device [22]. Also a transparent device is needed, which is no problem for PDMS but for steel and ceramics. The most common way to evaluate macromixing with a physical method is to investigate the RTD by analysing the dispersion of a tracer which is injected into the microfluidic device. CFD simulations offer the possibility to characterise mixing without time consuming experiments.

### 2.5.1 Residence Time Distribution (RTD)

The RTD describes the probability of a fluid element to pass through the reactor within a specific period of time. After injecting a tracer into the microfluidic device, the response is detected at the

outlet over time. The axial dispersion is caused by velocity fluctuations inside the microfluidic device and results in different residence times of fluid elements, giving the RTD [58, 80]. The tracer has to be inert, stable, easy detectable, should not be adsorbed at the channel walls and should not change density and viscosity of the solvent [32, 82]. Common tracers are dyes or electrolytes which are detected by UV/VIS absorption or conductivity, respectively. A classic experimental set-up, which was also used in this thesis is depicted in Figure 3.5.

### Input and Output Signal

In general, every input signal of the tracer is possible but pulse and step input are the most common ones [32]. When performing a step input the concentration of the tracer is instantaneous changed to a constant value at  $t = 0$ . The resulting signal is related to the input concentration  $c_0$  giving the cumulative age function  $F(t)$ . For the pulse input, a small volume (compared to the reactor volume) of tracer is injected within a short period of time. A recommended value for the input time is  $\Delta t < 0.01 t_{res}$ . The resulting signal at the output can be directly used to calculate the exit age distribution  $E(t)$ . The input and output signals as function of the time are depicted in Figure 2.14.

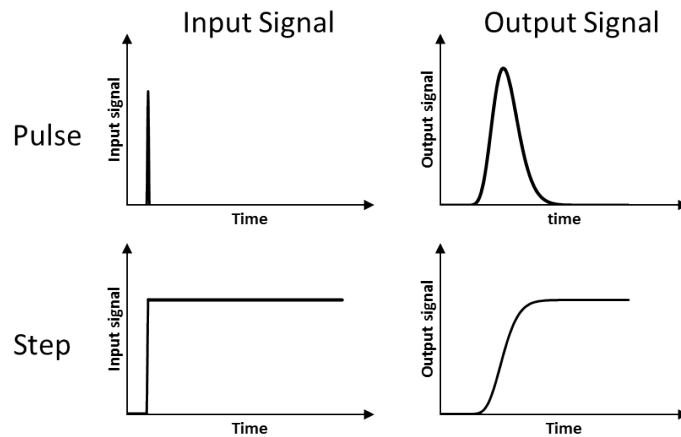


**Figure 2.14:** Input and output signals of pulse and step function of a plug flow reactor. At the pulse input the inlet flow is doped with a tracer. At the step input the reactor inlet is changed to a constant concentration of tracer. The output signal is dependent on the input signal and the type of reactor.

In microfluidics the input signals are usually realised with a 6-port injection valve which is switched by an actuator or manually. For the pulse input a sample loop is filled with a defined amount of tracer and after switching the valve, the tracer is injected into the microfluidic device. A step input is done by switching the valve from solvent to a constant tracer concentration. Electrically actuated valves have the advantage of short and reproducible switching times, which can not be guaranteed for manual switching valves [82, 83].

### Evaluation of RTD-Experiments

This section gives a summary of well known equations, for detailed information see [32, 80]. The relative output signal (ratio of signal to maximum signal) over time gives the cumulative age distribution  $F(t)$ . The exit age distribution  $E(t)$  is obtained by numerical differentiation of the  $F(t)$  curve:

$$E(t) = \frac{dF(t)}{dt} \quad (2.9)$$

Often the dimensionless time  $\theta$  is used and given as:

$$\theta = \frac{t}{t_{res}} \quad (2.10)$$

The normalised  $E(\theta)$  curve is determined as:

$$E(\theta) = E(t) \cdot t_{res} \quad (2.11)$$

Thereby  $t_{res}$  is the mean residence time which is defined as:

$$t_{res} = \int_0^{\infty} t \cdot E(t) dt \cong \sum_{t=0}^{\infty} t \cdot E(t) \cdot \Delta t \quad (2.12)$$

For interpretation of the RTD curves, the dimensionless Bodenstein number  $Bo$  is used, which is the ratio of convective mass transfer over axial dispersion and is given as:

$$Bo = \frac{u \cdot L_{char}}{D_{ax}} \quad (2.13)$$

Where  $u$  is the flow velocity,  $L_{char}$  is the characteristic length of the device and  $D_{ax}$  is the axial dispersion coefficient. A high Bodenstein number ( $Bo > 100$ ) is equivalent to low back mixing (i.e. plug flow) while a low Bodenstein number ( $Bo < 100$ ) indicates high back mixing [32]. In this thesis, the dispersion model is used for interpretation of the data. This model implies that there is no by-passing or short circuiting of fluid in the reactor and the conditions are illustrated in Figure 2.15. In experiments, the Bodenstein number is derived by calculation of the mean residence time  $t_{res}$  according to equation 2.12 and the variance  $\sigma_t^2$  of the RTD curve which is defined as:

$$\sigma_t^2 = \int_0^{\infty} (t - t_{res})^2 E(t) dt \cong \sum_{t=0}^{\infty} (t - t_{res})^2 E(t) \Delta t \quad (2.14)$$

In its dimensionless form, referred to the dimensionless time  $\theta$  the variance is defined as:

$$\sigma_{\theta}^2 = \frac{\sigma_t^2}{t_{res}^2} \quad (2.15)$$

For low back mixing, i.e. ideal plug flow, the Bodenstein number is given as:

$$Bo = \frac{2}{\sigma_{\theta}^2} \quad (2.16)$$

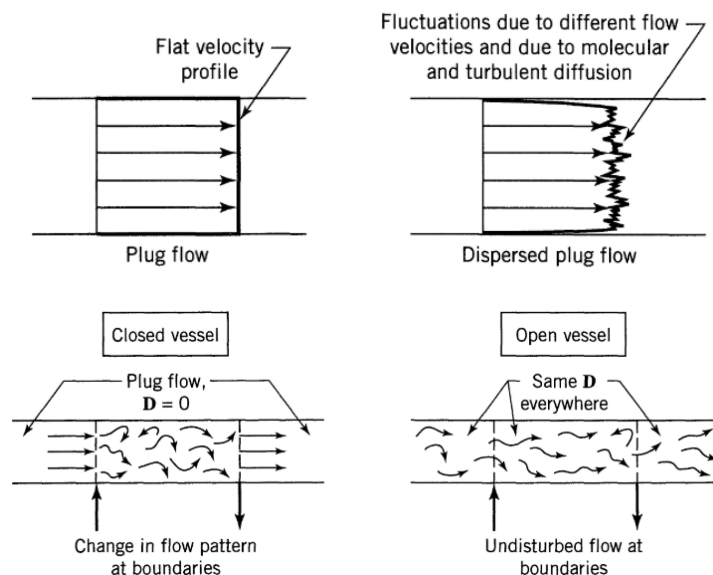


**Figure 2.15:** Top: Representation of ideal plug flow and dispersed plug flow. Bottom: Boundary conditions 'closed-closed' and 'open-open' for the in and outlet of a device according to the dispersion model [32].

These calculations are done iteratively. This means that first the Bodenstein number for low back mixing according to equation 2.16 is calculated. If the value is  $Bo > 100$  the assumption is fulfilled. If  $Bo < 100$  moderate or high back mixing is apparent leading to a variation of the model. In this case unfavorable flow conditions lead to an asymmetric RTD. Therefore the conditions of inlet and outlet of the reactor set the boundary conditions shown in Figure 2.15. From these boundaries different methods to calculate the Bodenstein number exist. The most common method uses the open-open conditions (Figure 2.15) and the algorithms for the description of the RTD-curve were developed by Levenspiel and Smith [32, 84]:

$$Bo_{o-o} = \frac{1}{\sigma_{\theta}^2} + \sqrt{\left(\frac{1}{\sigma_{\theta}^2}\right)^2 + \frac{8}{\sigma_{\theta}^2}} \quad (2.17)$$

It can be said that the RTD is well suited to get information about the macromixing performance of the reactor. RTD experiments provide information about concentration distributions which indeed influence chemical reactions. Nevertheless, to get information about the mixing performance on the molecular level, the RTD does not provide enough information. To access the molecular level mixing sensitive reactions are a possible approach.

## 2.5.2 Mixing Sensitive Reactions

In organic synthesis unwanted by-products or side reactions lead to low selectivity, as a result a lot of reaction work up has to be done. The most effective way to enhance the selectivity of chemical

reactions is catalysis. Another approach is to increase the mixing efficiency which also reduces side reactions and increases the selectivity. To investigate the mixing performance on a molecular scale, mixing sensitive reactions are well suited [22, 23, 64, 85–87]. These methods mostly use second-order reactions which are dependent on the mixing situation, demonstrated by their product distribution. The rate of a first-order reaction is unaffected by an inhomogeneous concentration distribution. Regions with concentration and reaction rate above average compensate those below average [23]. The way how the product distribution is determined by the mixing efficiency, is influenced by the ratio of mixing time and reaction time [88]. If the mixing time  $t_m$  is much shorter than the reaction time  $t_r$ , the reaction takes place in a homogeneous mixture. In this case no further improvement of the mixing performance is necessary. If the reaction is much faster than mixing, the reaction path is influenced by this concentration profile, resulting in side reactions [88–90]. Mixing sensitive reactions need to fulfil several characteristics [60, 90, 91]:

- Two or more reagents are involved providing a mixing dependence of the reaction.
- Fast, irreversible second-order reactions with a few (preferably two) products.
- The reaction kinetics and mechanism need to be fully defined. This includes knowledge about dependencies on pH, ionic strength, temperature and solvent. This provides that the product distribution is only dependent on mixing and not a chemical artefact.
- At least one of the reactions must be faster than the micromixing processes. The other one should be in the range or slower than the mixing process.
- All reactants should be soluble and stable to ensure a reliable analysis.
- Simple, inexpensive methods for analysis are essential.

Several mixing sensitive reaction systems are reported in literature [2, 22, 87, 89]. They can be divided into parallel-competitive (Figure 2.16) and consecutive-competitive (Figure 2.17) reactions. The principle is to carry out two reactions which both compete for one reactant. If mixing is ideal only the very fast primary reaction takes place. The secondary reaction is still fast, but slower than the first one thus it just reacts if a local excess of one reagent is present, i.e. non-ideal mixing. This results in a mixture of products indicating good or bad mixing. The homogeneous situation in Figure 2.16b and 2.17b can only be achieved if the mixing time  $t_m$  is much shorter than the reaction time  $t_r$ . In this case, the reaction between reagent A and B is preferred because the rate constant  $k_1 > k_2$  and as a result, the yield of S product approaches to zero. If the mixture is heterogeneous (Figure 2.16c and 2.17c), reagent A and B form the product R. Due to an inhomogeneous mixture, reactions only take place at the interface of the segregated fluids. After the instantaneous reaction of A and B, local overconcentration of C or R (depending on the reaction system) promote the secondary reaction. As a result, product S is formed which is used

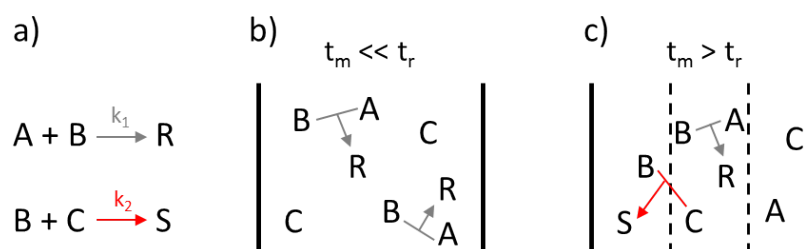


**Figure 2.16:** a) Scheme of a parallel-competitive reaction with  $k_1 > k_2$ . Reagent A and C are competing for reagent B giving the products R and S. b) In a homogeneous mixture the R product is preferred, due to different rate constants c) In a heterogeneous mixture also S product is formed due to local overconcentrations. Adapted from [88].

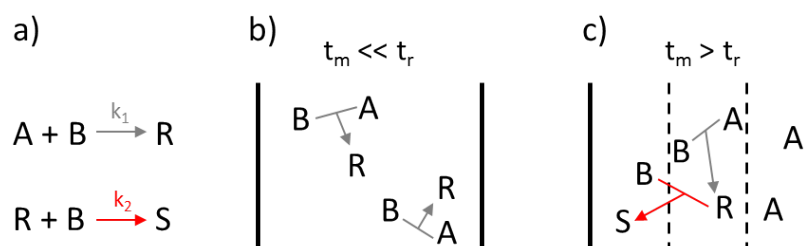
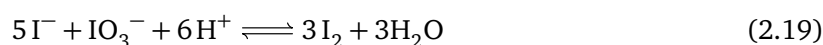


**Figure 2.17:** a) Scheme of a consecutive-competitive reaction with  $k_1 > k_2$ . The fast primary reaction between A and B gives product R. This product R competes with reagent A for reagent B giving product S. b) In a homogeneous mixture the R product is preferred, due to different rate constants c) In a heterogeneous mixture also the S product is formed due to local overconcentrations. Adapted from [88].

as indicator of the mixing quality. The higher the yield of the secondary product, the worse is the mixing quality [2, 22, 23, 88].

A common method of parallel-competitive mixing sensitive reactions to investigate microfluidic devices is the Villermaux/Dushman reaction published by Fournier et al. [22, 85, 86]. This reaction consists of a quasi-instantaneous acid-base neutralisation and a slower redox reaction.



A borate buffer solution containing  $I^-$  and  $IO_3^-$  is mixed with sulfuric acid providing a defined amount of  $H^+$  ions. In the case of ideal mixing, the acid is only consumed by the neutralisation which is much faster than the redox reaction. The formation of  $I_2$  is catalysed by  $H^+$  ions which are present, if the first reaction is incomplete, i.e. bad mixing [92]. The amount of formed iodine is detected as tri-iodide  $I_3^-$  complex by UV/VIS absorption. This reaction system has a few drawbacks: The concentration protocol for the experiments is often adapted to the devices, hindering comparison of different experiments. The kinetics and the mechanism of the reaction are not fully determined,

the products must be rapidly analysed in order to avoid iodine loss and disproportionation and the medium is oxidising which can have negative effects on the equipment [22, 66, 85, 88, 93, 94]. Due to the mentioned drawbacks, a consecutive-competitive reaction published by Bourne et al. [2] was used in this thesis and will be described in detail in the next section.

### Diazo coupling of 1-Naphthol and Diazotised Sulfanilic Acid

This mixing sensitive reaction system was developed to investigate micromixing in stirred tank reactors and was then improved and adapted to be used in microfluidics [22, 88–90, 95–98]. It is widely used for micromixing experiments because the reaction mechanism and reaction kinetics are fully determined [2, 88].



The consecutive-competitive system consists of a diazo coupling of A and B being 1-naphthol and diazotised sulfanilic acid respectively, as depicted in Figure 2.18. Reagent A is added in 20% excess to ensure 100% conversion of reagent B. First, two primary couplings of A and B result in the monoazo dyes p-R and o-R, and their secondary coupling yields in the final bisazo dye S. When first developed, Bourne et al. [2] did not take the formation of o-R into account. Afterwards his team determined the percentage of formation of o-R up to 7% [2]. To ensure maximum reaction rates and sensitivity to mixing the set standard conditions should be used. At these conditions (pH 9.9, T=25 °C, I=444.4 mM carbonate/bicarbonate buffer each 111.1 mM) the kinetics are fully defined and are given as  $k_{1p} = 12\,238 \pm 446 \text{ m}^3 \text{ mol}^{-1} \text{ s}^{-1}$ ,  $k_{1o} = 921 \pm 31 \text{ m}^3 \text{ mol}^{-1} \text{ s}^{-1}$ ,  $k_{2o} = 1.835 \pm 0.018 \text{ m}^3 \text{ mol}^{-1} \text{ s}^{-1}$ ,  $k_{2p} = 22.25 \pm 0.25 \text{ m}^3 \text{ mol}^{-1} \text{ s}^{-1}$  [2, 87].

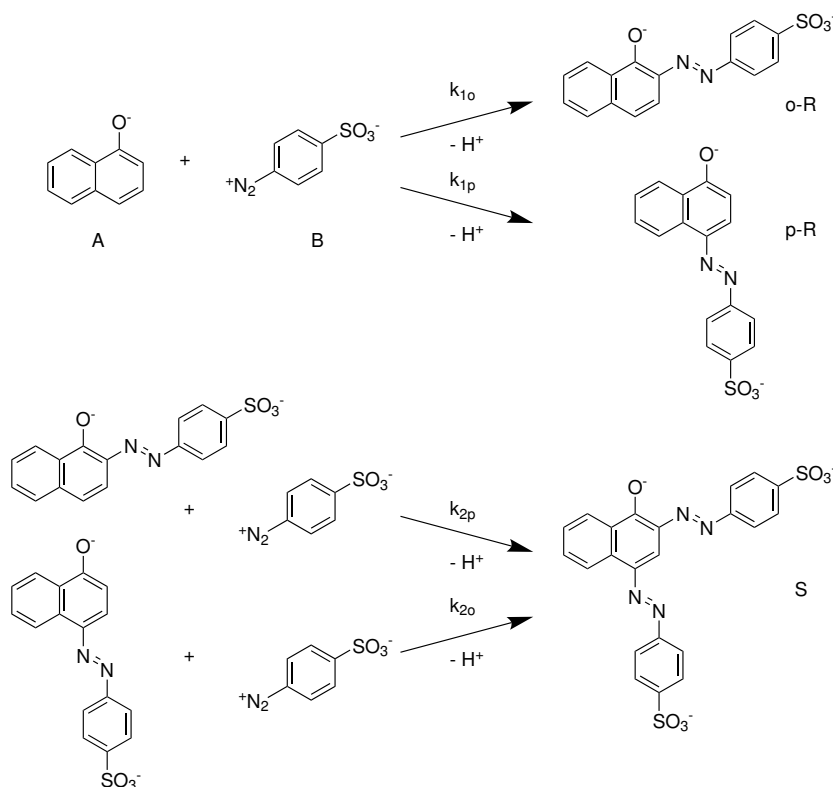


**Figure 2.18:** Scheme of the diazo coupling of 1-naphthol (A) and diazotised sulfanilic acid (B) giving the monoazo isomers p-R and o-R. The secondary coupling of p-R and o-R with B results in the bisazo dye S.

After the reaction is complete, the three dyes and unreacted 1-naphthol are present in the mixture. The sample is measured spectrophotometrically and the concentrations of the dyes are calculated using multiparameter regression as described in 5.4. With these concentrations the bisazo yield  $Y_S$  can be calculated according to

$$Y_S = \frac{2 \cdot c_S}{2 \cdot c_S + c_{oR} + c_{pR}} \quad (2.25)$$

and can be interpreted the following [23]:

- Kinetically controlled regime ( $t_r \gg t_m$ ); The much faster primary coupling leads to a bisazo yield of  $Y_S \ll 0.01$  because no secondary coupling takes place.
- Mixing controlled regime ( $t_r \ll t_m$ ); All monoazo dyes perform a secondary coupling resulting in  $Y_S = 1$ .
- Intermediate regime ( $t_r \approx t_m$ ); A mixing model for detailed analysis is necessary.

The useful range of this reaction system is  $0.04 \ll Y_S \ll 0.4$ . The lower value is referred to the sensibility of the used analytical technique. The higher value takes the stability of the bisazo dye S into account. Higher values of  $Y_S$  increase the probability of side reaction involving the S product [2, 60].

Drawbacks of this method are the non-straight forward synthesis of the dyes and reagents. Furthermore, reagents and dyes are not stable which means that solutions A and B have to be prepared every day and the products should be analysed within three hours [2, 88, 96, 98].

Due to the reaction times, this system is restricted for energy dissipation rates less than  $400 \text{ W kg}^{-1}$ . For high intensity mixers, Bourne et al. [89] improved the system using 2-naphthol as another reagent to investigate mixers with energy dissipation rates up to  $10^5 \text{ W kg}^{-1}$ . The improved reaction system consists of five reactions and four products which increases the complexity of kinetics and analysis [98]. As the system only using 1-naphthol is already sensitive to the application in this thesis, it was decided to use the reaction system which only uses 1-naphthol.

## 2.6 Model Reaction - Aerobic Oxidation of Grignard Reagents

For a detailed reactor design, knowledge about the reaction kinetics is necessary. The challenge of investigating the intrinsic kinetics of fast reactions is the limitation by heat and mass transfer. To evaluate the performance of 3D printed microreactors and to determine reaction kinetics in continuous flow, an aerobic oxidation of Grignard reagents to the corresponding phenol was chosen as model reaction. This reaction is a sustainable and inexpensive way to synthesise functionalized phenols [99]. This reaction is well suited for micro application, as it is very fast and can be categorised as type A reaction [1, 100]. The increased heat transfer in microfluidics eliminates local hot-spots and enables isothermic conditions [44]. This reaction is a green approach to form phenols as it uses oxygen as sustainable and inexpensive reagent [99].

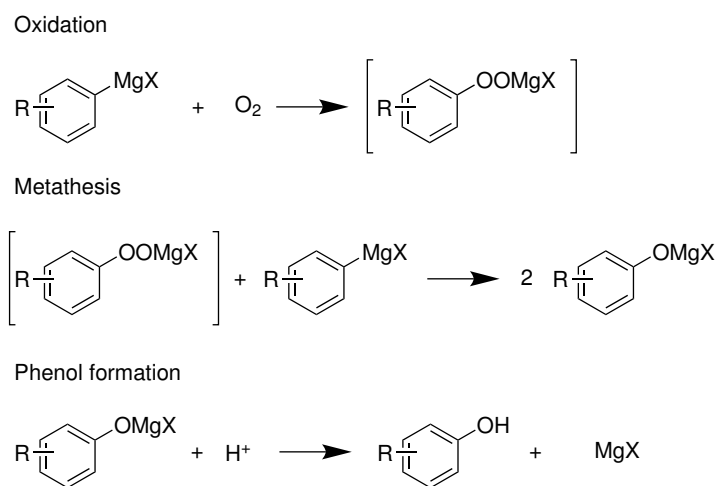


**Figure 2.19:** Proposed mechanism of the oxidation of Grignard reagents: First an aryl radical is formed by oxidation of an organo-magnesium species which then reacts to a organoperoxide. This reacts with another Grignard reagent to form a phenoxide. In a last step phenol is formed by acidification. Adapted from [99].

The mechanism is not fully investigated but it is believed as two-step reaction, involving an

electron transfer step between Grignard reagent and oxygen as seen in Figure 2.19. The formed peroxide intermediate reacts with another Grignard reagent to form phenoxide which is converted to phenol [99, 101].

To investigate the intrinsic kinetics of such a fast reaction in flow, quasi-instantaneous mixing is necessary. Otherwise the determined kinetic parameters are mixing dependent. To perform a kinetic analysis also the stoichiometric dosing of oxygen is essential which can be done by using a calibrated mass flow controller.

## 2.7 UV/VIS Spectroscopy

Analysis of the mixing sensitive reaction in section 2.5.2 is done with UV/VIS spectroscopy, which relies on the light absorption of a substance. Light is electromagnetic radiation which is characterised by its wavelength  $\lambda$ , frequency  $\nu$  and the speed of light  $c_{light}$  via:

$$c_{light} = \nu \cdot \lambda \quad (2.26)$$

The connection of light with energy is done with Planck's constant  $h = 6.63 \times 10^{-34}$  J s and given as

$$E = h \cdot \nu = \frac{h \cdot c_{light}}{\lambda} \quad (2.27)$$

where  $E$  is the energy of the radiation. Molecules with  $\pi$ -electrons or non-bonding electrons can absorb energy in the form of light, to excite these electrons to higher anti-bonding molecular orbitals. The wavelength of the absorbed light depends on the energy demand for excitation of electrons [102].

If light with the intensity  $I_0$  reaches a homogeneous media with path length  $l$ , the light intensity is decreased to  $I$  due to absorption of the media. This is known as the Lambert-Beer law and given as

$$A = \log \frac{I_0}{I} = \varepsilon \cdot c \cdot l \quad (2.28)$$

where  $A$  is the dimensionless absorption,  $c$  is the concentration of the absorbing media and  $\varepsilon$  is the molar extinction coefficient [102]. The absorption of  $n$  substances within one measurement are added together giving the total absorption as:

$$A_{tot} = \log \frac{I_0}{I} = \sum_{i=1}^n \varepsilon_i \cdot c_i \cdot l \quad (2.29)$$

This means, if the extinction coefficient for each wavelength of every substance is known, one can calculate the concentration of every substance. Lambert-Beer law (equations 2.28 and 2.29) can be applied if the following criteria are fulfilled [96, 102]:

- The absorbing substance is homogeneously distributed.
- The absorbing substance is present at a maximum concentration of  $10^{-2}$  mol L<sup>-1</sup>.

- No scattering of light due to scratches, particles or bubbles.
- The substances absorb independently of each other.
- The absorption is lower than one.

The absorption spectra is influenced by many parameters like temperature, pH value, ionic strength and polarity of the solvent. The analytical sensitivity and robust equipment are the reasons UV/VIS spectroscopy is a commonly useful technique.

---

## 3 Results and Discussion

Yield and selectivity of fast chemical reactions are highly influenced by the mixing efficiency of the reagents, because bad mixing can promote undesired side reactions. Detailed reactor design requires knowledge about the intrinsic reaction kinetics, without any limitations due to heat and mass transfer. The aim of this thesis is to design a set-up for kinetic measurements, of a very fast oxidation of Grignard reagents, in 3D printed microreactors. This reaction is performed at elevated pressure to dissolve oxygen in the solvent, followed by mixing the stream with the Grignard reagent. The very active Grignard reagent reacts instantly to the corresponding phenol. Achieving accurate kinetic results requires a geometry that provides fast mixing. To design the set-up, knowledge about the mixing performance of the created designs is necessary.

Therefore, the mixing performance of 3D printed microfluidic devices made of stainless steel (316 L) and ceramics (aluminium oxide) was investigated. For experimental analysis RTD measurements and mixing sensitive reactions were used. Different passive and active mixing designs were created and analysed. The mixing sensitive reaction was performed with all devices, while the RTD was only investigated for the CSTR-cascade v1 and the SAR-reactor. An overview of the devices and the corresponding experimental methods is listed in Table 3.1. The devices are meant to be used for the oxidation of Grignard reagents, which is a very fast and therefore mixing dependent reaction. Overall goal is to perform this fast reaction without mass transfer limitations to investigate the intrinsic kinetics. This data is necessary for detailed design of microfluidic devices.

The mixing sensitive reactions are done in aqueous media, RTD measurements in a mixture of water and ethanol, both at 25 °C. The oxidation of Grignard reagents is done in 2-methyl-tetrahydrofuran (2-methyl-THF) at different temperatures for kinetic analysis. To compare these varying conditions and channel geometries the dimensionless Reynolds number was used. The channel Reynolds number is calculated according to equation 2.1. The stirrer Reynolds number is calculated with

$$Re_{stirrer} = \frac{\rho \cdot n_{stirrer} d_{stirrer}^2}{\eta} \quad (3.1)$$

where  $\rho$  is the density of the solvent,  $n_{stirrer}$  is the rotational speed of the stirrer,  $d_{stirrer}$  is the diameter of the stirrer and  $\eta$  is the dynamic viscosity. The hydraulic diameter  $d_h$  is used to compare flow properties in non-circular channels. It is calculated with the cross-sectional area  $A$  and the perimeter  $P$  of the wetted cross-section and is given as:

$$d_h = 4 \cdot \frac{A}{P} \quad (3.2)$$

For circular channels, the hydraulic diameter is equal to the channel diameter. The highly complex structures of the 3D printed geometries change their channel diameter multiple times because of SAR-elements, mixing chambers and stirrers. The challenge relies in choosing the most expressive cross-section to calculate  $d_h$ . For each design, a representative region is used to calculate  $d_h$  and to compare the reactors at equal Reynolds numbers.

### 3.1 Description of the 3D printed Microfluidic Devices

**Table 3.1:** Overview of the investigated microfluidic devices and the corresponding experiments.

Microfluidic device	Material	Mixing sensitive reaction	RTD
Size-scaled-mixers	Steel	X	
Sphere-mixer	Steel		
Sphere-mixer	Ceramics	X	
T-mixer	Steel	X	
Split-and-recombine-reactor	Steel	X	X
CSTR-cascade v1	Steel	X	X
CSTR-cascade v1	Ceramics	X	X
CSTR-cascade v2	Steel	X	

Passive micromixers were designed and made of stainless steel and ceramics using 3D printing. They consist of one or more inlets, outlet and a mixing structure but do not have additional reaction volume. As benchmark, a simple T-mixer with two inlets and one outlet was used to compare the designed mixers with standard equipment. To provide enough volume for a complete reaction, the outlets were connected to a 1 m long capillary with a volume of 0.5 mL.

To investigate the influence of the channel size, three size-scaled-mixers were designed as depicted in Figure 3.1. This design has a croissant-shaped SAR-approach with seven SAR-sections, with an alternating offset of  $90^\circ$ . The mixing chamber splits into two channels with a semi-circular cross-section. These mixers have the same design, but their dimensions are scaled with factors of 0.75 and 0.5 referred to the large version. The semi-circles have radii of 1 mm, 0.75 mm and 0.5 mm resulting in hydraulic diameters of 1.222 mm, 0.917 mm, 0.611 mm for the large, medium and small version, respectively. These hydraulic diameters were chosen for the calculation of the Reynolds numbers.



**Figure 3.1:** Left: The size-scaled-mixers have the same design, but their dimensions are scaled with factors of 0.75 and 0.5 referred to the large version. Right: Rendered image of the mixing structure consisting of two semi-circles between each mixing chamber.

Figure 3.2 depicts the sphere-mixer, which has ten spherical mixing chambers which are connected by circular channels, with an alternating offset of  $90^\circ$ . The channel diameter is 0.8 mm resulting in an equal hydraulic diameter, being used for the calculation of the Reynolds number. This mixer was made of both materials to investigate the material influence on the mixing performance. Unfortunately the steel version was leaking when water was inserted, without applying pressure. Leakage occurred probably due to a low wall thickness in some regions, attributed to the fabrication process.

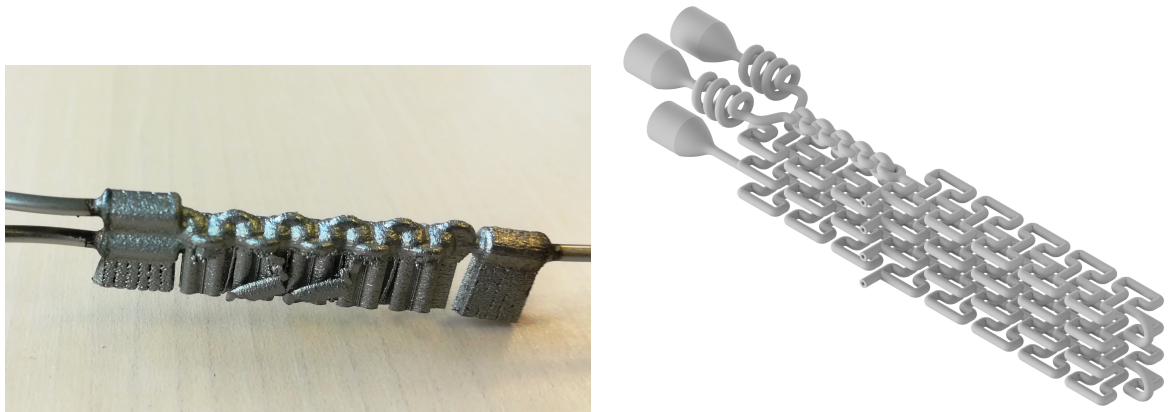


**Figure 3.2:** Left: The sphere-mixer has two inlets, one outlet and ten spherical mixing chambers. The mixing chambers are connected with two channels, with an alternating offset of  $90^\circ$ . Right: Rendered image of a reactor concept including the sphere-mixer as mixing section.

Figure 3.3 shows the SAR-reactor, consisting of two inlets which are mixed after a pre-cooling section. Then the combined streams use multiple split-and-recombine elements to ensure good mixing and enough reaction volume. In contrast to the mentioned passive mixers, this design

includes a mixing section and reaction volume and is fabricated in one piece. The channel diameter was chosen to be  $800\ \mu\text{m}$ . As reported in previous work [26], the design provides openings to remove unused powder from the printing process. Thereby, the remaining powder is removed by compressed air and ultrasonic treatment. After cleaning, these openings were closed by laser welding. Capillaries with  $1/16''$  outer diameter (OD) and  $0.03''$  inner diameter (ID) were attached to the inlet and outlet by laser welding to ensure proper connection of the reactor.

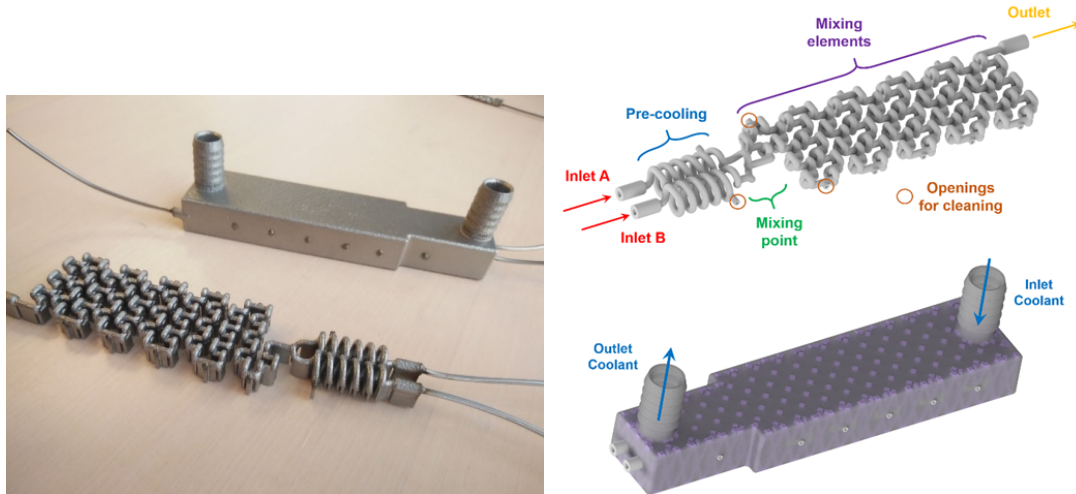


**Figure 3.3:** Left: 3D printed SAR-reactor with and without cooling, shell fabricated by SLM. Right: Rendered image of the SAR-reactor with and without cooling shell. The reactor consists of two inlets and a pre-cooling section, a mixing point and mixing elements which additionally ensure enough volume.

A CSTR-cascade was designed as active mixer and is depicted in Figure 3.4. The device was made of steel and ceramics to investigate the material influence. It consists of ten connected vessels with an internal diameter of  $3\ \text{mm}$ . The vessels are connected with  $800\ \mu\text{m}$  channels attached tangentially to the bottom part. As stirrers, spheroids with  $2.4\ \text{mm}$  width and  $2.7\ \text{mm}$  length are inserted in each vessel. The stirrers are agitated by a rotating magnetic field of a standard laboratory magnetic stirrer. The upper part of each vessel can be configured for different purposes by standard HPLC fittings. This allows the use of additional feed or quenching streams, sensors or plugging of the top part. At a marked position the vessels are not connected, indicating the inlet and outlet of the reactor.

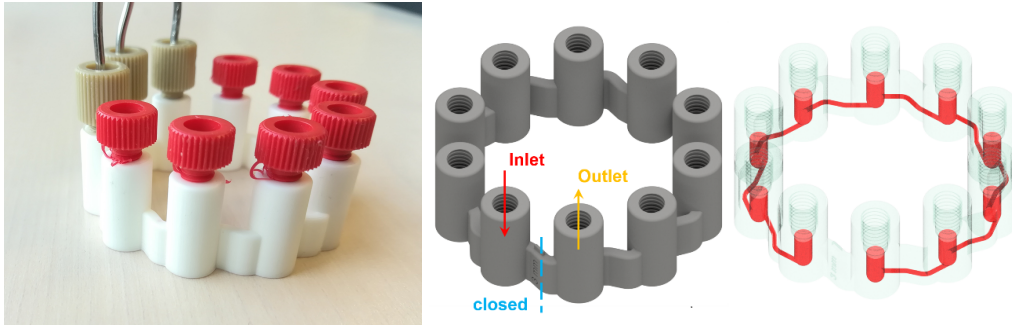


**Figure 3.4:** Left: CSTR-cascade v1 made of ceramics. The stainless steel version has the same design. Shavings are cut off from the red fittings. This indicates that the ceramic thread is not perfectly fitting to the thread of the standard HPLC fittings. This is attributed to shrinkage of ceramics during fabrication. Right: Rendered image of the CSTR-cascade v1 with highlighted channels and vessels.

### Connection of Microfluidic Devices

An important factor is the connection of the microfluidic devices to other equipment. In general, connection is done with standard HPLC tubings and fittings. Two options for the connection of stainless steel parts to other equipment exist. One is to directly weld steel capillaries to reactor inlet and outlet by laser welding. This capillary can be connected by standard fittings and connectors to other equipment. The other option is to use a standard thread cutter and then directly attach the fittings to the reactor. For both options an additional post-processing step is necessary which makes the choice to a matter of taste.

With microfluidics made of ceramics, laser welding or thread cutting are not possible. In contrast to steel, ceramics have no reasonable method to attach connectors in a post-processing step. However, the high resolution and the smooth surface of the LCM technology open the possibility to directly print the desired thread. With this customisation, it is possible to attach other devices by standard HPLC fittings. When the fittings were attached to the ceramic reactor, shavings were cut off the fittings as depicted in Figure 3.4. This indicates that the printed thread does not perfectly fit to the standard thread dimensions. In the fabrication process the ceramic parts are shrinking which has to be considered in the design process. By gaining more experience in the LCM process, the printing parameters can be optimised in the future. This allows the consideration of shrinkage in the design and fabrication process. Frequent connection and disconnection will lead to destruction of the standard HPLC fittings.

## 3.2 Macromixing - Residence Time Distribution

To investigate the macromixing performance of the SAR-reactor and the CSTR-cascade v1, the RTD was determined. The used basic set-up is depicted in Figure 3.5 and a step input was used as input signal. The step up signal was recorded when switching from no tracer to constant tracer

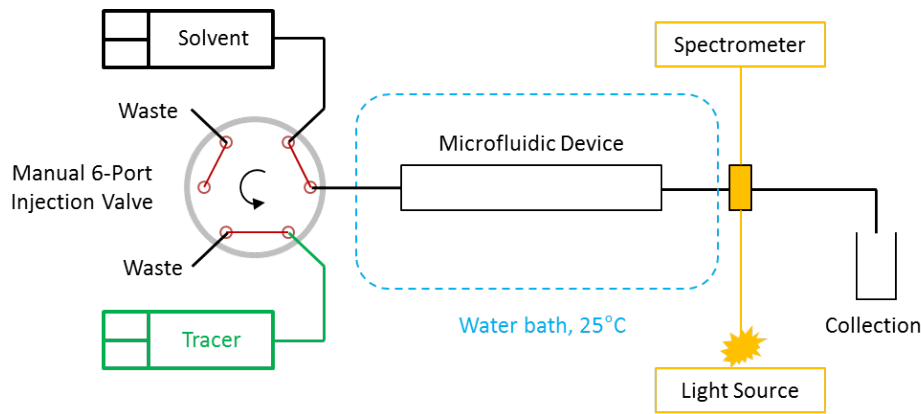


**Figure 3.5:** Experimental set-up for the determination of the RTD. By switching the manual 6-port injection valve, the input is changed from no tracer to a constant concentration of tracer. This step signal is detected by an inline UV/VIS flow cell connected to a spectrophotometer.

concentration. The step down signal was recorded the other way round. Solvent was a mixture of 12 wt% ethanol in water and as tracer a solution of 0.006 v% anisole in before mentioned solvent was used. The UV/VIS absorption of anisole over time was measured with a spectrophotometer at the outlet of the device. The Bodenstein number was calculated according to the open-open conditions as mentioned in the theoretical section 2.5.1.

### 3.2.1 Split-and-Recombine-Reactor

RTD measurements of the SAR-reactor were performed through one inlet, while the other one was blocked. Figure 3.6 illustrates the Bodenstein number of step up and step down experiments. Plug flow was obtained at Reynolds numbers between 50 and 60 which is referred to a water flow rate of approximately  $1.7 \text{ mL min}^{-1}$ . Plug flow behavior can be assumed for Bodenstein numbers  $Bo > 100$  indicating low axial dispersion [32]. The reactor volume was calculated as product of flow rate and mean residence time according to equation 2.12 and was determined to be  $461 \mu\text{L}$ . Gravimetric determination of the whole reactor volume resulted in  $665 \mu\text{L}$  and according to the CAD file the whole reactor volume was  $737 \mu\text{L}$ . Because one inlet with pre-cooling section was blocked for RTD experiments, the determined volume is lower than the gravimetric and the CAD volume. Additionally, the inlet and outlet regions as well as the attached capillaries result in deviations between the different volumes. Deviations between the gravimetric and the CAD volume are attributed to shrinkage and surface roughness of the fabricated devices.

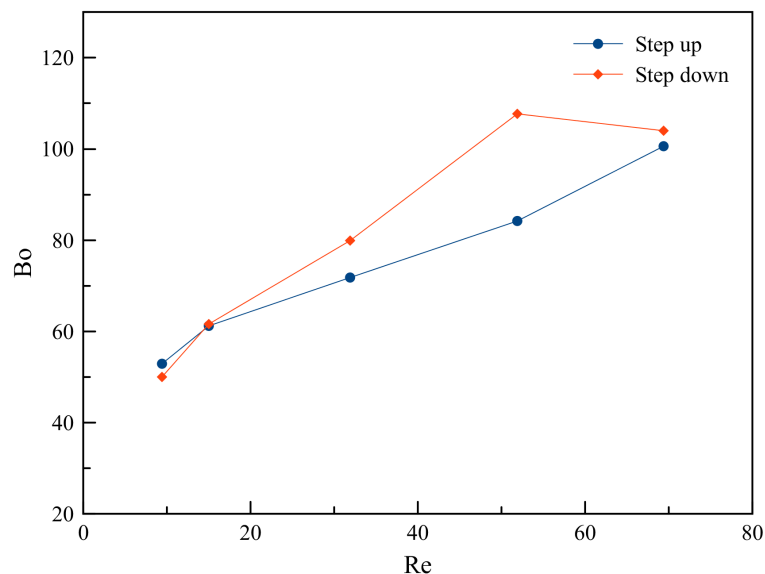


**Figure 3.6:** Bodenstein number against Reynolds number for the SAR-reactor. Step up and step down experiments were performed. Plug flow behaviour appears at Reynolds numbers between 50 and 60. The flow rates were  $0.5 \text{ mL min}^{-1}$ ,  $0.8 \text{ mL min}^{-1}$ ,  $1.7 \text{ mL min}^{-1}$ ,  $2.77 \text{ mL min}^{-1}$  and  $3.7 \text{ mL min}^{-1}$ .

### 3.2.2 CSTR-Cascade v1

Solvent and tracer were introduced in the first vessel and the last vessel was connected to the flow cell. The upper part of all other vessels was blocked with an HPLC plug. The RTD was determined for different flow rates and different rotational speeds. Figure 3.7 and Figure 3.8 depict the results for the CSTR-cascade v1 made of steel and ceramics, respectively. The determined Bodenstein number was  $Bo \approx 18$  for steel and  $Bo \approx 25$  for ceramics. No significant increase of the Bodenstein number with increasing RPM was found. The Bodenstein numbers of the CSTR-cascade v1 made of ceramics are a bit higher than the steel ones. This can be attributed to the smoother surface of ceramic reactors made by LCM. The rough surface of SLM fabricated reactors promotes dispersion and results in lower Bodenstein numbers. The reactor volumes were determined to be  $305 \mu\text{L}$  for steel and  $297 \mu\text{L}$  for ceramics. Gravimetric determinations of the reactor volumes were done with stirrers inside and connected fittings. It resulted in  $276 \mu\text{L}$  for steel and  $290 \mu\text{L}$  for ceramics. These low deviations are within the range of measurement errors.

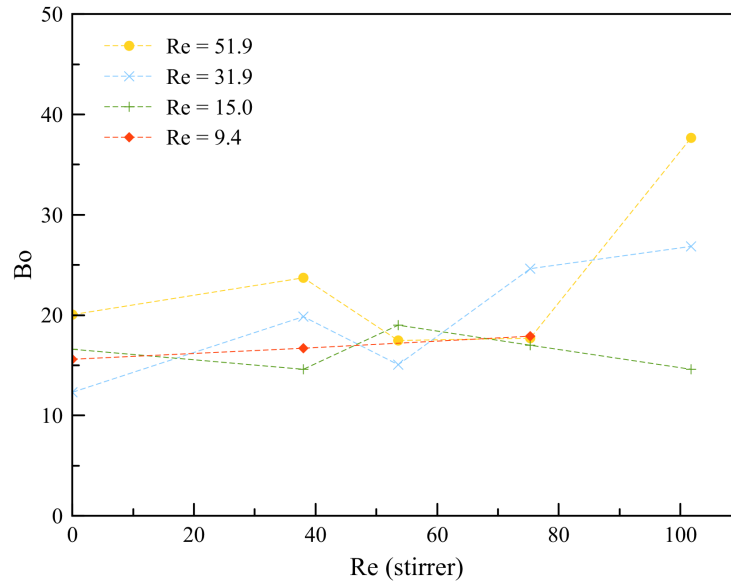


**Figure 3.7:** Bodenstein number of different flow rates against stirrer Reynolds number for the stainless steel CSTR-cascade v1. The flow rates were  $0.5 \text{ mL min}^{-1}$ ,  $0.8 \text{ mL min}^{-1}$ ,  $1.7 \text{ mL min}^{-1}$  and  $2.77 \text{ mL min}^{-1}$ .

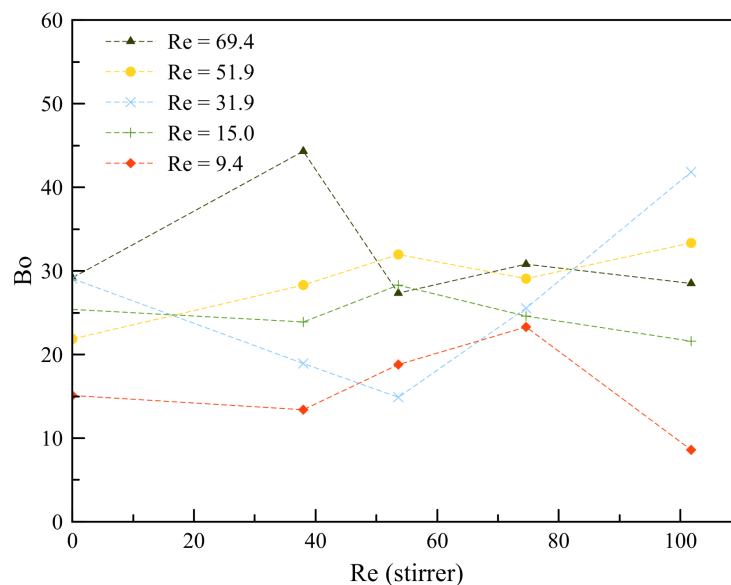


**Figure 3.8:** Bodenstein number of different flow rates against stirrer Reynolds number for the ceramic CSTR-cascade v1. The flow rates were  $0.5 \text{ mL min}^{-1}$ ,  $0.8 \text{ mL min}^{-1}$ ,  $1.7 \text{ mL min}^{-1}$ ,  $2.77 \text{ mL min}^{-1}$  and  $3.7 \text{ mL min}^{-1}$ .

RTD studies in literature recommend the use of two flow cells, one at the inlet and one at the outlet. This allows the compensation of deviations due to the injection valve, by using a mathematical approach based on convolution integral theorem [32, 83, 103]. Further improvement of the set-up

is possible by using a second flow cell at the reactor inlet and an electrical operated switching valve, ensuring reproducible injection times.

### 3.3 Micromixing - Mixing Sensitive Reactions

Experiments to characterise micromixing were done with mixing sensitive reactions published by Bourne et al. [2]. This system uses a consecutive-competitive diazo coupling of 1-naphthol and diazotised sulfanilic acid. When mixing is bad, only the secondary S-product is formed, indicated by its yield  $Y_S$ . This means if  $Y_S$  is low, mixing is fast and the reaction progress is not mass transfer limited, which is desired. This ensures high selectivity for fast chemical reactions in the investigated device. The used reaction scheme is depicted in Figure 2.18, set-up and procedure are depicted in Figure 3.9 and the experimental section 5.4.

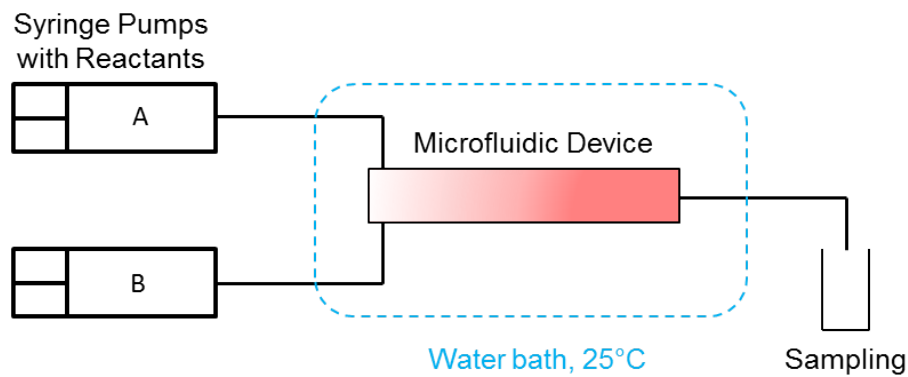


**Figure 3.9:** Experimental set-up for mixing sensitive reactions using a syringe pump with reactants, a microfluidic device at constant temperature of 25 °C and a sampling section.

The collected samples were diluted with buffer to achieve a concentration in the measurable range. UV/VIS absorption spectra were measured and the concentrations of each dye were calculated with a multi-parameter-regression method. The mixing performance was evaluated by calculation of the yield of the bisazo dye (S-product) which is given as [2]:

$$Y_S = \frac{2 \cdot c_S}{\bar{c}_{B0}} = \frac{2 \cdot c_S}{2 \cdot c_S + c_{oR} + c_{pR}} \quad (3.3)$$

To verify the correctness of the measurements, the mass balance ( $MB$ ) based on reagent B was calculated for each sample according to

$$\bar{c}_{B0} = \frac{c_B \cdot Q_B}{Q_A + Q_B} \quad (3.4)$$

$$MB = \frac{2 \cdot c_S + c_{oR} + c_{pR}}{\bar{c}_{B0}} \cdot 100\% \quad (3.5)$$

and closed within 8 %. Higher yields of S also lead to a worse mass balance (up to 20 % deviation) which was already reported in literature [88]. If the yield is  $0.04 < Y_S < 0.4$  the results are representative, higher yields can only be used qualitatively [2].

First, the dyes were synthesised to calibrate the UV/VIS absorption. Then the micromixing performance was investigated and compared, based on the Reynolds numbers of devices and operational points.

### 3.3.1 Calibration of the Dyes

#### 4-[(4-Sulfophenyl)azo]-1-naphthol (p-R)

The para monoazo dye was synthesised and calibrated as described in the experimental section 5.2. The calibration was done with standard conditions set by Bourne et al. [2], because the absorption of the substance is pH dependent. Solutions of different concentrations were prepared and analysed. The extinction coefficients  $\epsilon_{pR}$  were calculated according to Lambert-Beer law by equation 2.28. Comparison the obtained spectra with prior publications showed a good agreement. The maximum extinction coefficient near 516 nm differs around 1.3 % from published values [2, 90, 104]. It is assumed that this difference is not significant. The maximum extinction coefficients  $\epsilon_{pR}$  obtained in this work and as published in literature are shown in Table 3.2 and the spectra are depicted in Figure 3.10.

**Table 3.2:** Maximum extinction coefficients and the corresponding wavelengths of ortho- and para-isomer. The table represents data obtained within this work and literature references [2, 104].

Reference	para-isomer		ortho-isomer	
	$\epsilon_{pR}[m^2mol^{-1}]$	$\lambda[nm]$	$\epsilon_{oR}[m^2mol^{-1}]$	$\lambda[nm]$
This thesis	3151	514	2283	510
Bourne 1991	3171	514	2382	510
Wenger 1992	3190	515	2380	510

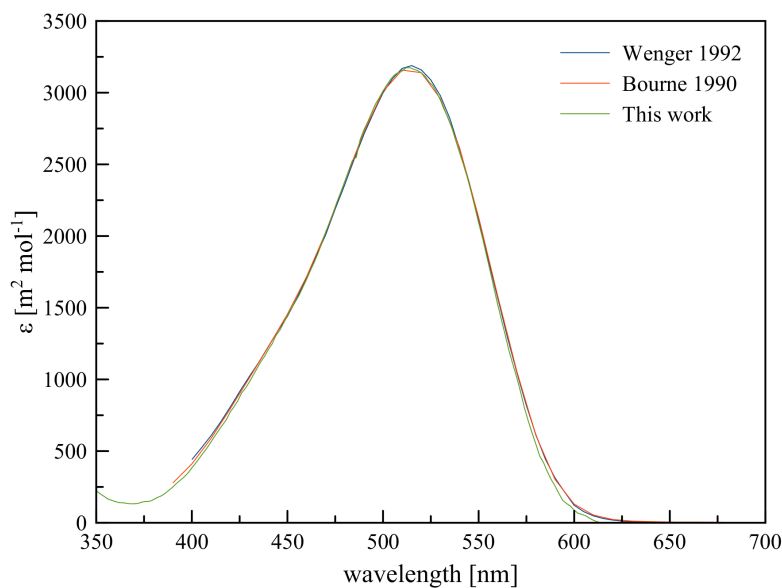


**Figure 3.10:** Absorption spectra of the para monoazo dye shows good agreement of this work, Bourne et al. [2] and Wenger et al. [104].

### 2-[(4-sulfophenyl)azo]-1-naphthol (o-R)

The ortho monoazo dye was synthesised and calibrated as described in the experimental section 5.2. Purification of this product was challenging. Multiple steps of recrystallisation and rinsing were necessary until the purity was satisfactory. A high loss of product and low yield of the synthesis were the consequence. After thin layer chromatography (TLC) showed only one spot, the extinction coefficient differed 4.2% from literature data. The obtained spectrum is similar in shape to the published spectra by Bourne et al. [2] and Wenger et al. [104], but the extinction coefficients differ in magnitude. The maximum extinction coefficients  $\epsilon_{oR}$  obtained in this work and as published in literature are shown in Table 3.2 and the spectra are depicted in Figure 3.11.

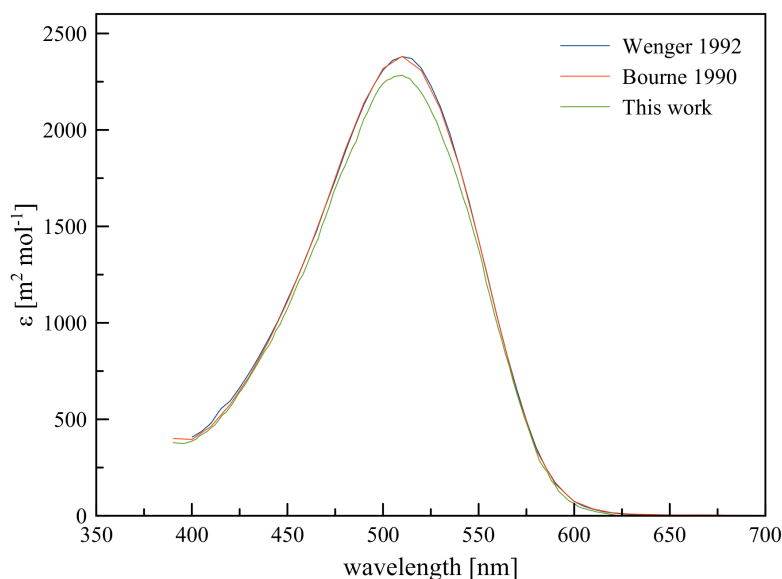


**Figure 3.11:** Absorption spectra of the ortho monoazo dye shows acceptable agreement of this work, Bourne et al. [2] and Wenger et al. [104].

### 2,4-Bis[(4-sulfophenyl)azo]-1-naphthol (S)

The yield of the bisazo dye is the indicator of the mixing quality. It can be obtained from both monoazo isomers by reaction with diazotised sulfanilic acid [2, 90, 104]. The knowledge of the absorption spectra is necessary for an accurate evaluation of the micromixing efficiency of the reactors. Literature has reported many problems in the synthesis and purification, in order to obtain a pure sample of the S-product. Published reference spectra have shown many variations in magnitude of the absorption spectra, but all of them show a saddle shape as shown in Figure 3.12. These differences are referred to problems in isolation, purification and quantification of the dye [90, 104]. Due to the reported problems in synthesis of the ortho-isomer and the S-product, it was decided to use the published extinction coefficients from Bourne et al. [2]. This data was checked by different researches and was also used in other micromixing studies without an own calibration [2, 88, 96, 98]. The used extinction coefficients of all dyes are listed in the appendix in Table 9.14.

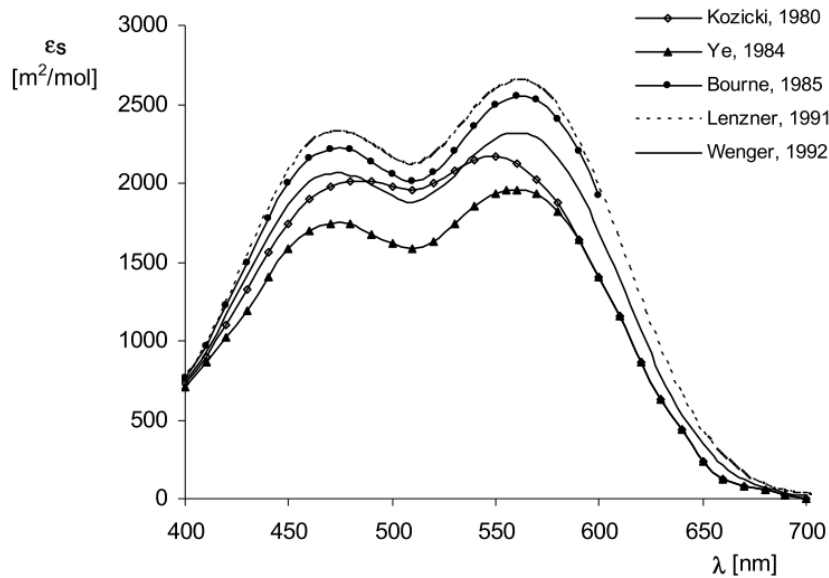


**Figure 3.12:** Different published absorption spectra of the bisazo dye. The differences are referred to problems with isolation, purification, quantification and instability of the pure S-product. This was reported by Wenger et al. [104] and illustrated by Nunes et al. [90].

### 3.3.2 Passive Mixers

The micromixing performance of the before mentioned passive mixers was investigated. Reagent A and B were introduced at different flow rates and a sample of the product solution was taken after three residence times. The product solution was diluted 1+10 with buffer and spectrophotometrically analysed. With a multi-parameter-regression using least square method the concentrations of the three dyes and the yield  $Y_S$  were calculated. The devices are compared with  $Y_S$  and the corresponding Reynolds number which refers to the flow rate. A high yield  $Y_S$  indicates bad mixing.

#### Size-Scaled-Mixers

To investigate the influence of the reactor size, the same mixing geometry in different size-scales was fabricated. The large version was also produced in a medium and a small version with scaling factors of 0.75 and 0.5, respectively. The mixing sensitive reactions were performed for the same flow rates and the results are depicted in Figure 3.13 (left). To compensate the geometry effects, the flow rates were converted to Reynolds numbers associated with the hydraulic diameter of each version, as depicted in Figure 3.13 (right).

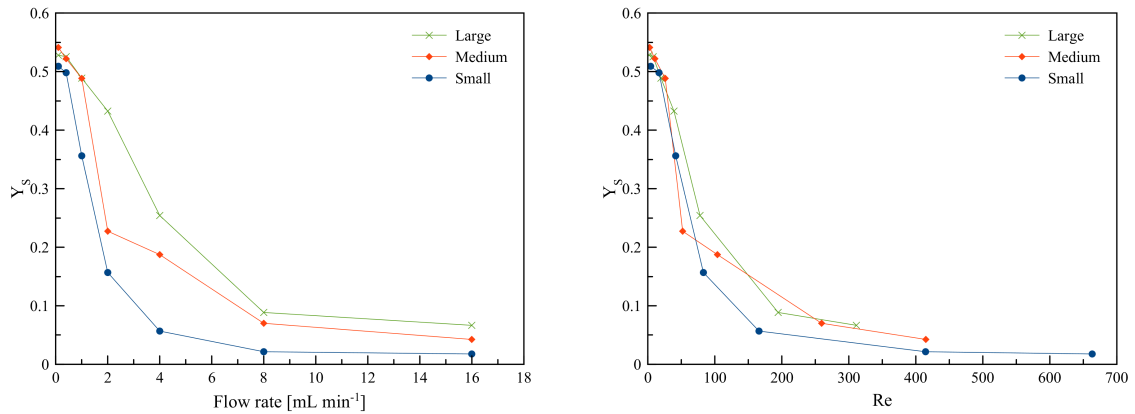


**Figure 3.13:** Experimental results of the bisazo dye yield  $Y_S$  as a function of the flow rate (left) and Reynolds number (right). The three size-scaled-mixers have the same geometry but in different scales. The smallest mixer performs best because of the higher flow velocity.

As expected, small reactors have a better performance at the same flow rate. This can be seen in the left plot in Figure 3.13. At a constant flow rate, the flow velocity is increased, if the channel diameter is reduced. High velocities lead to more turbulences (higher Reynolds number), and as a consequence to a better mixing performance. As shown in the right plot of Figure 3.13 the curves converge, indicating that at same Reynolds numbers the mixing performance is comparable for the size-scaled-mixers.

### Sphere-Mixer

The structure of the sphere-mixer is illustrated in Figure 3.2. The mixing chambers in combination with alternating offset of inlet and outlet of the chambers provide chaotic mixing. This device was made of steel and ceramics, but only the ceramic version was leak proof and able to be investigated. According to Figure 3.14, the bisazo yield is significantly decreased compared to the T-mixer, indicating an enhanced mixing performance of the ceramic sphere-mixer. The mass balance closed within 5% for  $Y_S < 0.4$  and within 17.5% for  $Y_S > 0.4$ .  $Y_S$  approaches zero at  $Re > 300$ , equal to a flow rate of  $10 \text{ mL min}^{-1}$ , indicating a kinetically limited regime. Compared to the smallest version of the size-scaled-mixers, the sphere-mixer performs better, even though the hydraulic diameter of the sphere-mixer is higher.

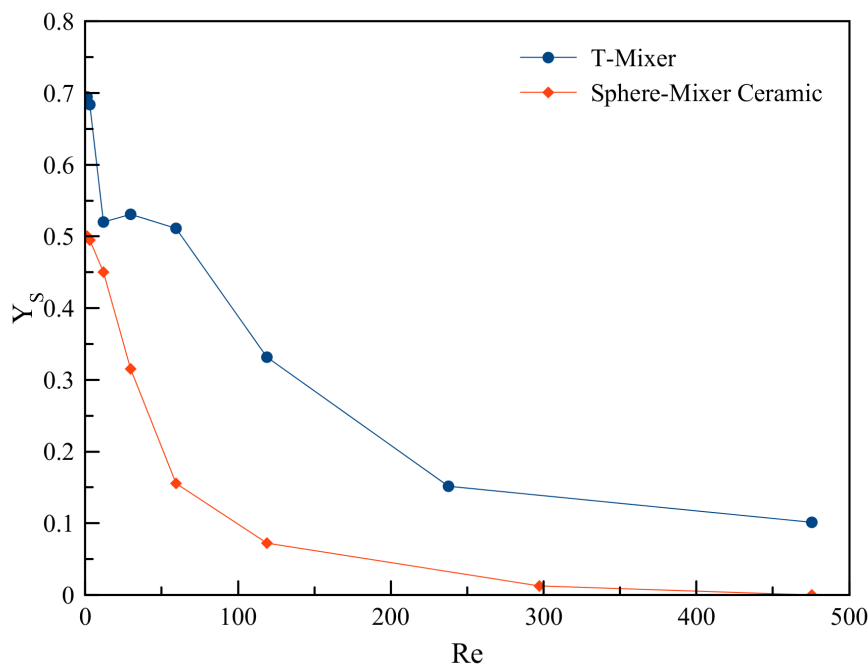


**Figure 3.14:** Experimental results of the bisazo dye yield  $Y_S$  as a function of the Reynolds number for the ceramic sphere-mixer and the standard T-mixer.

### Split-and-Recombine-Reactor (SAR-reactor)

The mixing sensitive reactions described in the experimental section were used to investigate the mixing performance of the SAR-reactor. Therefore different flow rates ( $0.04 \text{ mL min}^{-1}$ ,  $0.1 \text{ mL min}^{-1}$ ,  $0.4 \text{ mL min}^{-1}$ ,  $1 \text{ mL min}^{-1}$ ,  $1.75 \text{ mL min}^{-1}$ ,  $2 \text{ mL min}^{-1}$ ,  $4 \text{ mL min}^{-1}$ ,  $10 \text{ mL min}^{-1}$ ,  $16 \text{ mL min}^{-1}$ ) were used and the yield of the bisazo dye S was determined. Figure 3.15 shows the better performance of the SAR-reactor compared to the T-mixer. At all flow rates, the yield of the bisazo dye  $Y_S$  is lower, indicating more efficient mixing. The mixing point for the inlet streams of the SAR-reactor has a T-mixer-like design. But in difference to a simple T-mixer, the SAR-reactor has a more tangential-like mixing point, followed by a mixing section consisting of split-and-recombine elements. These two factors improve the mixing efficiency and lead to a better performance than the simple T-mixer.

As mentioned before, the devices are meant to be used for the oxidation of Grignard reagents. The selectivity of this reaction is mixing dependent due to its high reaction rate. The given process conditions for the Grignard oxidation are at  $Re = 52$ . Even through the much better performance of the SAR-reactor compared to the T-mixer, the yield of  $Y_S = 0.14$  indicates that the conditions are in an intermediate regime between kinetically controlled ( $Y_S \ll 0.01$ ) and mixing controlled regime ( $Y_S = 1$ ) [23]. As mentioned before, the yield must respect the limits  $0.04 < Y_S < 0.4$  to be reliable. From Figure 3.15 it can be concluded that the values for very low Reynolds numbers can

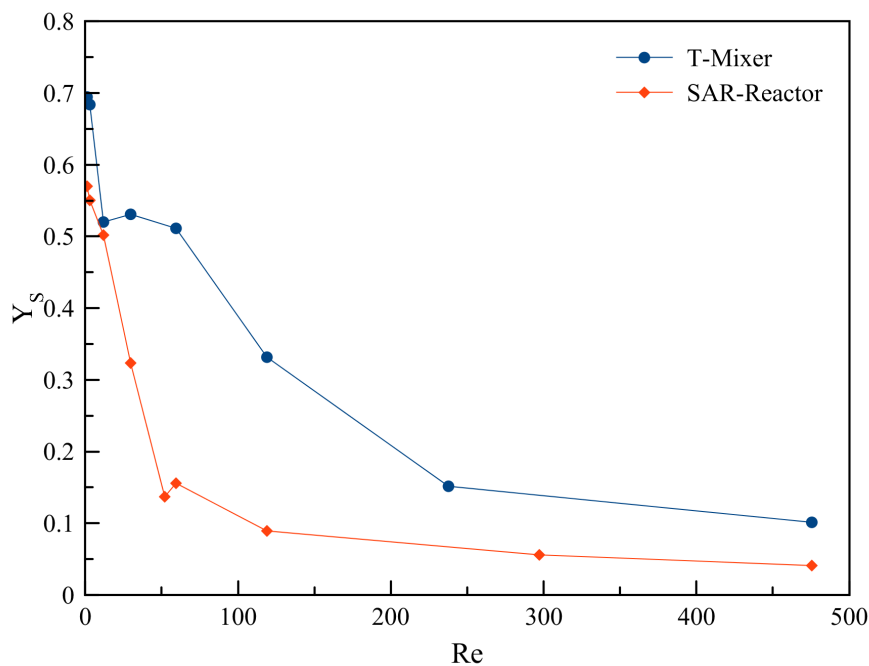


**Figure 3.15:** Experimental results of the bisazo dye yield  $Y_S$  as a function of the Reynolds number for the SAR-reactor and a T-mixer.

only be considered qualitatively.

The checked mass balance closed within  $\pm 8\%$ . It was observed that the error in the mass balance increased with higher yields of the bisazo dye. This indicates that a significant amount of B is not converted to the mentioned dyes and instead unidentified side products are formed [60, 88]. The higher the yield of the S-product gets, the higher is the risk of a reaction with diazonium ions. This leads to a loss of S-product and formation of unstable products [2]. The deviation in the mass balance is systemic and increases with increasing  $Y_S$ , thus the qualitative conclusions of the experiments are still valid [88, 90].

### 3.3.3 Active Mixers - CSTR-Cascade

In contrast to passive mixers, active mixers induce mixing by application of external forces. The advantage is that the mixing efficiency can be influenced independently of the flow rate by adjusting the stirrer speed. Therefore a CSTR-cascade was fabricated and investigated. The CSTR-cascade is placed on a laboratory magnetic stirrer and by setting the RPM of the magnetic stirrer, tiny magnetic spheroids in each vessel start to rotate. The CSTR-cascade v1 is compared with the SAR-reactor and a T-mixer with a connected steel coil with 1/16" OD, 0.03" ID and 1 m length, giving a volume of 0.5 mL. The flow rate is converted into a representative Reynolds number to compare their mixing performance. The set RPM are used for calculation of the stirrer Reynolds number according to

equation 3.1. The real rotational speed of the stirrers differs from the set value because the liquid flow influences the rotation at higher flow rates. It was not possible to check the real rotational speed of the stirrers.

Figure 3.16 depicts the yield of the S product as function of the channel Reynolds number between the vessels. For every flow rate three stirrer speeds, no rotation ( $Re = 0$ ), 500 RPM ( $Re = 53.8$ ) and 1000 RPM ( $Re = 107.5$ ) were analysed. It was observed that at low flow rates stirring has a

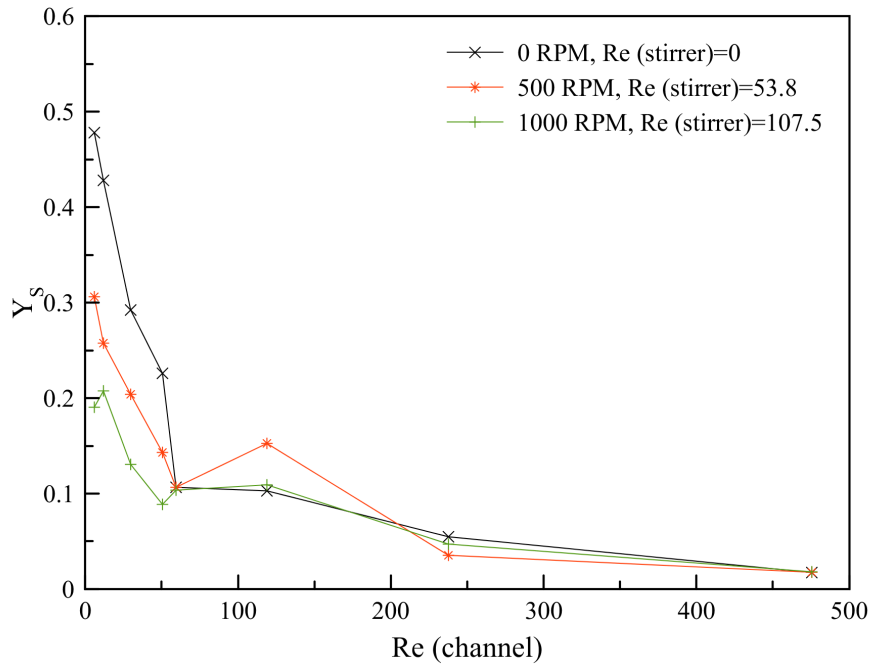


**Figure 3.16:** Experimental results of the bisazo dye yield  $Y_S$  as a function of the Reynolds number referring to the flow rate, for different stirring speeds of the CSTR-cascade v1.

strong effect on the bisazo yield  $Y_S$  as it decreases from 0.48 to 0.19. With higher flow rates, the effect of the stirrer decreases. It becomes negligible at  $Re > 200$  because no significant change of  $Y_S$  with the stirrer speed can be seen. For  $Y_S < 0.4$  the mass balance closed within  $\pm 9\%$ . For  $Re(\text{channel}) = 119$  at 500 RPM the error was  $-17.8\%$ , which explains the deviation from the trend of the curve.

These results show that the CSTR-cascade v1 has a good mixing performance, indicated by a low bisazo yield  $Y_S$ . The advantage is that also at low flow rates the CSTR-cascade v1 mixes better than passive mixers. This favours the application at low flow rates beneficial compared to the SAR-reactor or the T-mixer as illustrated in Figure 3.17.

The CSTR-cascade v1 without stirring has a comparable performance as the SAR-reactor because in this case, they are both passive mixers. The stirrers act as internal mixing structures where the streams pass around the spheroids, which has the same effect as the SAR elements of the SAR-reactor. With induced rotation the mixing performance increases as mentioned above. Especially at low flow

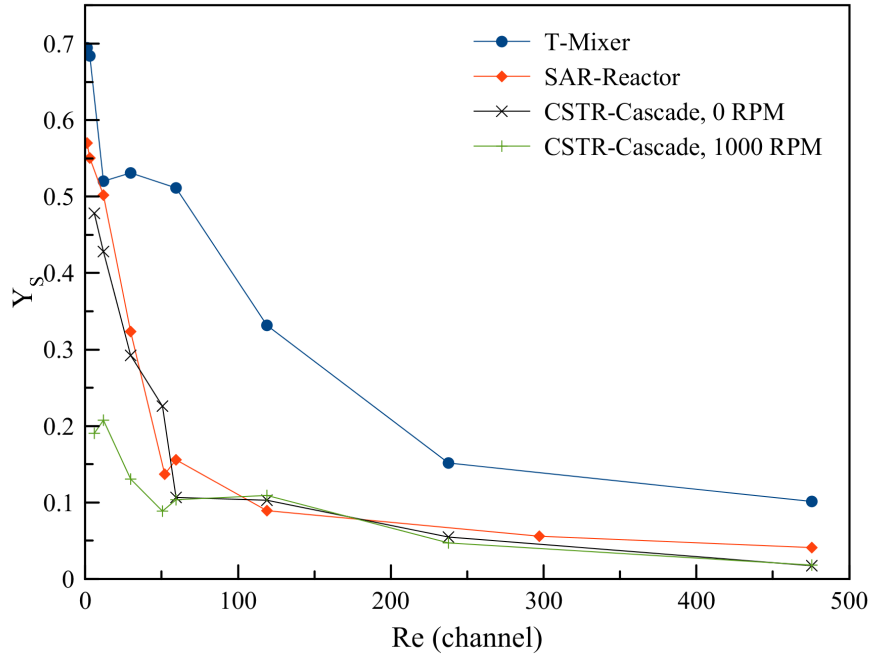


**Figure 3.17:** Experimental results of the bisazo dye yield  $Y_S$  as a function of the Reynolds number referring to the flow rate of T-mixer and SAR-reactor, CSTR-cascade v1 without stirring and with 1000 RPM.

rates this reactor is beneficial.

In a further step the influence of the stirring direction on the bisazo yield was investigated. Therefore mixing sensitive reactions were performed for different flow rates ( $0.4 \text{ mL min}^{-1}$ ,  $1.7 \text{ mL min}^{-1}$  and  $4 \text{ mL min}^{-1}$ ) in clockwise (CW) and counter-clockwise (CCW) rotational direction. Figure 3.18 illustrates the difference of the rotational direction. Because the inlet and outlet are located in a tangential position, the stirrer can turn in the same direction as the inlet flow or against the inlet flow direction. It has to be mentioned that the flow itself can influence the stirrer, which can have an effect of acceleration or deceleration of the rotational speed of the stirrer. This can have an influence on the mixing performance, especially at low flow rates. At higher flow rates the mixing performance is dominated by the flow velocity and the influence of the stirrer becomes negligible.

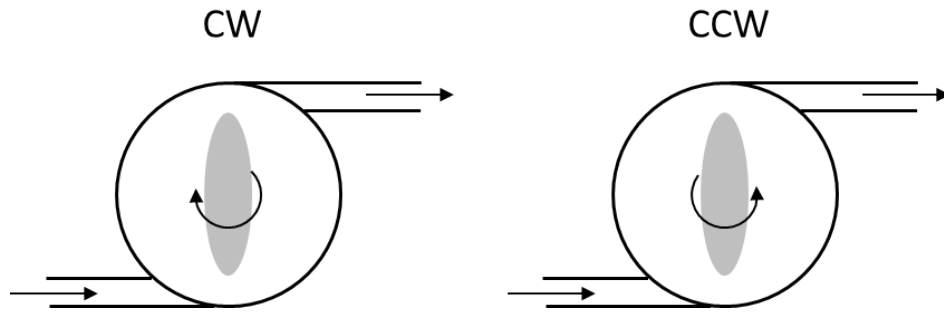


**Figure 3.18:** Schematic illustration of the rotational direction of the stirrer in a vessel: Left: In clockwise rotation, the stirrer acts against the inlet flow. Right: In counter-clockwise rotation, the stirrer turns in direction of the flow at the vessel inlet.

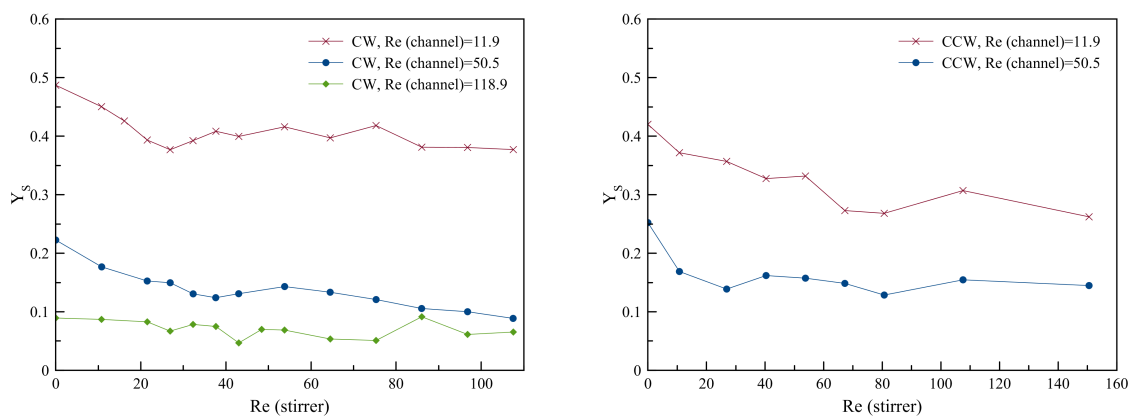


**Figure 3.19:** Experimental results of the bisazo dye yield  $Y_S$  as a function of the stirrer Reynolds number for different channel Reynolds numbers: Left: Clockwise rotation of the stirrer. Right: Counter-clockwise rotation of the stirrer.

The overall performance increases with the rotational speed for both cases as depicted in Figure 3.19. At  $Re = 11.9$  the CCW rotation performed with a lower bisazo yield than the CW rotation. These values can only be used qualitatively because the  $Y_S$  values are sometimes out of the reliable range of  $0.04 < Y_S < 0.4$ . At higher flow rates, the CW rotation performs slightly better as seen at  $Re = 50.5$ . At  $Re = 118.9$ , the rotational speed has no significant influence on the bisazo yield.

### 3.4 Material Influence on the Mixing Performance

The influences of the material and the fabrication technique on the performance of the devices are of major interest for the application and design of micro reactors. As mentioned in section 2.3, both materials are compatible with organic solvents and have high mechanical strength and temperature resistance. Ceramics are slightly better in thermal and chemical resistance (i.e. involved corrosive

reactants), which qualifies them for applications that can not be covered by stainless steel [37, 55]. Steel parts fabricated by SLM have a higher surface roughness than ceramic parts, which can influence the mixing performance of the devices. Therefore two designs, CSTR-cascade v1 and sphere-mixer, were manufactured from stainless steel and ceramics via SLM or LCM, respectively. Unfortunately the steel version of the sphere-mixer leaked in the mixing section, therefore, it was not analysed.

The influence of the surface roughness was investigated with the CSTR-cascade v1 made of steel and ceramics. Mixing sensitive reactions were performed for both materials and the results are illustrated in Figure 3.20. The used flow rate was  $1.7 \text{ mL min}^{-1}$  corresponding to the Reynolds number  $Re = 52$  of the Grignard oxidation reaction conditions. Stirring was induced by a laboratory magnetic stirrer which was set between 0 RPM and 1000 RPM. The results indicated a similar mixing efficiency for both materials. Without stirring the bisazo yields were  $Y_S = 0.22$  and  $Y_S = 0.25$  for steel and ceramics respectively. Stirring reduced the yield to  $Y_S = 0.09$  at 1000 RPM for both materials. The ceramic CSTR-cascade v1 gave slightly lower yields than the steel CSTR-cascade v1, but a significant difference was not observed. The mass balance closed within 6 % for all operation points indicating reliable results. This is either referred to the sensitivity of the experimental method or the surface roughness has no significant influence.

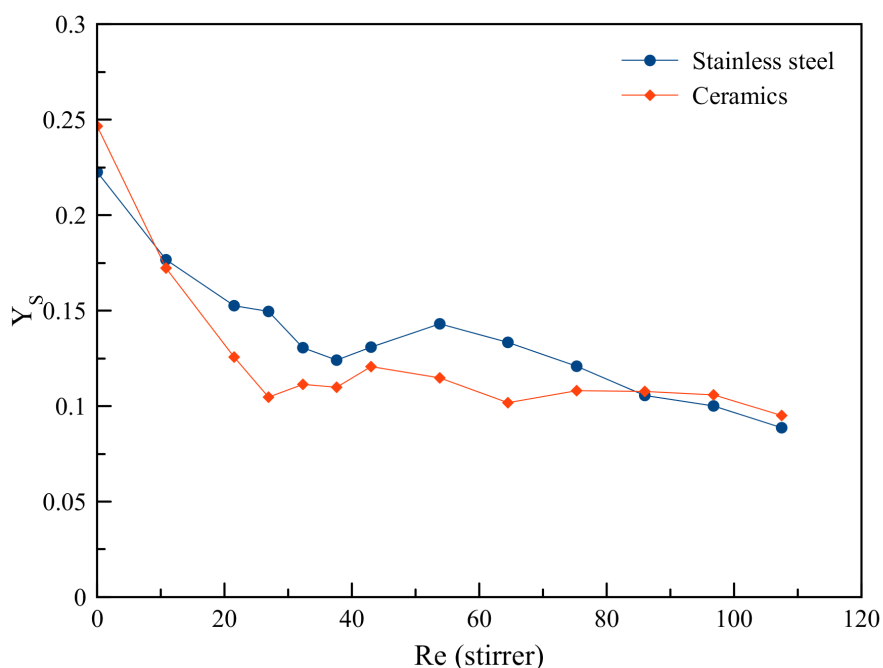


**Figure 3.20:** Experimental results of the bisazo dye yield  $Y_S$  as a function of the stirrer Reynolds number for CSTR-cascade v1 made of steel and ceramics. The flow rate was  $1.7 \text{ mL min}^{-1}$  corresponding to the Reynolds number for the model reaction conditions  $Re = 52$ . The stirrer speed was set between 0 RPM and 1000 RPM.

In section 3.2.2 the RTD results of the CSTR-cascade v1 made of both materials are depicted in Figure 3.7 and Figure 3.8. The calculated Bodenstein numbers of the ceramic version are slightly higher than the steel version. This is also attributed to the smoother surface of the ceramic parts. Roughness induces dispersion and as a result the Bodenstein number is lowered.

### 3.5 Optimisation Approaches of the CSTR-Cascade v1

The design and geometry of the CSTR-cascade v1 was optimised to ensure a good mixing performance and improve handling of the device. Therefore, the vessels of the CSTR-cascade v2 were sheathed with a cooling shell as depicted in Figure 3.21. This shell can be directly connected to a thermostat, ensuring simple handling of the device and a constant temperature inside the vessels.

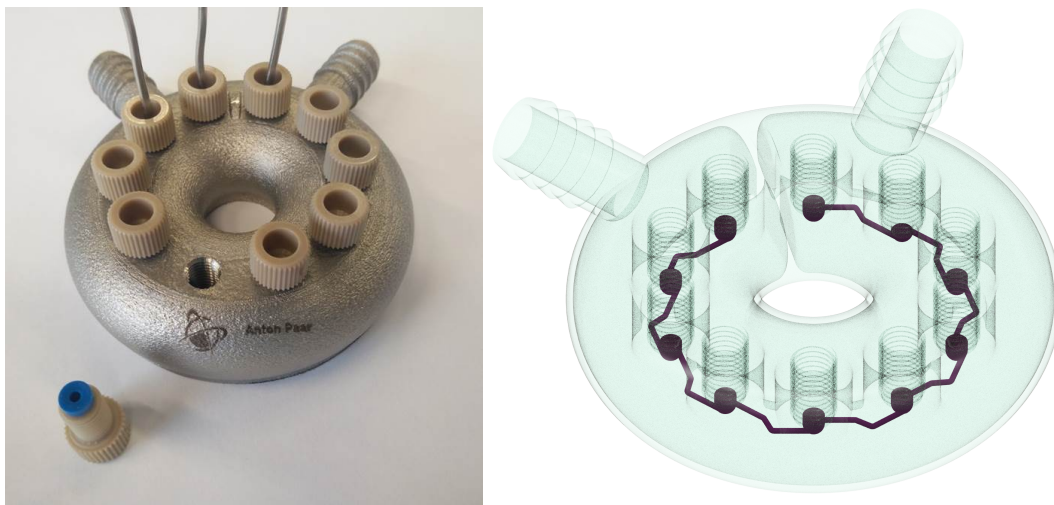


**Figure 3.21:** Left: Optimised CSTR-cascade v2 with cooling shell and new flat bottom fittings. Right: Rendered image of the new designed CSTR-cascade v2 with highlighted channels and vessels.

The first approach of the CSTR-cascade v1 used conical 10-32 HPLC fittings which resulted in a dead volume between fitting and vessel wall, highlighted in Figure 3.22a. This dead volume is disadvantageous for the reactor performance. It was not possible to reduce the vessel diameter because the used stirrers had to be inserted after 3D printing. To overcome this problem, the type of fitting was changed from conical to flat bottom fittings for the optimised CSTR-cascade v2. A steel version of this design was manufactured.

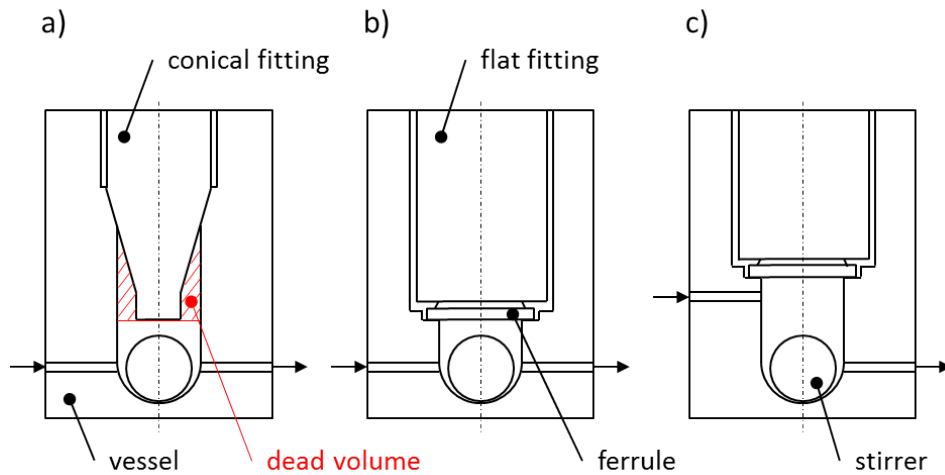


**Figure 3.22:** a) Scheme of the CSTR vessel with stirrer and conical fitting. Between fitting and vessel a dead volume is generated. b) Scheme of the new design with flat bottom fittings and an additional ferrule. The dead volume was removed. c) To ensure enough space for analytical probes the vessel height was increased. The inlet channel was moved to a higher position to ensure mixing in the whole vessel.

The design of the CSTR-cascade is also meant to insert analytical probes through the fittings in each vessel. To ensure enough space for the sensors, the height of the vessels was increased as shown in Figure 3.22c. This resulted in a higher reactor volume and the possibility of poor mixing in the top region. To provide sufficient mixing in the upper part of the vessel, the inlet channel was moved to a higher position. This design was not fabricated yet. Figure 3.23 shows the new 1/4-28" flat bottom HPLC fitting and an additional ferrule which is pressed against a sealing area provided by the vessel design, depicted in Figure 3.22b. With this design, the dead volume at the top of the vessel was eliminated.



**Figure 3.23:** Right: First the conical HPLC fittings were used which generated a dead volume. Left: The new flat bottom fittings have an additional ferrule as sealing, which eliminated the dead volume.

The micromixing performance of the new CSTR-cascade v2, with the design of Figure 3.22b, was checked and the results are depicted in Figure 3.24. At low stirring speeds,  $Y_S$  of the optimised

design is lower. This indicates that the dead volume of the CSTR-cascade v1 had an influence on the micromixing performance for low rotational speeds.

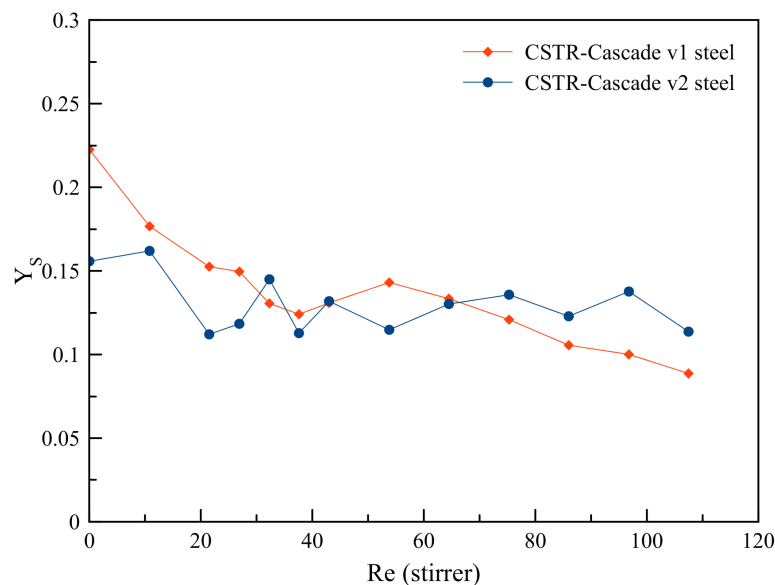


**Figure 3.24:** Experimental results of the bisazo dye yield  $Y_s$  as a function of the stirrer Reynolds number for the optimised CSTR-cascade v2 and the first CSTR-cascade v1, both made of steel. The flow rate was  $1.7 \text{ mL min}^{-1}$ . The stirrer speed was chosen between 0 RPM and 1000 RPM in clockwise direction.

### 3.6 Kinetic Measurements in Flow

For detailed reactor design the intrinsic kinetics of a chemical reaction need to be known. This requires a kinetic measurement without any limitations due to heat or mass transfer, which is challenging for very fast reactions. The described mixing experiments and RTD measurements of the designed reactors showed a good mixing performance. The results indicated a low mixing limitation and allowed the use of the reactors for kinetic measurements of the model reaction mentioned in section 2.6.

As model reaction the aerobic oxidation of Grignard reagents to the corresponding phenols was chosen. The oxidation of a Grignard reagents involved 4-chlorophenylmagnesium bromide and pure oxygen, both dissolved in 2-methyl-THF. This reaction was carried out at  $1 \text{ mL min}^{-1}$  2-methyl-THF,  $1.5 \text{ mL min}^{-1}$  oxygen (at norm conditions) and  $0.126 \text{ mL min}^{-1}$  of the Grignard reagent, resulting in a stoichiometric ratio of 1:1 of oxygen and reagent. The conditions were  $0^\circ\text{C}$  and 7 bar. The RTD and mixing sensitive reaction were carried out at equal Reynolds numbers to obtain similar flow behaviour. The experimental set-up for kinetic measurements is depicted in Figure 3.25. One equivalent of oxygen is dosed with an MFC and mixed with 2-methyl-THF to absorb  $\text{O}_2$  in a 1 mL steel coil. This feed is pumped with pump 1. The second feed is a 1 M solution of Grignard reagent

dissolved in 2-methyl-THF and is added to the first feed in the mixing section of the reactor. The Grignard reagent is placed in a 1 mL sample loop and injected with a 6-port injection valve by pump 2, using 2-methyl-THF. The streams are combined in the mixing section of the SAR-reactor which was used for these tests. Downstream, a BPR ensures a constant system pressure of 7 bar, allowing the whole oxygen to dissolve in the solvent. Afterwards the reaction is quenched by 0.5 M hydrochloric acid. Absorption coil and reactor were placed in a water bath of a thermostat to ensure a constant temperature. The capillaries upstream and downstream of the BPR were made of transparent PFA to check for oxygen bubbles. All other coils and capillaries were made of stainless steel with 1/16" OD and 0.03" ID.

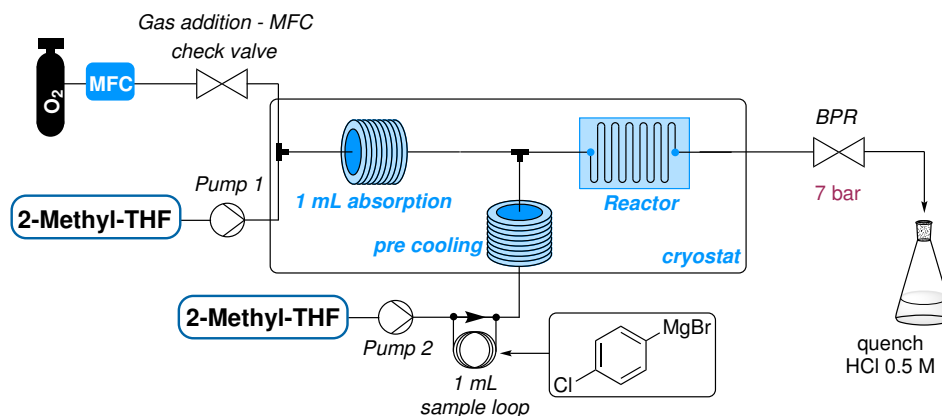


**Figure 3.25:** Set-up for kinetic measurements of an oxidation of Grignard reagents in flow. Adapted from [100].

Kinetics can be investigated by performing the reaction at different temperatures and then analyse the product solution with HPLC or GC-MS to determine the product concentrations. A scale at the outlet was used to check the flow rate over time. Pump 1, pump 2 and the scale were controlled via a LabVIEW program which sets the flow rates of both pumps and records pressures, set flow rates as well as a measured flow rate of the scale.

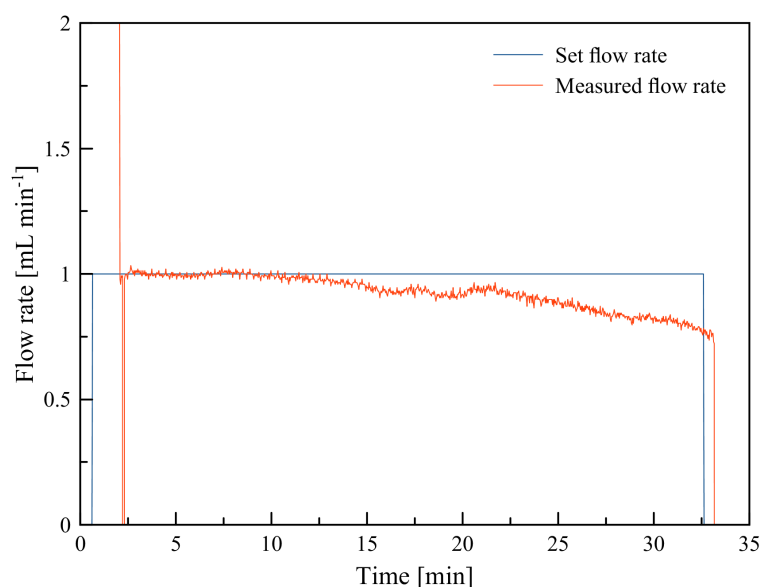
Because the evaluation of the mixing performance gave promising results, the SAR-reactor was used for kinetic measurements of the Grignard oxidation. After the set-up was assembled further pre-tests to check tightness, pressure and flow behaviour of the complex system were performed. While performing these tests several problems occurred.

Figure 3.26 depicts the set flow rate and the measured flow rate over time of one experiment. To simplify the system no oxygen was introduced and only pump 1 and a BPR with 5 bar were used. The oxygen and the reagent inlet were plugged. Pump 1 was set to a constant flow rate of  $1 \text{ mL min}^{-1}$  of 2-methyl-THF and the flow rate was measured with a scale at the outlet. Over 30 min the flow rate decreased from  $1 \text{ mL min}^{-1}$  to  $0.77 \text{ mL min}^{-1}$  which is a relative decrease of 23%. No leaks were found and the averaged system pressure was constant for the whole time. This decrease may refer to swelling of seals in the pump due to 2-methyl-THF. It seems that the used HPLC pumps

**Table 3.3:** Set flow rates of test runs for kinetic measurements.

Stream	Flow rate [mL/min]
Pump 1	0.5
Pump 2	0.063
Oxygen	0.5

are not suitable for long term experiments with this solvent.

**Figure 3.26:** Set and measured flow rate of 2-methyl-THF against time.

To remove the solvent effect on the pumps, isopropyl alcohol was used in further tests which showed constant flow rates. In a next step the system was equipped with oxygen and both pumps were connected to the system. An adjustable BPR was set to 8 bar and the set flow rates are listed in Table 3.3. Figure 3.27 depicts the pressure at pump 1 over time. The pressure periodically fluctuated and over time it increased. In this set-up, no check valve between system and MFC was used. The MFC has a maximum pressure of 10 bar and when the system pressure was higher, the pressure was released manually by opening the purge valve of the pump. This was done to avoid damage to the MFC and is demonstrated with the instant pressure drops in Figure 3.27. A constant pressure was not reached within three hours. The periodic fluctuation can be attributed to the heterogeneous system because the used BPR is not meant to be used for two phase applications. Undissolved oxygen bubbles can act as springs which also explains the fluctuating pressure.

Further tests were made with water and oxygen in order to save solvent. To prevent damage to the MFC, a check valve was implemented between mixing point and MFC. The BPR was set

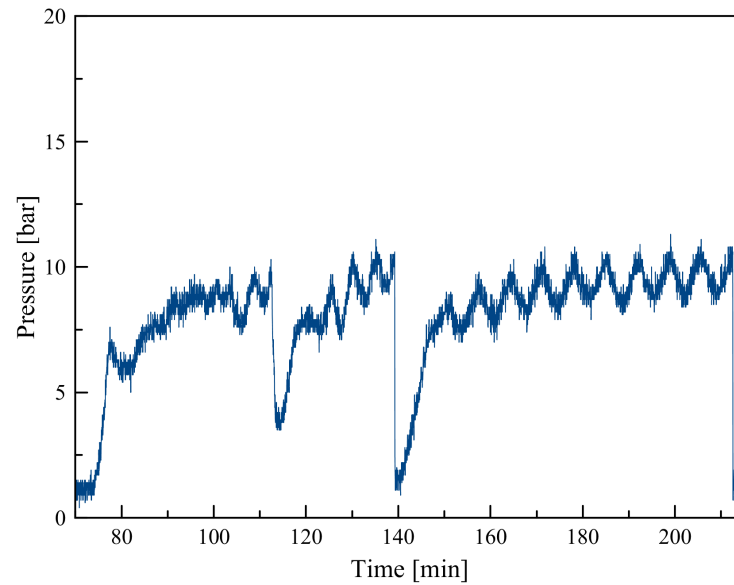


**Figure 3.27:** Pressure measured at pump 1 of a test run with isopropyl alcohol and oxygen.

to 8 bar and the set flow rates are listed in Table 3.3. It was observed that the oxygen was fully dissolved in the system. After the BPR, slugs were formed due to the atmospheric pressure in this region. Unfortunately, within 150 min the system pressure did not reach a steady value as depicted in Figure 3.28. After starting at around 8 bar the pressure increased until it reached around 11 bar. Then the pressure dropped down to the starting value and increased again. It seemed like something plugged the system which was blown out at some pressure but still the system did not reach a steady state. Possible reasons are contamination of the channels by particles from previous applications or non-removed particles from the fabrication process. Again, maybe the used BPR was not suitable for two phase applications.

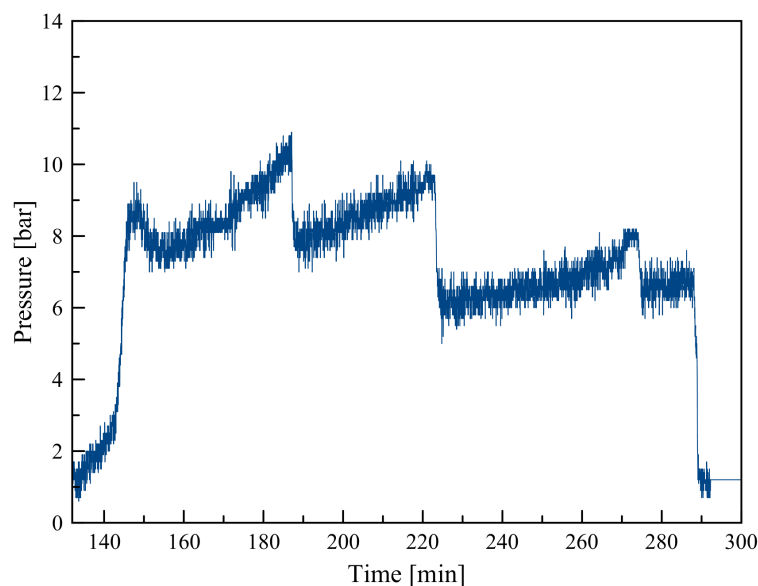


**Figure 3.28:** Pressure measured at pump 2 of a test run with water and oxygen. The pressure did not reach a steady value and after shifting upwards, it dropped down instantly at some point. This behaviour is attributed to the BPR which is not meant to be used for heterogeneous systems.

These test runs showed that further improvement is necessary until kinetics can be determined in flow. Many problems occurred due to the heterogeneous system which complicated to keep the system pressure constant. If the system pressure is not reached yet, but oxygen is already introduced, it may not be fully dissolved. In this case the generated slugs act as springs which interfere with the performance of the BPR. A BPR specially designed for heterogeneous applications could lead to a steady system pressure.

This set-up consists of two pumps and an MFC, which results in complex pressure and flow conditions because the equipment influences each other. The used HPLC pumps suffer from solvent incompatibility and pulsations. High pressure syringe pumps, which run with less pulsation, would be an alternative. This type of pumps allows the use of aggressive solvents because the only wetted parts are the syringes which can be easily exchanged. As the syringes run out of liquid over time, a fully continuous process is hard to realise with syringe pumps. Another alternative would be gear pumps with an attached MFC for liquids. In general, more sensors with inline monitoring and regulation of critical parameters can lead to a smoother process regulation. This has the drawbacks of costs, complexity and the risk of over regulation, resulting in oscillating parameters due to inter dependencies.

---

## 4 Conclusion and Outlook

The aim of this thesis was the experimental characterisation of 3D printed microreactors made of stainless steel and ceramics. To achieve the objectives, first the literature concerning MRS, mixing, mixing characterisation and additive manufacturing was reviewed. Characterisation of the mixing performance of different designs was done with a set of mixing sensitive reactions. Additionally, the RTD of two designs was investigated. To gain information about the influence of the used material and manufacturing method, experiments were performed for the same designs made of steel and ceramics. Based on the obtained information, optimisation approaches of the designs were developed. Finally, a set-up for the determination of reaction kinetics in flow, using the 3D printed microreactors was developed.

The used 3D printing processes in this thesis were SLM and LCM for stainless steel and ceramics, respectively. Steel and ceramics have a better resistance against chemicals, temperature and pressure than PDMS which is the usual material. Parts made of steel can be post-processed, e.g. by welding or thread cutting, to ensure proper connection to other equipment. Contrary, this is not possible for ceramics, but it is possible to directly print a thread which allows the connection of standard HPLC fittings.

For the novel 3D printed microreactors the concepts of active and passive mixing were applied using different designs. As passive mixer designs a croissant-shaped mixer in three size-scales, a sphere-mixer with spherical mixing chambers and a SAR-reactor with multiple SAR-elements were fabricated. Active mixing is done with a CSTR-cascade v1 consisting of ten connected CSTR-vessels with internal stirrers. The CSTR-cascade v1 and the sphere-mixer were made of stainless steel and ceramics to evaluate influences based on material and fabrication process. Unfortunately the steel version of the sphere-mixer was not leak proof.

To evaluate the macromixing performance of the SAR-reactor and the CSTR-cascade v1, the RTD was determined. Therefore a step input with anisole as tracer was done for different flow rates and rotational speeds. The Bodenstein number was calculated as a measure for plug flow behaviour and was determined according to the dispersion model. The SAR-reactor has plug flow behaviour at a flow rate of  $1.7 \text{ mL min}^{-1}$ . The CSTR-cascade v1 has Bodenstein numbers of approximately 20 indicating high back mixing. The ceramic version has slightly higher Bodenstein numbers which

is referred to the smoother surface of ceramics compared to steel. Determination of the reactor volume using the mean residence time, CAD and gravimetric data agreed well for the CSTR-cascades.

The micromixing performance was characterised with a mixing sensitive diazo coupling involving 1-naphthol and diazotised sulfanilic acid. Synthesis and purification of the reaction products was not satisfying and prohibited a calibration. Therefore, literature data [2] was used for analysis. The obtained results indicate that all designs show a better mixing performance than a standard T-mixer which was used as benchmark. The size-scaled mixers show better mixing performance for the smallest version. This is because at equal flow rates the flow velocity increases for smaller channel diameters, which is beneficial for the mixing performance. The best mixing performance is achieved with the sphere-mixer. The SAR-reactor and the CSTR-cascade show a comparable good performance. Especially at low flow rates, the rotating stirrers increase the mixing performance significantly. In general, the mixing performance increases with the rotational speed, but at higher flow rates the flow velocity becomes the dominant mixing effect. Ceramics showed a slightly better micromixing performance than steel, which is surprising but might be attributed to the smoother surface.

To optimise the design of the CSTR-cascade v1, the type of fitting was changed from a conical shaped to a flat bottom HPLC fitting for the optimised CSTR-cascade v2. This reduced the dead volume in each vessel resulting in a better micromixing performance at low flow rates. A cooling shell was designed to allow direct connection of the CSTR-cascade v2 to a thermostat. To provide enough space for sensor probes, the vessels were designed higher.

For detailed reactor design the intrinsic kinetics without any heat or mass transfer limitations are necessary. The designed mixers are well suited for kinetic measurements. A set-up for kinetic measurements of a fast aerobic oxidation of Grignard reagents was designed. Pre-tests of the set-up concerning tightness and solvent compatibility lead to problems. A steady state with constant pressure and flow rate was not achieved for different solvents and process parameters. This is attributed to a low compatibility of the solvent for the chosen model reaction with the HPLC pumps and the complexity of the whole system. Without a steady state, measurements of the kinetic properties are impossible.

Although further improvement is necessary, the objectives of this thesis were accomplished. All in all, a method to characterise the micromixing performance of mixers was successfully implemented. New, improved designs can be investigated and compared to optimise the geometry of active and passive mixers. The use of stainless steel and ceramics offers the possibility of extreme process conditions which were not accessible yet. The CSTR-cascade can be equipped with multiple analysis tools to investigate reactions in more detail, providing data for effective reactor design.

---

## 5 Experimental

### 5.1 Equipment

#### UV/VIS Spectrophotometer

An Avantes AvaLight-DS-DUV, equipped with a deuterium lamp, was used as light source for UV/VIS measurements and an Avantes AvaSpec-ULS2048 was used as detector. They were connected with two optic fibres FC-UV400-1-FIA-SR and a Flow Cell-Z-10 from Avantes with 10 mm optical path length.

#### Pumps

To ensure a constant flow rate with low pulsation, Landgraf Laborsysteme Spritzenpumpe LA-120, equipped with HSW 50 mL(60 mL) Soft-Ject Luer syringes were used for RTD and mixing sensitive reactions.

The set-up for kinetic measurements was equipped with two Knauer Azura P4.1S V6870 HPLC pumps. Pump 1 had a 50 mL titanium pump head. Pump 2 had a 10 mL stainless steel pump head.

#### Laboratory Magnetic Stirrer

To set exact rotational speeds for experiments with the CSTR-cascade, an IKA RCT Standard laboratory magnetic stirrer was used. The RPM are digitally displayed and can be set between 0 RPM and 1400 RPM in steps of 10 RPM.

#### 6-Port Injection Valve

For injection of RTD-tracer and the injection of Grignard reagent in kinetic measurements, a 6-Port Medium Pressure Injection Valve V-450 from IDEX Health & Science LLC was used.

#### Mass Flow Controller

The oxygen stream for kinetic measurements was controlled with a mass flow controller from Vögtlin instruments, type GSC-A9SA-DD21 with a range from 0 mL min<sup>-1</sup> to 25 mL min<sup>-1</sup>.

## 5.2 Preparation of Reagents

### Buffer

222.2 mmol (23.551 g) of  $\text{Na}_2\text{CO}_3$  and 222.2 mmol (18.667 g) of  $\text{NaHCO}_3$  were dissolved in 1 L deionised water. This resulted in a pH of 9.9 and an ionic strength of 888.8 mM. The buffer was used to dissolve 1-naphthol for the mixing sensitive reactions. For spectrophotometric measurements the buffer stock was diluted 1+1 with deionised water, resulting in an ionic strength of 444.4 mM.

### Reagent A - 1-Naphthol Solution

A 1.2 mM solution of 1-naphthol was prepared by dissolving 0.12 mmol (17.3 mg) 1-naphthol in 100 mL carbonate/bicarbonate buffer (each 222.2 mM) at room temperature, under intense stirring and exclusion of light. Dissolution took about one hour. This solution was prepared fresh every morning before the experiments, stored cool and dark, thus excluding any decomposition [88, 96].

### Reagent B - Diazotised Sulfanilic Acid

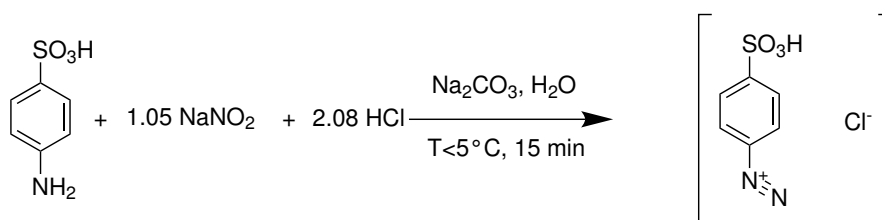


**Figure 5.1:** Reaction scheme for the preparation of diazotatised sulfanilic acid according to [96].

Diazotised sulfanilic acid was prepared as a 10 mM stock solution. For experiments, the stock solution was diluted 1+9 with deionised water, ensuring a 1 mM reaction solution B.

For the 10 mM stock, 0.5 mmol (53 mg)  $\text{Na}_2\text{CO}_3$  were dissolved in 30 mL water. 1 mmol (173.2 mg) of sulfanilic acid was added and the solution was cooled in an ice bath. After dissolution, another 20 mL water and 1.05 mmol (72.4 mg) of sodium nitrite ( $\text{NaNO}_2$ ) were added and dissolved, resulting in a pale yellow solution. 2.08 mmol (2.08 mL) of 1 M hydrochloric acid were added dropwise and stirred for 15 minutes, keeping the temperature below  $5^\circ\text{C}$ . Excess of nitrite was destroyed by addition of 0.05 mmol (4.9 mg) sulphamic acid and stirring for 10 minutes. The mixture was filled up to a volume of 100 mL with water. This solution was prepared fresh every morning before the experiments, stored cool and dark, thus excluding any decomposition [96].

## 4-[(4-Sulfo-phenyl)azo]-1-naphthol (p-R)

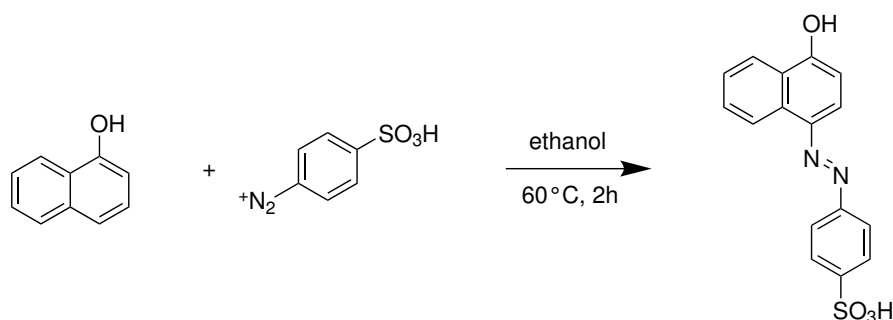


**Figure 5.2:** Reaction scheme for synthesis of the para-R-product according to [2].

7 mmol sulfanilic acid were diazotised and dropwise added to 7 mmol (1 g) 1-naphthol, dissolved in 5 mL ethanol. The mixture instantaneously turned dark brown-red and was heated up to 60 °C for two hours. The mixture was cooled to room temperature within 4 hours to induce precipitation. The dark red-green precipitate was separated by filtration and rinsed with acetone. Purification was done by triple recrystallisation from ethanol/water (50:50 v/v) [2, 105]. To achieve sufficient purity, the dried product was rinsed multiple times with ethanol and water (50:50 v/v). TLC on silica gel 60  $F_{254}$  showed one spot at  $R_f = 0.8$  under UV light, with ethyl acetate and methanol as eluent (1.8:1 v/v) [90]. The product is obtained as the free acid with a molecular weight of  $328.34 \text{ g mol}^{-1}$  [2, 90, 104]. Extinction coefficients are listed in the appendix (Table 9.14).

## 2-[(4-Sulfo-phenyl)azo]-1-naphthol (o-R)

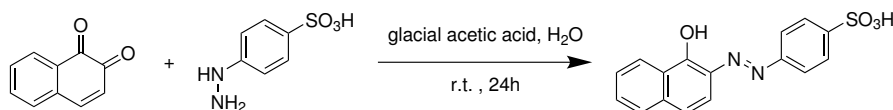


**Figure 5.3:** Reaction scheme for synthesis of the ortho-R-product according to [2].

A suspension of 3.75 mmol (773 mg) 4-hydrazino benzene sulphonic acid hemihydrate in 2 mL deionised water was prepared. Another suspension of 3.75 mmol (593 mg) 1,2-naphthoquinone in 6 g glacial acetic acid was prepared and added to the first suspension, forming a dark red suspension. The mixture was stirred for 24 h at room temperature. Precipitated product was dissolved by addition of approximately 1 mL water and unreacted reagents were separated by filtration. The dye was precipitated by addition of sodium chloride and filtered to remove water soluble impurities. Purification was done by hot filtration and recrystallisation from water. Therefore the solid product was dissolved in a minimum amount of hot water and filtered. The solution was slowly cooled to room temperature, later in an ice bath. The solution was filtered and the solid was washed with cold water [2, 90]. TLC on silica gel 60  $F_{254}$  showed one spot at  $R_f = 0.72$  under UV light, with

ethyl acetate and methanol as eluent (1.8:1 v/v) [90]. The product is obtained as the mono sodium salt with a molecular weight of  $350.33 \text{ g mol}^{-1}$  [2, 90, 104]. Extinction coefficients are listed in the appendix in Table 9.14.

### 5.3 UV/VIS Calibration of the Dyes

Calibration solutions of the dyes contained up to  $0.05 \text{ mol m}^{-3}$  dye, in a carbonate/bicarbonate (each  $111.1 \text{ mM}$ ) buffer with pH 9.9 and ionic strength of  $444.4 \text{ mM}$  at  $25 \text{ }^\circ\text{C}$ . The absorption was measured at wavelengths from  $350 \text{ nm}$  to  $700 \text{ nm}$  in steps of  $2 \text{ nm}$ . A baseline was measured with pure buffer.

### 5.4 Mixing Sensitive Reactions

Mixing reactions were performed with a  $1.2 \text{ mM}$  1-naphthol solution in a carbonate/bicarbonate buffer (pH 9.9, ionic strength  $888.8 \text{ mM}$ ) (Solution A) and a  $1 \text{ mM}$  solution of diazotised sulfanilic acid (Solution B). The experimental set-up is shown in Figure 3.9 and the reaction system in Figure 2.18. Equal volumetric flow rates were achieved by the use of a syringe pump, containing both solutions in separate syringes. The microfluidic devices and the pump were connected with capillaries ( $1/16''$  OD,  $0.03''$  ID) and standard HPLC fittings. After the microfluidic devices, the product solution of each operation point was collected. About  $1 \text{ mL}$  was sampled and stored dark until analysis. To reach a steady state, the system was flushed for at least three residence times before taking a sample.

For experiments with the CSTR-cascade, the first vessel was connected with 1-naphthol and the coupling reaction started in the second vessel, by addition of diazotised sulfanilic acid.

#### Evaluation of Mixing Sensitive Reactions

For UV/VIS-measurements,  $0.5 \text{ mL}$  of the product solution were diluted with  $5 \text{ mL}$  buffer (pH 9.9, ionic strength  $444.4 \text{ mM}$ ), to achieve a concentration in the measurable range of the Avantes flow cell, being approximately  $0.04 \text{ mM}$ . In the AVASOFT software, the 'Integration Time' was set to  $5 \text{ ms}$  and 'Averaging' was set to 500. Dark and light spectra were recorded with buffer (pH 9.9, ionic strength  $444.4 \text{ mM}$ ). The measured absorption was exported at wavelengths between  $390 \text{ nm}$  and  $700 \text{ nm}$  with intervals of  $10 \text{ nm}$ . The concentration of each dye was determined by measuring the total absorption of the samples. The total absorption is given by [2]:

$$A = \varepsilon_{pR} \cdot c_{pR} \cdot l + \varepsilon_{oR} \cdot c_{oR} \cdot l + \varepsilon_S \cdot c_S \cdot l \quad (5.1)$$

where  $\varepsilon$  is the molar extinction coefficient of a dye at a specific wavelength,  $c$  is the dye concentration and  $l$  is optical path length. By knowing the extinction coefficients of all components for each measured wavelength, it is possible to calculate each concentration using standard-multi-parameter-regression with least square fitting method. This was done using a MATLAB

code which is given in the appendix (Section 9.7). Equation 5.1 can be applied, if Lambert-Beer law is valid. This is the case for independently absorbing components and absorption in the range between 0.1 and 1 [96].

Due to overlapping of the absorption spectra, UV/VIS-analyses gives inadequate resolution between the monoazo dyes (p-R, o-R). Bourne et al. [2] proved with HPLC analysis that the sum of monoazo dyes can be determined correctly with spectrophotometric analysis.

## 5.5 Residence Time Distribution

A syringe pump was equipped with two syringes, containing either solvent or tracer. A connected 6-port injection valve enabled the injection of tracer into the microfluidic device, which was detected with an inline UV/VIS flow cell at the outlet of the reactor. Solvent was a mixture of 12 wt% ethanol in water. As tracer 0.006 v% anisole in before mentioned solvent was used. A baseline correction was done by measurement of the absorption, at wavelengths where anisole does not absorb light (500 nm-506 nm). In AVASOFT the 'Integration Time' was set to 1.05 ms and 'Averaging' was set to 500. Values were saved every 400 ms. The set-up is shown in Figure 3.5. To perform either a step input or a pulse input, the injection valve needs to be connected properly as shown in Figure 5.4. For the step input the reactor input was switched from zero tracer to a constant concentration of tracer.

The SAR-reactor was connected with one inlet, while the other one was blocked. The 6-port injection valve was connected with the first vessel of the CSTR-cascade with a 3 cm long steel capillary with 1/16" OD and 0.03" ID.

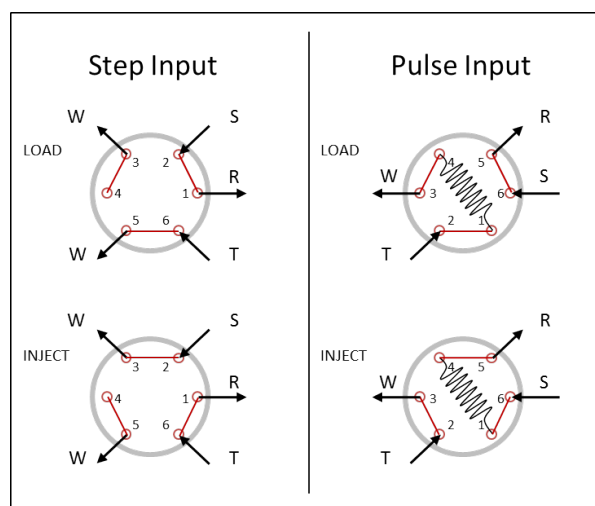


**Figure 5.4:** Switch positions of the 6-port injection valve. A step input switches from no tracer to a constant concentration of tracer. With a sample loop, a defined amount of tracer is injected, called a pulse input. (S) Solvent, (T) Tracer, (R) Reactor, (W) Waste.

---

## 6 References

- [1] D. M. Roberge, L. Ducry, N. Bieler, P. Cretton, B. Zimmermann, “Microreactor Technology : A Revolution for the Fine Chemical and Pharmaceutical Industries ?”, *Chemical Engineering and Technology* **2005**, *28*, 318–323.
- [2] J. R. Bourne, O. M. Kut, J. Lenzner, H. Maire, “Kinetics of the Diazo Coupling between 1-Naphthol and Diazotized Sulfanilic Acid”, *Industrial and Engineering Chemistry Research* **1990**, *29*, 1761–1765.
- [3] S. L. Lee, T. F. O’Connor, X. Yang, C. N. Cruz, S. Chatterjee, R. D. Madurawe, C. M. Moore, L. X. Yu, J. Woodcock, “Modernizing Pharmaceutical Manufacturing: from Batch to Continuous Production”, *Journal of Pharmaceutical Innovation* **2015**, *10*, 191–199.
- [4] A. Adamo, R. L. Beingessner, M. Behnam, J. Chen, T. F. Jamison, K. F. Jensen, J. C. M. Monbaliu, A. S. Myerson, E. M. Revalor, D. R. Snead, T. Stelzer, N. Weeranoppanant, S. Y. Wong, P. Zhang, “On-demand continuous-flow production of pharmaceuticals in a compact, reconfigurable system”, *Science* **2016**, *352*, 61–67.
- [5] M. B. Plutschack, K. Gilmore, P. H. Seeberger, “The Hitchhiker ’ s Guide to Flow Chemistry”, *Chemical Reviews* **2017**, *117*, 11796–11893.
- [6] Continuous Pharmaceuticals, <https://www.continuouspharma.com/technology/> (visited on 09/25/2018).
- [7] Food and Drug Administration, Strategic plan for preventing and mitigating drug shortages, tech. rep. October, **2013**, pp. 1–40.
- [8] B. Gutmann, D. Cantillo, C. O. Kappe, “Continuous-Flow Technology — A Tool for the Safe Manufacturing of Active Pharmaceutical Ingredients”, *Angewandte Chemie - International Edition* **2015**, *54*, 6688–6728.
- [9] P. Poehlauer, J. Manley, R. Broxterman, M. Ridemark, “Continuous Processing in the Manufacture of Active Pharmaceutical Ingredients and Finished Dosage Forms: An Industry Perspective”, *Organic Process Research & Development* **2012**, *16*, 1586–1590.
- [10] Food and Drug Administration, Pharmaceutical CGMPs for the 21s Century - A risk-based approach, tech. rep. September, **2004**, p. 32.

- 
- [11] International Council of Harmonisation, June 2018, Kobe, Japan, **2018**, <http://www.ich.org/ichnews/press-releases/view/article/ich-assembly-kobe-japan-june-2018.html> (visited on 09/10/2018).
- [12] D. T. McQuade, P. H. Seeberger, “Applying Flow Chemistry: Methods, Materials, and Multistep Synthesis”, *The Journal of Organic Chemistry* **2013**, *78*, 6384–6389.
- [13] K. Geyer, J. D. C. Codøe, P. H. Seeberger, “Microreactors as Tools for Synthetic Chemists — The Chemists Round- Bottomed Flask of the 21st Century ?”, *Chem. Eur. J* **2006**, *12*, 8434–8442.
- [14] N. Kockmann, M. Gottsponer, B. Zimmermann, D. M. Roberge, “Enabling continuous-flow chemistry in microstructured devices for pharmaceutical and fine-chemical production”, *Chemistry - A European Journal* **2008**, *14*, 7470–7477.
- [15] W. Ehrfeld, V. Hessel, V. Haverkamp, “Microreactors”, *Ullmann’s Encyclopedia of Industrial Chemistry* **2012**, 173–198.
- [16] R. L. Hartman, K. F. Jensen, “Microchemical systems for continuous-flow synthesis”, *Lab Chip* **2009**, *9*, 2495–2507.
- [17] K. Ward, Z. H. Fan, “Mixing in microfluidic devices and enhancement methods”, *Journal of Micromechanics and Microengineering* **2015**, *25*, 1–18.
- [18] G. Cai, L. Xue, H. Zhang, J. Lin, “A review on micromixers”, *Micromachines* **2017**, *8*, 1–27.
- [19] N. Kockmann, “Pressure loss and transfer rates in microstructured devices with chemical reactions”, *Chemical Engineering and Technology* **2008**, *31*, 1188–1195.
- [20] V. Hessel, H. Löwe, F. Schönfeld, “Micromixers - A review on passive and active mixing principles”, *Chemical Engineering Science* **2005**, *60*, 2479–2501.
- [21] J. Aubin, D. F. Fletcher, J. Bertrand, C. Xuereb, “Characterization of the mixing quality in micromixers”, *Chemical Engineering and Technology* **2003**, *26*, 1262–1270.
- [22] J. Aubin, M. Ferrando, V. Jiricny, “Current methods for characterising mixing and flow in microchannels”, *Chemical Engineering Science* **2010**, *65*, 2065–2093.
- [23] J. R. Bourne, “Mixing and the Selectivity of Chemical Reactions”, *Organic Process Research & Development* **2003**, *7*, 471–508.
- [24] W. Ehrfeld, K. Golbig, V. Hessel, H. Löwe, T. Richter, “Characterization of mixing in micromixers by a test reaction: Single mixing units and mixer arrays”, *Industrial and Engineering Chemistry Research* **1999**, *38*, 1075–1082.
- [25] A. Alam, K. Y. Kim, “Mixing performance of a planar micromixer with circular chambers and crossing constriction channels”, *Sensors and Actuators B: Chemical* **2013**, *176*, 639–652.
-

- 
- [26] B. Gutmann, M. Köckinger, G. Glotz, T. Ciaglia, E. Slama, M. Zadavec, S. Pfanner, M. C. Maier, H. Gruber-Wölfler, C. Oliver Kappe, “Design and 3D printing of a stainless steel reactor for continuous difluoromethylations using fluoroform”, *Reaction Chemistry & Engineering* **2017**, *2*, 919–927.
- [27] A. J. Capel, S. Edmondson, S. D. Christie, R. D. Goodridge, R. J. Bibb, M. Thurstans, “Design and additive manufacture for flow chemistry”, *Lab on a Chip* **2013**, *13*, 4583–4590.
- [28] A. K. Au, W. Huynh, L. F. Horowitz, A. Folch, “3D-Printed Microfluidics”, *Angewandte Chemie - International Edition* **2016**, *55*, 3862–3881.
- [29] N. Bhattacharjee, A. Urrios, S. Kang, A. Folch, “The upcoming 3D-printing revolution in microfluidics”, *Lab on a Chip* **2016**, *16*, 1720–1742.
- [30] S. Chatterjee, FDA Perspective on Continuous Manufacturing, **2012**.
- [31] R. M. Felder, R. W. Rousseau, *Elementary principles of chemical processes*, 3rd ed., Hoboken, NJ Wiley, **2005**, p. 675.
- [32] O. Levenspiel, *Chemical Reaction Engineering*, 3rd ed., John Wiley & Sons, New York, **1999**, p. 686.
- [33] D. Webb, T. F. Jamison, “Continuous flow multi-step organic synthesis”, *Chemical Science* **2010**, *1*, 675–680.
- [34] Y. Xia, G. M. Whitesides, “Soft Lithography”, *Angewandte Chemie - International Edition* **1998**, *37*, 550–575.
- [35] R. Vinu, *Gas-Liquid and Gas-Liquid-Solid Reactors*, **2017**, pp. 273–342.
- [36] M. N. Kashid, A. Renken, L. Kiwi-Minsker, “Gas-liquid and liquid-liquid mass transfer in microstructured reactors”, *Chemical Engineering Science* **2011**, *66*, 3876–3897.
- [37] N. Kockmann, O. Brand, G. K. Fedder, C. Hierold, J. G. Korvink, *Micro Process Engineering*, Vol. 39, 1st, (Ed.: N. Kockmann), Wiley-VCH Verlag GmbH&Co. KGaA, Weinheim, **2006**, pp. 561–563.
- [38] E. K. Sackmann, A. L. Fulton, D. J. Beebe, “The present and future role of microfluidics in biomedical research”, *Nature* **2014**, *507*, 181–189.
- [39] G. Panke, T. Schwalbe, W. Stirner, S. Taghavi-Moghadam, G. Wille, “A Practical Approach of Continuous Processing to High Energetic Nitration Reactions in Microreactors”, *Synthesis* **2003**, 2827–2830.
- [40] V. Hessel, H. Löwe, “Organic synthesis with microstructured reactors”, *Chemical Engineering and Technology* **2005**, *28*, 267–284.
- [41] V. Hessel, B. Cortese, M. H. de Croon, “Novel process windows - Concept, proposition and evaluation methodology, and intensified superheated processing”, *Chemical Engineering Science* **2011**, *66*, 1426–1448.
-

- 
- [42] C. Wiles, P. Watts, "Continuous flow reactors: A perspective", *Green Chemistry* **2012**, *14*, 38–54.
- [43] M. Damm, T. N. Glasnov, C. O. Kappe, "Translating high-temperature microwave chemistry to scalable continuous flow processes", *Organic Process Research and Development* **2010**, *14*, 215–224.
- [44] R. L. Hartman, J. P. McMullen, K. F. Jensen, "Deciding whether to go with the flow: Evaluating the merits of flow reactors for synthesis", *Angewandte Chemie - International Edition* **2011**, *50*, 7502–7519.
- [45] C.-y. Lee, W.-t. Wang, C.-c. Liu, L.-m. Fu, "Passive mixers in microfluidic systems : A review", *Chemical Engineering Journal* **2016**, *288*, 146–160.
- [46] V. Hessel, S. Hardt, H. Löwe, *Chemical Micro Process Engineering*, Wiley-VCH Verlag GmbH&Co. KGaA, Weinheim, **2004**, p. 674.
- [47] P. Plouffe, A. Macchi, D. M. Roberge, "From batch to continuous chemical synthesis-a toolbox approach", *Organic Process Research and Development* **2014**, *18*, 1286–1294.
- [48] N. Kockmann, *Transport Phenomena in Micro Process Engineering*, Springer-Verlag, Berlin Heidelberg, **2008**, p. 365.
- [49] F. Lévesque, N. J. Rogus, G. Spencer, P. Grigorov, J. McMullen, D. A. Thaisrivongs, I. Davies, J. R. Naber, "Advancing Flow Chemistry Portability: A Simplified Approach to Scaling Up Flow Chemistry", *Organic Process Research and Development* **2018**.
- [50] P. N. Nge, C. I. Rogers, A. T. Woolley, "Advances in microfluidic materials, functions, integration, and applications", *Chemical Reviews* **2013**, *113*, 2550–2583.
- [51] J. N. Lee, C. Park, G. M. Whitesides, "Solvent Compatibility of Poly(dimethylsiloxane)-Based Microfluidic Devices", *Analytical Chemistry* **2003**, *75*, 6544–6554.
- [52] A. J. Capel, A. Wright, M. J. Harding, G. W. Weaver, Y. Li, R. A. Harris, S. Edmondson, R. D. Goodridge, S. D. Christie, "3D printed fluidics with embedded analytic functionality for automated reaction optimisation", *Beilstein Journal of Organic Chemistry* **2017**, *13*, 111–119.
- [53] I. Yadroitsev, I. Smurov, "Surface morphology in selective laser melting of metal powders", *Physics Procedia* **2011**, *12*, 264–270.
- [54] Lithoz GmbH, LITHOZ Company Folder, 1060 Vienna, **2018**, [http://www.lithoz.com/application/files/6315/2465/8479/LITHOZ%7B%5C\\_%7DGeneralFolder%7B%5C\\_%7D2018%7B%5C\\_%7DE.pdf](http://www.lithoz.com/application/files/6315/2465/8479/LITHOZ%7B%5C_%7DGeneralFolder%7B%5C_%7D2018%7B%5C_%7DE.pdf) (visited on 01/07/2019).
- [55] R. Knitter, D. Goehring, P. Risthaus, J. Hauszelt, "Microfabrication of ceramic microreactors", *Microsystem Technologies* **2001**, *7*, 85–90.
-

- 
- [56] N. Travitzky, A. Bonet, B. Dermeik, T. Fey, I. Filbert-Demut, L. Schlier, T. Schlordt, P. Greil, "Additive manufacturing of ceramic-based materials", *Advanced Engineering Materials* **2014**, *16*, 729–754.
- [57] M. Schwentenwein, J. Homa, "Additive manufacturing of dense alumina ceramics", *International Journal of Applied Ceramic Technology* **2015**, *12*, 1–7.
- [58] E. L. Paul, V. a. Atiemo-obeng, S. M. Kresta, *Handbook of Industrial Mixing*, (Ed.: E. L. Paul), John Wiley & Sons, New Jersey, **2004**, p. 1432.
- [59] Z. Mao, C. Yang, "Micro-mixing in chemical reactors: A perspective", *Chinese Journal of Chemical Engineering* **2017**, *25*, 381–390.
- [60] J. Baldyga, J. R. Bourne, *Turbulent Mixing and Chemical Reactions*, John Wiley & Sons, Chichester, **1999**.
- [61] M. Mory, *Fluid Mechanics for Chemical Engineering*, John Wiley & Sons, Hoboken, NJ, **2011**, p. 422.
- [62] Y. K. Suh, S. Kang, "A Review on Mixing in Microfluidics", *Micromachines* **2010**, *1*, 82–111.
- [63] A. A. Mouza, C. M. Patsa, F. Schönfeld, "Mixing performance of a chaotic micro-mixer", *Chemical Engineering Research and Design* **2008**, *86*, 1128–1134.
- [64] J. M. Ottino, S. Wiggins, "Introduction: Mixing in microfluidics", *Philosophical Transactions of the Royal Society A: Mathematical Physical and Engineering Sciences* **2004**, *362*, 923–935.
- [65] E. A. Mansur, Y. Mingxing, W. Yundong, D. Youyuan, "A State-of-the-Art Review of Mixing in Microfluidic Mixers", *Chinese Journal of Chemical Engineering* **2008**, *16*, 503–516.
- [66] L. Falk, J. Commenge, "Performance comparison of micromixers", *Chemical Engineering Science* **2010**, *65*, 405–411.
- [67] N. T. Nguyen, Z. Wu, "Micromixers - A review", *Journal of Micromechanics and Microengineering* **2005**, *15*.
- [68] W. Wang, S. Zhao, T. Shao, Y. Jin, Y. Cheng, "Visualization of micro-scale mixing in miscible liquids using  $\mu$ -LIF technique and drug nano-particle preparation in T-shaped micro-channels", *Chemical Engineering Journal* **2012**, *192*, 252–261.
- [69] D. S. Kim, S. H. Lee, T. H. Kwon, C. H. Ahn, "A serpentine laminating micromixer combining splitting/recombination and advection", *Lab on a Chip* **2005**, *5*, 739–747.
- [70] S. Hardt, H. Pennemann, F. Schönfeld, "Theoretical and experimental characterization of a low-Reynolds number split-and-recombine mixer", *Microfluidics and Nanofluidics* **2006**, *2*, 237–248.
- [71] A. D. Stroock, S. K. Dertinger, A. Ajdari, H. A. Stone, "Chaotic Mixer for Microchannels", *Science* **2002**, *295*, 647–652.
-

- 
- [72] H. Song, J. Tice, R. F. Ismagilov, "A Microfluidic System for Controlling Reaction Networks in Time", *Angewandte Chemie International Edition* **2003**, *42*, 1433–7851.
- [73] A. Günther, K. F. Jensen, "Multiphase microfluidics: From flow characteristics to chemical and materials synthesis", *Lab on a Chip* **2006**, *6*, 1487–1503.
- [74] V. Hessel, P. Angeli, A. Gavriilidis, H. Löwe, "Gas-liquid and gas-liquid-solid microstructured reactors: Contacting principles and applications", *Industrial and Engineering Chemistry Research* **2005**, *44*, 9750–9769.
- [75] A. Günther, S. A. Khan, M. Thalmann, F. Trachsel, K. F. Jensen, "Transport and reaction in microscale segmented gas–liquid flow", *Lab Chip* **2004**, *4*, 278–286.
- [76] L.-H. Lu, K. S. Ryu, C. Liu, "A magnetic microstirrer and array for microfluidic mixing", *Journal of Microelectromechanical Systems* **2002**, *11*, 462–469.
- [77] S. H. Lee, D. Van Noort, J. Y. Lee, B. T. Zhang, T. H. Park, "Effective mixing in a microfluidic chip using magnetic particles", *Lab on a Chip* **2009**, *9*, 479–482.
- [78] X. Zhu, E. S. Kim, "Microfluidic motion generation with acoustic waves", *Sensors and Actuators A: Physical* **1998**, *66*, 355–360.
- [79] I. Glasgow, N. Aubry, "Enhancement of microfluidic mixing using time pulsing", *Lab on a Chip* **2003**, *3*, 114–120.
- [80] S. R. Gobert, S. Kuhn, L. Braeken, L. C. Thomassen, "Characterization of Milli- and Microflow Reactors: Mixing Efficiency and Residence Time Distribution", *Organic Process Research and Development* **2017**, *21*, 531–542.
- [81] V. Hessel, S. Hardt, H. Lowe, F. Schonfeld, "Laminar Mixing in Different Interdigital Micromixers : I . Experimental Characterization", *AIChE Journal* **2003**, *49*, 566–577.
- [82] D. Bošković, Dissertation, Technischen Universität Ilmenau, **2010**, p. 175.
- [83] D. Bošković, S. Loebbecke, "Modelling of the residence time distribution in micromixers", *Chemical Engineering Journal* **2007**, *135*, 138–146.
- [84] O. Levenspiel, W. K. Smith, "Notes on the diffusion-type model for the longitudinal mixing of fluids in flow", *Chemical Engineering Science* **1957**, *6*, 227–233.
- [85] M. C. Fournier, L. Falk, J. Villermaux, "A new parallel competing reaction system for assessing micromixing efficiency - Experimental approach", *Chemical Engineering Science* **1996**, *51*, 5053–5064.
- [86] P. Guichardon, L. Falk, J. Villermaux, "Characterisation of micromixing efficiency by the iodide-iodate reaction system. Part II: Kinetic study", *Chemical Engineering Science* **2000**, *55*, 4245–4253.
- [87] M. Jasińska, "Test reactions to study efficiency of mixing", *Chemical and Process Engineering - Inżynieria Chemiczna i Procesowa* **2015**, *36*, 171–208.
-

- 
- [88] S. Schwolow, J. Hollmann, B. Schenkel, T. Röder, “Application-oriented analysis of mixing performance in microreactors”, *Organic Process Research and Development* **2012**, *16*, 1513–1522.
- [89] J. R. Bourne, O. M. Kut, J. Lenzner, “An Improved Reaction System To Investigate Micromixing in High-Intensity Mixers”, *Industrial and Engineering Chemistry Research* **1992**, *31*, 949–958.
- [90] I. M. da Silva Nunes, PhD thesis, Universidade do Porto, **2007**, p. 256.
- [91] J. R. Bourne, P. Rys, K. Suter, “Mixing effects in the bromination of resorcin”, *Chemical Engineering Science* **1977**, *32*, 711–716.
- [92] J. M. Commenge, L. Falk, “Villermaux-Dushman protocol for experimental characterization of micromixers”, *Chemical Engineering and Processing: Process Intensification* **2011**, *50*, 979–990.
- [93] J. R. Bourne, “Comments on the iodide-iodate method for characterising micromixing”, *Chemical Engineering Journal* **2008**, *140*, 638–641.
- [94] L. Falk, J. M. Commenge, *Characterization of Mixing and Segregation in Homogeneous Flow Systems. In Micro Process Engineering: A Comprehensive Handbook, Vol. 32*, 1st ed., (Eds.: V. Hessel, A. Renken, J. C. Schouten, J.-I. Yoshida), Wiley-VCH Verlag GmbH & Co. KGaA, Weinheim, Germany, **2009**, pp. 162–165.
- [95] S. Ehlers, K. Elgeti, T. Menzel, G. Wießmeier, “Mixing in the offstream of a microchannel system”, *Chemical Engineering and Processing: Process Intensification* **2000**, *39*, 291–298.
- [96] K. Malecha, L. J. Golonka, J. Bałdyga, M. Jasińska, P. Sobieszuk, “Serpentine microfluidic mixer made in LTCC”, *Sensors and Actuators B: Chemical* **2009**, *143*, 400–413.
- [97] J. R. Bourne, S. Yu, “Investigation of micromixing in stirred tank reactors using parallel reactions”, *Industrial & Engineering Chemistry Research* **1994**, *33*, 41–55.
- [98] P. Guichardon, L. Falk, M. Andrieu, “Experimental Comparison of the Iodide-Iodate and the Diazo Coupling Micromixing Test Reactions in Stirred Reactors”, *Chemical Engineering Research and Design* **2001**, *79*, 906–914.
- [99] Z. He, T. F. Jamison, “Continuous-flow synthesis of functionalized phenols by aerobic oxidation of grignard reagents”, *Angewandte Chemie - International Edition* **2014**, *53*, 3353–3357.
- [100] M. C. Maier, R. Lebl, P. Sulzer, J. Lechner, T. Mayr, M. Zadavec, E. Slama, S. Pfanner, C. Schmölder, P. Pöchlauer, C. O. Kappe, H. Gruber-Woelfler, “Development of customized 3D printed stainless steel reactors with inline oxygen sensors for aerobic oxidation of Grignard reagents in continuous flow”, *Reaction Chemistry & Engineering* **2019**, DOI 10.1039/C8RE00278A.
-

- [101] J. F. Garst, C. D. Smith, A. C. Farrar, "Radical Intermediates in the Oxygenation of Phenylmagnesium Bromide. Evidence from Aromatic Phenylation", *Journal of the American Chemical Society* **1972**, *94*, 7707–7710.
- [102] M. Hesse, H. Meier, B. Zeeh, *Spektroskopische Methoden in der organischen Chemie*, 6th ed., Georg Thieme Verlag, Stuttgart, **2005**, p. 429.
- [103] J. T. Adeosun, A. Lawal, "Residence-time distribution as a measure of mixing in T-junction and multilaminated/elongational flow micromixers", *Chemical Engineering Science* **2010**, *65*, 1865–1874.
- [104] K. S. Wenger, E. H. Dunlop, I. D. MacGillp, "Investigation of the chemistry of a diazo micromixing test reaction", *AIChE Journal* **1992**, *38*, 1105–1114.
- [105] K. H. Slotta, W. Franke, "Zur Konstitution der Azo-Indicatoren", *Berichte der deutschen chemischen Gesesellschaft* **1931**, *64*, 86–94.
- [106] H. ur Rehman, M. Ansari, "Density, Viscosity, and Electrical Conductivity Measurements on the Ternary System H<sub>2</sub>O + C<sub>2</sub>H<sub>5</sub>OH + LiCl over the Entire Ranges of Solvent Composition and LiCl Solubility from (-5 to +50) °C", *Journal of Chemical & Engineering Data* **2008**, *53*, 2072–2088.
- [107] B. Nowicka, A. Kacperska, J. Barczyńska, A. Bald, S. Taniewska-Osińska, "Viscosity of solutions of NaI and CaCl<sub>2</sub> in water-ethanol and of NaI in water-tetrahydrofuran mixtures", *Journal of the Chemical Society Faraday Transactions 1: Physical Chemistry in Condensed Phases* **1988**, *84*, 3877–3884.
- [108] C. Vallés, E. Pérez, A. M. Mainar, J. Santafé, M. Domínguez, "Excess enthalpy, density, speed of sound, and viscosity for 2-methyltetrahydrofuran + 1-butanol at (283.15, 298.15, and, 313.15) K", *Journal of Chemical and Engineering Data* **2006**, *51*, 1105–1109.

---

## 7 List of Figures

1.1	Illustration of a pharmaceutical production chain with multiple, disconnected batch processes for primary (left) and secondary (right) manufacturing [6]. . . . .	1
2.1	A simple depiction of batch (top) and continuous (bottom) manufacturing. Adapted from [3]. . . . .	4
2.2	Zones of a standard two feed microfluidic system. The modules can be used repetitively and interchangeably to enlarge the system [5]. . . . .	8
2.3	Illustration of the required channel diameter depending on the reaction kinetics and the heat sensitivity/generation of the reaction [47]. . . . .	10
2.4	Left: Scheme of the selective laser melting/sintering (SLM/SLS) manufacturing process. SLS sinters the material together while SLM uses the laser to achieve a full melt of the material [28]. Right: Scheme of the lithography-based ceramic manufacturing (LCM) technique. a) building platform, b) wiper blade, c) vat, d) light source. Adapted from [54]. . . . .	13
2.5	Illustration of the exchange of molecules through an interfacial area by molecular diffusion: a) initial conditions with complete separation of two fluids; b) random state during diffusion process [62]. . . . .	14
2.6	Illustration of the effect of multilamination of streams. The interfacial area is increased and at the same time the diffusion path length is decreased leading to an enhanced mixing efficiency. Adapted from [62]. . . . .	15
2.7	Examples of active and passive mixing approaches. Active mixing is induced by external forces and passive mixing solely uses the mixer geometry [20, 67]. . . . .	16
2.8	Left: Colored experimental $\mu$ -LIF results for increasing Re numbers (from left to right) for a T-mixer. Pure red denotes 100% liquid A and pure blue denotes 0% [68]. Right: Schematic illustration of basic passive mixer designs: a) T-mixer, b) Y-mixer, c) concept of parallel lamination and d) concept of hydrodynamic focusing [67]. . . .	17
2.9	Examples of SAR-mixers: Left: F-shaped SAR concept published by Kim et al. [69]; Right: Chain-like SAR concept published by Hardt et al. [70]. . . . .	17

---

2.10	Examples for chaotic advection: Left: At high Reynolds numbers obstacles at the wall (a), in the channel (b) or zig-zag arrangements (c) showed good mixing performance [67]; Right: Scheme of the staggered herringbone micromixer and the produced vortices [71]. . . . .	18
2.11	Left: a) Scheme of two inlets in a standard micro channel with slow mixing and high dispersion. b) Proposed multiphase micromixer with efficient mixing inside the droplets [72]. Right: Illustration of different gas-liquid flow regimes in microstructures. The gas flow rate increases from top to bottom [5]. . . . .	19
2.12	Left: Fluorescence micrographs of a fluorescent and a non-fluorescent stream in a mixing chamber: a) Chamber without particles shows no mixing enhancement, i.e. diffusive mixing. b) Non-rotating magnetic particles in the chamber lead to enhanced but incomplete mixing. c) Mixing chamber with rotating particles generates efficient mixing. Adapted from [77]. Right: Scheme of an acoustically driven micromixer published by Zhu et al. [78]. . . . .	20
2.13	Numerical simulation of pulsed flow in a simple T-mixer with a mean velocity of $1 \text{ mm s}^{-1}$ for both inlet streams. Left: Control case without any pulsing indicates bad mixing. Right: Pulsed flow with a 90 degree phase difference. The graph shows the mean velocities as a function of time. The numerical simulation shows enhanced mixing for various times. Adapted from [79]. . . . .	21
2.14	Input and output signals of pulse and step function of a plug flow reactor. At the pulse input the inlet flow is doped with a tracer. At the step input the reactor inlet is changed to a constant concentration of tracer. The output signal is dependent on the input signal and the type of reactor. . . . .	22
2.15	Top: Representation of ideal plug flow and dispersed plug flow. Bottom: Boundary conditions 'closed-closed' and 'open-open' for the in and outlet of a device according to the dispersion model [32]. . . . .	24
2.16	a) Scheme of a parallel-competitive reaction with $k_1 > k_2$ . Reagent A and C are competing for reagent B giving the products R and S. b) In a homogeneous mixture the R product is preferred, due to different rate constants c) In a heterogeneous mixture also S product is formed due to local overconcentrations. Adapted from [88].	26
2.17	a) Scheme of a consecutive-competitive reaction with $k_1 > k_2$ . The fast primary reaction between A and B gives product R. This product R competes with reagent A for reagent B giving product S. b) In a homogeneous mixture the R product is preferred, due to different rate constants c) In a heterogeneous mixture also the S product is formed due to local overconcentrations. Adapted from [88]. . . . .	26
2.18	Scheme of the diazo coupling of 1-naphthol (A) and diazotised sulfanilic acid (B) giving the monoazo isomers p-R and o-R. The secondary coupling of p-R and o-R with B results in the bisazo dye S. . . . .	28

---

---

2.19	Proposed mechanism of the oxidation of Grignard reagents: First an aryl radical is formed by oxidation of an organo-magnesium species which then reacts to a organoperoxide. This reacts with another Grignard reagent to form a phenoxide. In a last step phenol is formed by acidification. Adapted from [99]. . . . .	29
3.1	Left: The size-scaled-mixers have the same design, but their dimensions are scaled with factors of 0.75 and 0.5 referred to the large version. Right: Rendered image of the mixing structure consisting of two semi-circles between each mixing chamber. . .	34
3.2	Left: The sphere-mixer has two inlets, one outlet and ten spherical mixing chambers. The mixing chambers are connected with two channels, with an alternating offset of 90°. Right: Rendered image of a reactor concept including the sphere-mixer as mixing section. . . . .	34
3.3	Left: 3D printed SAR-reactor with and without cooling, shell fabricated by SLM. Right: Rendered image of the SAR-reactor with and without cooling shell. The reactor consists of two inlets and a pre-cooling section, a mixing point and mixing elements which additionally ensure enough volume. . . . .	35
3.4	Left: CSTR-cascade v1 made of ceramics. The stainless steel version has the same design. Shavings are cut off from the red fittings. This indicates that the ceramic thread is not perfectly fitting to the thread of the standard HPLC fittings. This is attributed to shrinkage of ceramics during fabrication. Right: Rendered image of the CSTR-cascade v1 with highlighted channels and vessels. . . . .	36
3.5	Experimental set-up for the determination of the RTD. By switching the manual 6-port injection valve, the input is changed from no tracer to a constant concentration of tracer. This step signal is detected by an inline UV/VIS flow cell connected to a spectrophotometer. . . . .	37
3.6	Bodenstein number against Reynolds number for the SAR-reactor. Step up and step down experiments were performed. Plug flow behaviour appears at Reynolds numbers between 50 and 60. The flow rates were 0.5 mL min <sup>-1</sup> , 0.8 mL min <sup>-1</sup> , 1.7 mL min <sup>-1</sup> , 2.77 mL min <sup>-1</sup> and 3.7 mL min <sup>-1</sup> . . . . .	38
3.7	Bodenstein number of different flow rates against stirrer Reynolds number for the stainless steel CSTR-cascade v1. The flow rates were 0.5 mL min <sup>-1</sup> , 0.8 mL min <sup>-1</sup> , 1.7 mL min <sup>-1</sup> and 2.77 mL min <sup>-1</sup> . . . . .	39
3.8	Bodenstein number of different flow rates against stirrer Reynolds number for the ceramic CSTR-cascade v1. The flow rates were 0.5 mL min <sup>-1</sup> , 0.8 mL min <sup>-1</sup> , 1.7 mL min <sup>-1</sup> , 2.77 mL min <sup>-1</sup> and 3.7 mL min <sup>-1</sup> . . . . .	39
3.9	Experimental set-up for mixing sensitive reactions using a syringe pump with reactants, a microfluidic device at constant temperature of 25 °C and a sampling section.	40
3.10	Absorption spectra of the para monoazo dye shows good agreement of this work, Bourne et al. [2] and Wenger et al. [104]. . . . .	42

---

---

3.11	Absorption spectra of the ortho monoazo dye shows acceptable agreement of this work, Bourne et al. [2] and Wenger et al. [104]. . . . .	43
3.12	Different published absorption spectra of the bisazo dye. The differences are referred to problems with isolation, purification, quantification and instability of the pure S-product. This was reported by Wenger et al. [104] and illustrated by Nunes et al. [90].	44
3.13	Experimental results of the bisazo dye yield $Y_S$ as a function of the flow rate (left) and Reynolds number (right). The three size-scaled-mixers have the same geometry but in different scales. The smallest mixer performs best because of the higher flow velocity. . . . .	45
3.14	Experimental results of the bisazo dye yield $Y_S$ as a function of the Reynolds number for the ceramic sphere-mixer and the standard T-mixer. . . . .	46
3.15	Experimental results of the bisazo dye yield $Y_S$ as a function of the Reynolds number for the SAR-reactor and a T-mixer. . . . .	47
3.16	Experimental results of the bisazo dye yield $Y_S$ as a function of the Reynolds number referring to the flow rate, for different stirring speeds of the CSTR-cascade v1. . . . .	48
3.17	Experimental results of the bisazo dye yield $Y_S$ as a function of the Reynolds number referring to the flow rate of T-mixer and SAR-reactor, CSTR-cascade v1 without stirring and with 1000 RPM. . . . .	49
3.18	Schematic illustration of the rotational direction of the stirrer in a vessel: Left: In clockwise rotation, the stirrer acts against the inlet flow. Right: In counter-clockwise rotation, the stirrer turns in direction of the flow at the vessel inlet. . . . .	50
3.19	Experimental results of the bisazo dye yield $Y_S$ as a function of the stirrer Reynolds number for different channel Reynolds numbers: Left: Clockwise rotation of the stirrer. Right: Counter-clockwise rotation of the stirrer. . . . .	50
3.20	Experimental results of the bisazo dye yield $Y_S$ as a function of the stirrer Reynolds number for CSTR-cascade v1 made of steel and ceramics. The flow rate was $1.7 \text{ mL min}^{-1}$ corresponding to the Reynolds number for the model reaction conditions $Re = 52$ . The stirrer speed was set between 0 RPM and 1000 RPM. . . . .	51
3.21	Left: Optimised CSTR-cascade v2 with cooling shell and new flat bottom fittings. Right: Rendered image of the new designed CSTR-cascade v2 with highlighted channels and vessels. . . . .	52
3.22	a) Scheme of the CSTR vessel with stirrer and conical fitting. Between fitting and vessel a dead volume is generated. b) Scheme of the new design with flat bottom fittings and an additional ferrule. The dead volume was removed. c) To ensure enough space for analytical probes the vessel height was increased. The inlet channel was moved to a higher position to ensure mixing in the whole vessel. . . . .	53

---

---

3.23	Right: First the conical HPLC fittings were used which generated a dead volume. Left: The new flat bottom fittings have an additional ferrule as sealing, which eliminated the dead volume. . . . .	53
3.24	Experimental results of the bisazo dye yield $Y_S$ as a function of the stirrer Reynolds number for the optimised CSTR-cascade v2 and the first CSTR-cascade v1, both made of steel. The flow rate was $1.7 \text{ mL min}^{-1}$ . The stirrer speed was chosen between 0 RPM and 1000 RPM in clockwise direction. . . . .	54
3.25	Set-up for kinetic measurements of an oxidation of Grignard reagents in flow. Adapted from [100]. . . . .	55
3.26	Set and measured flow rate of 2-methyl-THF against time. . . . .	56
3.27	Pressure measured at pump 1 of a test run with isopropyl alcohol and oxygen. . . . .	57
3.28	Pressure measured at pump 2 of a test run with water and oxygen. The pressure did not reach a steady value and after shifting upwards, it dropped down instantly at some point. This behaviour is attributed to the BPR which is not meant to be used for heterogeneous systems. . . . .	58
5.1	Reaction scheme for the preparation of diazotatised sulfanilic acid according to [96].	62
5.2	Reaction scheme for synthesis of the para-R-product according to [2]. . . . .	63
5.3	Reaction scheme for synthesis of the ortho-R-product according to [2]. . . . .	63
5.4	Switch positions of the 6-port injection valve. A step input switches from no tracer to a constant concentration of tracer. With a sample loop, a defined amount of tracer is injected, called a pulse input. (S) Solvent, (T) Tracer, (R) Reactor, (W) Waste. . . . .	65

---

## 8 List of Tables

2.1	Surface-to-volume ratios for various reactors. Calculated for half filled round-bottom flasks with static liquid. Adapted from [5]. . . . .	6
3.1	Overview of the investigated microfluidic devices and the corresponding experiments.	33
3.2	Maximum extinction coefficients and the corresponding wavelengths of ortho- and para-isomer. The table represents data obtained within this work and literature references [2, 104]. . . . .	41
3.3	Set flow rates of test runs for kinetic measurements. . . . .	56
9.2	Substance data of the used solvents. Unless otherwise stated the temperature is 25 °C.	82
9.3	RTD results of the SAR-reactor. . . . .	83
9.4	RTD results of the stainless steel CSTR-cascade. . . . .	83
9.5	RTD results of the ceramic CSTR-cascade. . . . .	84
9.6	Results of mixing sensitive reactions of the size-scaled-mixers. . . . .	85
9.7	Results of mixing sensitive reactions of sphere-mixer, SAR-reactor and T-mixer. . . . .	85
9.8	Results of mixing sensitive reactions of CSTR-cascade v1 made of stainless steel and ceramics. The stirrers turned clockwise and the flow rate was 1.7 mL min <sup>-1</sup> resulting in $Re(channel) = 52$ . . . . .	86
9.9	Results of mixing sensitive reactions of CSTR-cascade v1 made of stainless steel. The stirrers turned in clockwise direction. . . . .	87
9.10	Results of mixing sensitive reactions of CSTR-cascade v1 made of stainless steel. The stirrers turned in counter-clockwise direction. . . . .	87
9.11	Results of mixing sensitive reactions of CSTR-cascade v1 made of ceramics. The stirrers turned in clockwise direction. . . . .	88
9.12	Results of mixing sensitive reactions of the optimised CSTR-cascade v2 made of stainless steel with flow rate 1.7 mL min <sup>-1</sup> resulting in $Re(channel) = 52$ . The stirrers turned in clockwise direction. . . . .	88
9.13	List of used chemicals and solvents. . . . .	89
9.14	Extinction coefficients for p-R, o-R and S product at the investigated wavelengths. Data obtained from Bourne et al. [2] at 25 °C, pH 9.9, $I = 444.4 \text{ mol L}^{-1}$ . . . . .	93

---

## 9 Appendix

### 9.1 Abbreviations and Symbols

#### Abbreviations

2D	Two dimensional
3D	Three dimensional
API	Active pharmaceutical ingredient
BPR	Back pressure regulator
CAD	Computer aided design
CFD	Computational fluid dynamics
CSTR	Continuous stirred-tank reactor
CW	Clockwise
CCW	Counter-clockwise
FDA	Food and drug administration
FEP	Fluorinated ethylene propylene
GC-MS	Gas chromatography - mass spectroscopy
HPLC	High performance liquid chromatography
ID	Inner diameter
LCM	Lithography-based ceramic manufacturing
MFC	Mass flow controller
MRS	Microreaction systems
$\mu$ -LIF	Micro laser induced fluorescence
NPW	Novel process windows
o-R	Ortho-isomer of diazo coupling
OD	Outer diameter
p-R	Para-isomer of diazo coupling
PAT	Process analytical technology
PEEK	Polyether ether ketone
PFA	Perfluoroalkoxy alkane
PTFA	Polytetrafluoroethylene
PDMS	Polydimethylsiloxane

---

RPM	Rounds per minute
RTD	Residence time distributions
S	Bisazo product of diazo coupling
SAR	Split-and-recombine
SLM	Selective laser melting
SLS	Selective laser sintering
SOP	Standard operating procedure
THF	Tetrahydrofuran
TLC	Thin layer chromatography
UV/VIS	Ultraviolet-visible

**Symbols**

$A$	Cross-sectional area, [m <sup>2</sup> ]
$A$	Absorption, [–]
$Bo$	Bodenstein number, [–]
$c$	Concentration, [mol m <sup>-3</sup> ]
$k_r$	Reaction rate constant, [(mol/m <sup>3</sup> ) <sup>1-n</sup> · s <sup>-1</sup> ]
$d$	Channel diameter, [m]
$d_{stirrer}$	Stirrer diameter, [m]
$d_h$	Hydraulic diameter, [m]
$Da_i$	Damkoehler number i, [–]
$D_{ax}$	Axial dispersion coefficient, [m <sup>2</sup> s <sup>-1</sup> ]
$D_{mol}$	Diffusion coefficient, [m <sup>2</sup> s <sup>-1</sup> ]
$\Delta H_r$	Heat of reaction, [J mol <sup>-1</sup> ]
$E$	Energy, [J]
$E$	Exit age function, [s <sup>-1</sup> ]
$F$	Cumulative age function, [–]
$h$	Planck's constant, [J s]
$I$	Intensity, [W m <sup>-2</sup> ]
$l$	Optical path length, [m]
$l$	Channel length, [m]
$L_{char}$	Characteristic length, [m]
$MB$	Mass balance, [%]
$n$	Order of reaction, [–]
$n_{stirrer}$	Rotational speed, [s <sup>-1</sup> ]
$\Delta p$	Pressure drop, [Pa]
$P$	Perimeter, [m]
$Pe$	Peclét number, [–]

$Q$	Volumetric flow rate, [ $\text{m}^3 \text{s}^{-1}$ ]
$Re$	Reynolds number, [–]
$t$	Time, [s]
$t_m$	Mixing time, [s]
$t_r$	Reaction time, [s]
$t_{res}$	Mean residence time, [s]
$\Delta T_w$	Fluid-to-wall temperature difference, [K]
$u$	Flow velocity, [ $\text{m s}^{-1}$ ]
$U_t$	Overall heat transfer coefficient, [ $\text{W m}^{-2} \text{K}^{-1}$ ]
$V$	Volume, [ $\text{m}^3$ ]
$V_R$	Reactor volume, [ $\text{m}^3$ ]
$Y_S$	Yield of S-Product, [–]

**Greek symbols**

$\varepsilon_i$	Molar extinction coefficient, [ $\text{m}^2 \text{mol}^{-1}$ ]
$\varepsilon_{diss}$	Energy dissipation rate, [ $\text{W kg}^{-1}$ ]
$\eta$	Dynamic viscosity, [Pa s]
$\theta$	Dimensionless time, [–]
$\lambda$	Wavelength, [nm]
$\lambda_f$	Channel friction factor, [–]
$\nu$	Frequency, [ $\text{s}^{-1}$ ]
$\nu$	Kinematic viscosity, [ $\text{m}^2 \text{s}^{-1}$ ]
$\rho$	Density, [ $\text{kg m}^{-3}$ ]
$\sigma_t^2$	Variance, [ $\text{s}^2$ ]

**9.2 Substance Data****Table 9.2:** Substance data of the used solvents. Unless otherwise stated the temperature is 25 °C.

Substance	Parameter	Value and unit
<b>Water</b>	Density	997.1 $\text{kg m}^{-3}$ [106]
	Dynamic viscosity	0.894 mPa s [106]
<b>Ethanol:Water 12:88 wt%</b>	Density	980.8 $\text{kg m}^{-3}$ [106]
	Dynamic viscosity	1.388 mPa s [107]
<b>2-methyl-THF</b>	Density	849.5 $\text{kg m}^{-3}$ [108]
	Dynamic viscosity at 0 °C	0.592 mPa s

### 9.3 Results Residence Time Distribution

**Table 9.3:** RTD results of the SAR-reactor.

Flow rate mL.min <sup>-1</sup>	Re(channel) [-]	Step up		Step down	
		Bo [-]	$t_{res}$ [-]	Bo [-]	$t_{res}$ [-]
0.5	9.4	52.9	45	50	50
0.8	15	61.2	30.4	61.6	30.3
1.7	31.9	71.8	15.1	79.9	15.7
2.77	51.9	84.2	11	107.7	11.9
3.7	69.4	100.6	8.7	104	8.8

**Table 9.4:** RTD results of the stainless steel CSTR-cascade.

Flow rate [mL.min <sup>-1</sup> ]	Re(channel) [-]	Rotational speed [RPM]	Re(stirrer) [-]	Step up		Step down	
				Bo [-]	$t_{res}$ [s]	Bo [-]	$t_{res}$ [s]
0.5	9.4	0	0.0	15.6	34.3	10.1	10.1
0.5	9.4	560	38.0	16.7	27.4	10	27.4
0.5	9.4	1110	75.3	17.9	34.8	15.2	32
0.8	15.0	0	0.0	16.6	23.2	10.4	20.8
0.8	15.0	560	38.0	14.6	21.4	42.4	47.4
0.8	15.0	790	53.6	19	24.1	16.4	24.1
0.8	15.0	1110	75.3	17	20.6	11.3	17.2
0.8	15.0	1500	101.8	14.6	21.3	11.5	18.7
1.7	31.9	0	0.0	12.31	12.3	15.2	13.2
1.7	31.9	560	38.0	19.85	11	15.6	10.2
1.7	31.9	790	53.6	15.06	10.3	10.1	11.1
1.7	31.9	1110	75.3	24.63	10.8	15.3	11
1.7	31.9	1500	101.8	26.85	10	16.4	10.5
2.77	51.9	0	0.0	20.05	7.8	18.3	18.3
2.77	51.9	560	38.0	23.72	7.7	21.7	7.4
2.77	51.9	790	53.6	17.47	7.7	12	6.5
2.77	51.9	1110	75.3	17.7	8.4	12.9	7.5
2.77	51.9	1500	101.8	37.67	6.9	12.3	7.2

**Table 9.5:** RTD results of the ceramic CSTR-cascade.

Flow rate [mL min <sup>-1</sup> ]	Re(channel) [-]	Rotational speed [RPM]	Re(stirrer) [-]	Step up		Step down	
				Bo [-]	$t_{res}$ [s]	Bo [-]	$t_{res}$ [s]
0.25	4.7	0	0.0	20.5	56.7	11.2	59.9
0.25	4.7	790	53.6	14.5	55.6	13	58.4
0.25	4.7	1500	101.8	14.5	53.1	9.3	57
0.5	9.4	0	0.0	15.1	28.6	15.5	30
0.5	9.4	560	38.0	13.4	29.6	11.7	27.1
0.5	9.4	790	53.6	18.8	29.5	11.9	27.1
0.5	9.4	1100	74.6	23.3	28.5	8.2	26.9
0.5	9.4	1500	101.8	8.6	31.9	12.1	29.1
0.8	15	0	0.0	25.4	21.7	23.6	22.3
0.8	15	560	38.0	23.9	19.1	18	18.4
0.8	15	790	53.6	28.3	19.6	18.3	17.7
0.8	15	1110	75.3	24.6	16.6	18.8	17.8
0.8	15	1500	101.8	21.6	19	18.7	17
1.7	31.9	0	0.0	29.08	10.7	17.9	11.1
1.7	31.9	560	38.0	18.93	10.4	26.3	11.3
1.7	31.9	790	53.6	14.89	11.2	28.5	10.4
1.7	31.9	1110	75.3	25.54	9.7	21.4	10
1.7	31.9	1500	101.8	41.84	9.9	17.2	9.2
2.77	51.9	0	0.0	21.87	7.3	17.1	6.4
2.77	51.9	560	38.0	28.31	8.5	21.8	8
2.77	51.9	790	53.6	31.97	10	23.4	9.2
2.77	51.9	1110	75.3	29.08	9.8	27.6	9.9
2.77	51.9	1500	101.8	33.35	10	25.5	9
3.7	69.4	0	0.0	29.18	6.4	18.9	5.8
3.7	69.4	560	38.0	44.32	8	26.9	7.9
3.7	69.4	790	53.6	27.35	8.8	26.9	9
3.7	69.4	1110	75.3	30.81	7.2	29.8	8.4
3.7	69.4	1500	101.8	28.51	8	25	8.4

## 9.4 Results Mixing Sensitive Reactions

**Table 9.6:** Results of mixing sensitive reactions of the size-scaled-mixers.

Flow rate [mL.min <sup>-1</sup> ]	Small			Medium			Large		
	Re [-]	Y <sub>S</sub> [-]	MB [%]	Re [-]	Y <sub>S</sub> [-]	MB [%]	Re [-]	Y <sub>S</sub> [-]	MB [%]
0.1	4.1	0.5092	14.2	2.6	0.5413	24.2	1.9	0.5281	32.4
0.4	16.6	0.4982	24.9	10.4	0.5221	15.1	7.8	0.5255	23
1.0	41.5	0.3562	3.31	25.9	0.4885	4.16	19.5	0.4889	12.5
2.0	82.9	0.1568	-0.38	51.9	0.2274	-5.2	38.9	0.4326	7.8
4.0	165.9	0.0568	-1.97	103.8	0.1874	-6.63	77.8	0.2542	1.35
8.0	414.6	0.0215	3.32	259.4	0.0701	1.79	194.5	0.0886	-1.9
16.0	663.4	0.0177	4.84	415.0	0.0425	2	311.3	0.0666	-1.13

**Table 9.7:** Results of mixing sensitive reactions of sphere-mixer, SAR-reactor and T-mixer.

Flow rate [mL.min <sup>-1</sup> ]	Sphere-mixer			SAR-reactor		T-mixer	
	Re [-]	Y <sub>S</sub> [-]	MB [%]	Y <sub>S</sub> [-]	MB [%]	Y <sub>S</sub> [-]	MB [%]
0.04	1.2	0.5004	17.5	0.57	38.4	0.6945	15.7
0.1	3	0.495	15.2	0.5504	20.7	0.6839	16.0
0.4	11.9	0.4503	9.8	0.5019	15.6	0.5201	-5.3
1.0	29.7	0.3153	5.03	0.3235	5.8	0.5309	-5.9
1.7	52	-	-	0.1368	-1.9	-	-
2.0	59.4	0.1556	5.4	0.1558	3.5	0.5113	-7.6
4.0	118.9	0.0723	4.9	0.0893	1.3	0.3316	3.7
10.0	297.2	0.0126	2.04	0.0559	1.8	0.1516	-1.5
16.0	475.5	0	1.54	0.041	6.6	0.1013	-1.4

**Table 9.8:** Results of mixing sensitive reactions of CSTR-cascade v1 made of stainless steel and ceramics. The stirrers turned clockwise and the flow rate was  $1.7 \text{ mL min}^{-1}$  resulting in  $Re(channel) = 52$ .

Rotational speed [RPM]	Re(stirrer) [–]	Stainless steel		Ceramics	
		$Y_S$ [–]	MB [%]	$Y_S$ [–]	MB [%]
0	0	0.2226	-0.54	0.2466	3.5
100	10.8	0.1767	2.65	0.1723	-6.2
200	21.5	0.1526	2.87	0.1257	0.28
250	26.9	0.1496	2.33	0.1047	0.27
300	32.3	0.1306	2.01	0.1114	-0.92
350	37.6	0.1241	2.13	0.1099	-0.41
400	43	0.1309	1.9	0.1207	-0.78
500	53.8	0.1431	1.72	0.1148	-0.25
600	64.5	0.1334	2.08	0.1018	-0.71
700	75.3	0.1209	2.01	0.1081	-1.1
800	86	0.1056	1.54	0.1077	-1.1
900	96.8	0.1001	0.67	0.1059	-1.4
1000	107.5	0.0887	0.63	0.0951	-0.72

**Table 9.9:** Results of mixing sensitive reactions of CSTR-cascade v1 made of stainless steel. The stirrers turned in clockwise direction.

Flow rate [ $\text{mL min}^{-1}$ ]		0.4		1.0		1.7		4.0	
Reynolds number [–]		11.9		29.7		50.5		118.9	
Rotational speed [RPM]	Re(stirrer) [–]	$Y_S$ [–]	MB [%]	$Y_S$ [–]	MB [%]	$Y_S$ [–]	MB [%]	$Y_S$ [–]	MB [%]
0	0	0.487	14.4	0.279	8.3	0.223	-0.54	0.089	-0.8
100	10.8	0.450	9.4	0.200	8.8	0.177	2.65	0.087	-1
150	21.5	0.426	6.8	0.183	8.4	0.153	2.87	0.083	-2.2
200	26.9	0.393	5.8	0.172	7.1	0.150	2.33	0.067	-0.8
250	32.3	0.377	4.8	0.158	8.2	0.131	2.01	0.078	-1.6
300	37.6	0.392	5.5	0.161	10.3	0.124	2.13	0.075	-1.7
350	37.6	0.408	5.7	0.164	4.1	-	-	0.047	-2.9
400	43	0.400	0.3	0.166	5.97	0.131	1.9	0.070	-0.5
500	53.8	0.416	6	0.140	6.7	0.143	1.72	0.069	-1.3
600	64.5	0.397	6	0.152	10.3	0.133	2.08	0.054	-2.3
700	75.3	0.418	6	0.139	0.91	0.121	2.01	0.051	-2.2
800	86	0.381	7.5	0.145	5.3	0.106	1.54	0.092	-5.96
900	96.8	0.381	5.8	0.112	5.3	0.100	0.67	0.061	-1.1
1000	107.5	0.377	5.8	0.094	3.1	0.089	0.63	0.065	-1.6

**Table 9.10:** Results of mixing sensitive reactions of CSTR-cascade v1 made of stainless steel. The stirrers turned in counter-clockwise direction.

Flow rate [ $\text{mL min}^{-1}$ ]		0.4		1.7	
Reynolds number [–]		11.9		50.5	
Rotational speed [RPM]	Re(stirrer) [–]	$Y_S$ [–]	MB [%]	$Y_S$ [–]	MB [%]
0	0.0	0.420	14.6	0.252	3.8
100	10.8	0.372	15.5	0.169	1.9
250	26.9	0.357	9.9	0.139	0.7
375	40.3	0.328	13.2	0.162	1.8
500	53.8	0.332	10.6	0.157	1.4
625	67.2	0.273	8.2	0.149	2.3
750	80.7	0.268	11.5	0.129	1.8
1000	107.5	0.307	11.5	0.155	0.9
1400	150.6	0.262	6.5	0.145	1.2

**Table 9.11:** Results of mixing sensitive reactions of CSTR-cascade v1 made of ceramics. The stirrers turned in clockwise direction.

Rotational speed [RPM]		0		500		1000	
Re(stirrer) [–]		0		53.8		107.5	
Flow rate [mL min <sup>-1</sup> ]	Re(channel) [–]	Y <sub>S</sub> [–]	MB [%]	Y <sub>S</sub> [–]	MB [%]	Y <sub>S</sub> [–]	MB [%]
0.2	5.9	0.5	16.9	0.306	-6.23	0.1905	-1.59
0.4	11.9	0.4	13.6	0.258	0.299	0.2076	-0.18
1	29.7	0.3	-0.51	0.204	-8.97	0.1306	-4.16
1.7	50.5	0.2	4.36	0.143	-3.4	0.0887	-3.2
2	59.4	0.1	-3.73	0.107	-3.15	0.1036	-4.42
4	118.9	0.1	-8.23	0.153	-17.8	0.1092	-6.59
8	237.7	0.1	-6.61	0.035	-3.36	0.0471	-7.84
16	475.5	0.0	-6.24	0.018	-5.64	0.0181	-6.14

**Table 9.12:** Results of mixing sensitive reactions of the optimised CSTR-cascade v2 made of stainless steel with flow rate 1.7 mL min<sup>-1</sup> resulting in  $Re(channel) = 52$ . The stirrers turned in clockwise direction.

Rotational speed [RPM]	Re(stirrer) [–]	Y <sub>S</sub> [–]	MB [%]
0	0.0	0.1558	5.8
100	10.8	0.1620	3.1
200	21.5	0.1121	2.7
250	26.9	0.1184	5.5
300	32.3	0.1450	6
350	37.6	0.1128	5.6
400	43.0	0.1319	7.8
500	53.8	0.1148	5.6
600	64.5	0.1302	4.2
700	75.3	0.1358	6.6
800	86.0	0.1229	7.5
900	96.8	0.1377	1.5
1000	107.5	0.1137	2.1

## 9.5 List of Chemicals

**Table 9.13:** List of used chemicals and solvents.

Substance	CAS-Nr.	Supplier	Product Nr.	LOT Nr.
1-Naphthol	90-15-3	Merck	8.22289.0250	S7173389
2-Naphthol	135-19-3	Merck	8.22290.0250	S7049090811
Sodium carbonate anhydrous	497-19-8	Fluk	71351	7277051408C02
Sodium hydrogen carbonate	144-55-8	Roth	0965.3	07785579
Sulfanilic acid	121-57-3	Merck	1.00686.0250	K45733786702
Sodium nitrite	7632-00-0	Roth	8604.1	192186023
Sodium chloride	7647-14-5	Roth	9265.2	144212672
Hydrochloric acid	7647-01-0	Roth	4625.1	359107937
Naphthalene 1,2-dione	524-42-5	TCI	339949	FCB063892
4-hydrazinobenzenesulphamic acid hemihydrate	854689-079	Apollo Scientific	OR70100	AS418553
Sulfamic acid	5329-14-6	Roth	4714.1	272182249
Acetic acid	64-19-7	Sigma Aldrich	A6283-100ML	SZBE3170V
Ethanol	64-175	Roth	K928.2	128269168
Methanol	67-56-1	Roth	8388.2	451178333
Ethyl acetate	141-78-6	Chem-Lab NV	CL00.0502.2500	26.0760506
2-Methyltetrahydrofuran	96-47-9	Sigma Aldrich	673277-2L	SHBj4237

## 9.6 SOP-Residence Time Distribution

As shown in figure 3.5 syringe pump, 6-port injection valve, microfluidic device and Avantes flow cell are connected to each other using capillaries (1/16" OD, 0.03" ID) and corresponding fittings. Keep the distance between valve, microfluidic device and flow cell as short as possible to reduce falsification of results. An exact connection scheme of the 6-port injection valve is shown in figure 5.4.

In AVASOFT the 'Integration Time' was set to 1.05 ms and 'Averaging' was set to 500.

1. Turn on the Avantes station and the deuterium lamp (blue toggle switch) and let it warm up for 15 min.
2. Flush the flow cell with the used solvent.
3. Turn on the shutter (red toggle switch) and start the measurement (start/stop button).
4. Take a light reference of the used solvent (white light bulb).
5. Turn off the shutter (red toggle switch) and take a dark reference (dark light bulb).
6. Turn on the shutter and stop the measurement (start/stop button).
7. Press the 'Time Series' button to add a continuous measurement. Add another 'Time Series' to perform a baseline correction.
8. Set the method of one tab as ansiole measurement with absorption measurement between 268 nm and 274 nm.
9. Set the method of the second tab as baseline correction with absorption measurement between 500 nm and 506 nm.
10. Set the time steps of the data export to EXCEL, depending on residence time of your device.
11. Start the measurement (start/stop button).
12. When the signal of the solvent is constant, switch the valve to "Inject" at a defined time to introduce the tracer.
13. When the signal of the tracer is constant switch the valve back to the "Load" position to perform a step-down signal.
14. Clean the flow cell with deionised water and ethanol and turn off the deuterium lamp (blue toggle switch).
15. Turn off the Avantes station after 15 min.

The exported data gives an EXCEL sheet with absorption data of the two wavelength ranges at specific times.

## 9.7 SOP-Mixing Sensitive Reaction

After preparation of all solutions, connect the syringe pump with the microfluidic device as illustrated in figure 3.9. Heat the water bath to 25 °C and place the microfluidic device in it. After setting the desired flow rate, the microfluidic device is flushed for at least three residence times to reach a steady state. Afterwards 1 mL is sampled and stored dark.

In AVASOFT the 'Integration Time' was set to 5 ms and 'Averaging' was set to 500.

1. Turn on the Avantes station and the deuterium lamp (blue toggle switch) and let it warm up for 15 min.
2. Set the data export wavelength between 390 nm and 700 nm in steps of 10 nm.
3. Flush the flow cell with buffer solution (ionic strength 444.4 mM).
4. Turn on the shutter (red toggle switch) and start the measurement (start/stop button).
5. Take a light reference of the buffer (white light bulb).
6. Turn off the shutter (red toggle switch) and take a dark reference (dark light bulb).
7. Turn on the shutter and stop the measurement (start/stop button).
8. Start the measurement (start/stop button) and switch to the absorption mode (A) in AVASOFT.
9. Suck the sample through the flow cell using a syringe.
10. Press 'file'->'export'->'ASCII' to store the data in a .txt-file.
11. Clean the flow cell with deionised water and ethanol and turn off the deuterium lamp (blue toggle switch).
12. Turn off the Avantes station after 15 min.

The exported .txt-files are adapted to be used with the MATLAB code:

- Remove the header and every blank space.
- Convert every *comma* into a *dot* (',' → '.').
- Convert every *semicolon* into *blank space* (';' → ' ').

The MATLAB code and the .txt-files are saved in the same folder so Matlab can import the files.

## MATLAB code

```

daten = dir('*.txt'); % loads every .txt file within this folder
numfiles = numel(daten); %number of files loaded

flow=[0.5 1]; %flowvector - flows QA+QB [mL/min]
c_B=10*9.987/99.763/2 %concentration of sulfanilic acid for Mass Balance
f_dilution=[5.5397/0.4912 5.5243/0.4841]; %dilution factor
mass(buffer+sample)/mass(sample)
absorption = nan((700-390)/10+1,numfiles); % absorbtption matrix is generated
Massenbilanz = nan(1, numfiles); % mass balance matrix is generated
YS = nan(size(Massenbilanz)); %Yield Ys Matrix is generated

l=0.01; %optical path length of flow cell [m]
ext_coeff=[277.6 400.6 654.7;411.2 395.5 761.3;588.7 463.6 972.2;794.2
576.6 1246.9;1009.6 722.5 1544.1;1227.8 901.8 1830.4;1456.9 1110.6
2074.9;1717.1 1345.8 2245.5;2025.7 1611.5 2318.7;2382.1 1892.3
2311.7;2728.4 2140.4 2246.2;3009.6 2317.9 2157.5;3158.5 2381.6
2116.9;3140.3 2308.0 2175.0;2959.1 2108.3 2311.4;2618.4 1809.4
2467.4;2133.5 1431.3 2590.4;1583.6 1018.4 2647.4;1057.6 638.6 2618.8;609.6
343.8 2486.1;302.7 166.1 2259.7;130.2 74.8 1964.2;54.1 35.3 1618.4;23.2
15.7 1265.7;11.6 8.7 936.1;7.9 6.6 652.1;4.7 4.2 428.7;4.4 4.2 271.9;4.1
4.4 191.2;2.5 2.7 89.1;2.2 2.8 48.9;1.6 2.1 28.3].*l; %epsilon[m^2/mol] *
optical path length[m]; For every wavelength between 390nm and 700 nm a
extinction coefficient for p-R, o-R and S is listed

lb=[0;0;0];%lower boundary for concentration
ub=[1;1;1];%upper boundary for concentration
options=optimoptions('lsqin','Algorithm','interior-
point','Display','iter');%optional

figure
hold on
xlabel('Flow [mL/min]')
ylabel('XS')
for k=1:numfiles
    currentfile = daten(k); %loads each file after each other
    currentdata = load(currentfile.name); %loads data into file
    absorption(:, k) = currentdata(:, 5); % saves data from column 5 in
.txt file into absorption matrix
    d = currentdata(:, 5); %saves data into d vector
    c = f_dilution.*lsqin(ext_coeff,d,[],[],[],[],lb,ub,[],options); %
performs linear regression with least square method and calculates
concentration of p-R, o-R and S
    Massenbilanz(k) = (c_B-c(1)-c(2)-2*c(3))/c_B*100; %massbalance (cB-cp-
cO-cS)/cB
    XS(k)=2*c(3)/(c(1)+c(2)+2*c(3));
    plot(flow, XS, '*') %plots the YS of each file over the set flows.
end

```

**Table 9.14:** Extinction coefficients for p-R, o-R and S product at the investigated wavelengths. Data obtained from Bourne et al. [2] at 25 °C, pH 9.9,  $I = 444.4 \text{ mol L}^{-1}$ .

Wavelength [nm]	Extinction coefficients [ $\text{m}^2 \text{mol}^{-1}$ ]		
	para-isomer (p-R)	ortho-isomer (o-R)	S-product
390	277.6	400.6	465.7
400	411.2	395.5	761.3
410	588.7	463.6	972.2
420	794.2	576.6	1246.9
430	1009.6	722.5	1544.1
440	1227.8	901.8	1830.4
450	1456.9	1110.6	2074.9
460	1717.1	1345.8	2245.5
470	2025.7	1611.5	2318.7
480	2382.1	1892.3	2311.7
490	2728.4	2140.4	2246.2
500	3009.6	2317.9	2157.5
510	3158.5	2381.6	2116.9
520	3140.3	2308.0	2175.0
530	2959.1	2108.3	2311.4
540	2618.4	1809.4	2467.4
550	2133.5	1431.3	2590.4
560	1583.6	1018.4	2647.4
570	1057.6	638.6	2618.8
580	609.6	343.8	2486.1
590	302.7	166.1	2259.7
600	130.2	74.8	1964.2
610	54.1	35.3	1618.4
620	23.2	15.7	1265.7
630	11.6	8.7	936.1
640	7.9	6.6	652.1
650	4.7	4.2	428.7
660	4.4	4.2	271.9
670	4.1	4.4	161.2
680	2.5	2.7	89.1
690	2.2	2.8	48.9
700	1.6	2.1	28.3